Diffusion in Aerobic Granular Sludge

van den Berg, L.

DOI
10.4233/uuid:2e5c2d37-20af-48f9-a926-593e8a7aa5a6

Publication date
2022

Document Version
Final published version

Citation (APA)
van den Berg, L. (2022). *Diffusion in Aerobic Granular Sludge*. [Dissertation (TU Delft), Delft University of Technology]. https://doi.org/10.4233/uuid:2e5c2d37-20af-48f9-a926-593e8a7aa5a6

DIFFUSION IN AEROBIC GRANULAR SLUDGE

Lenno van den Berg

Diffusion in Aerobic Granular Sludge

Lenno van den Berg

Diffusion in Aerobic Granular Sludge

Proefschrift

ter verkrijging van de graad van doctor

aan de Technische Universiteit Delft,

op gezag van de Rector Magnificus, prof.dr.ir. T.H.J.J. van der Hagen,

voorzitter van het College voor Promoties,

in het openbaar te verdedigen op

dinsdag 7 juni 2022 om 15:00 uur

door

Leendert VAN DEN BERG

Master of Science in Civil Engineering,

Master of Science in Life Science and Technology,

Technische Universiteit Delft, Nederland

geboren te Zeist, Nederland

Dit proefschrift is goedgekeurd door de promotoren.

Samenstelling promotiecommissie bestaat uit:

Rector Magnificus	voorzitter
Prof.dr.ir. M.K. de Kreuk	Technische Universiteit Delft, *promotor*
Prof.dr.ir. M.C.M. van Loosdrecht	Technische Universiteit Delft, *promotor*
Onafhankelijke leden:	
Prof.dr.ir. J.B. van Lier	Technische Universiteit Delft
Prof.dr.ir. E.I.P. Volcke	Universiteit Gent
Prof.dr.ir. C. Picioreanu	King Abdullah Univ. of Science and Technology
Prof.dr.rer.nat. H. Horn	Karlsruher Institut für Technologie
Dr. Y. Lin	Technische Universiteit Delft
Prof.dr. D. Brdjanovic	IHE Delft/Technische Universiteit Delft, reservelid

The research presented in this thesis was performed at the Sanitary Engineering Section, Department of Watermanagement, Faculty of Civil Engineering, Delft University of Technology, The Netherlands. The research was financially supported by the NWO VIDI grant 016.168.320.

Cover illustration: Multiple overlapping paths that were generated with a random walk simulation in two dimensions. Diffusion is often approximated as a random walk process.

ISBN 978-94-6366-534-6

Printed by Proefschrift-aio.nl

An electronic version of this dissertation is available at http://repository.tudelft.nl/

Contents

Summary

A large part of the wastewater produced worldwide is discharged without any treatment. This has several negative consequences, including the spread of diseases and contamination of the environment. One method to treat wastewater is called aerobic granular sludge (AGS), an advanced, compact technology that uses granules. Granules are spherical aggregates of microorganisms and biopolymers. Different microorganisms break down different pollutants within the granules. The microorganisms rely on the mass transfer of pollutants into the granule. This occurs through diffusion, a passive mode of transport that is driven by a concentration difference.

Diffusion is an essential aspect of AGS as well as other biofilm processes. Most previous research has shown that diffusion in granules and biofilms is a complex process. The diffusion behaviour varies between biofilms, within the biofilm, and between different molecules. At the same time, granule and biofilm models use a simple approach to describe diffusion. These models often use a single diffusion coefficient for the entire granule or biofilm. It is unclear how valid these simplifications are and how much they influence the accuracy of the model outcomes. In this dissertation, we studied different aspects of diffusion in granules to verify and extend previous research on the complexity of diffusion. The resulting information was then used to evaluate the impact on granule models.

It is well-known that diffusion in granules is influenced by the granule density. The density can be measured readily and it is often used to predict diffusion coefficients in a granule. However, multiple methods exist to measure granule density. In Chapter 2 we evaluated four commonly used methods: the pycnometer method, the percoll density gradient method, the dextran blue method, and the settling velocity method. We found that all methods besides the settling velocity method, yielded comparable and reliable results.

The granules are heterogeneous structures, with a density that differs throughout the granule. In Chapter 3, we visualized the heterogeneous structures of different granules with magnetic resonance imaging, a unique and non-invasive method. The granules displayed heterogeneous structures that include high- and low-density regions, water-like voids, and solid inclusions. However, large and connected channels were not observed. This is in contrast with previous studies that used imaging methods with extensive sample processing. Our findings suggest that the larger channels observed in

previous studies are an artefact of the sample processing and not a structural feature of the granules.

The effect of the observed heterogeneous structures on the kinetic properties of AGS was evaluated in Chapter 4. Nuclear magnetic resonance methods were used to measure the self-diffusion coefficients of water inside granules of different origin. The self-diffusion coefficients in the granules were around 70% of the self-diffusion coefficients of free water, for the granules from all origins. However, there was no clear correlation between the structure of the granules and the local diffusion coefficients. A reaction-diffusion model was used to evaluate the effect of six different heterogeneous diffusion scenarios on the flux of substrate into a granule. The model revealed that there were only minor differences (< 5%) between the different scenarios, indicating that heterogeneous diffusion does not have a significant influence on the process performance of AGS.

The diffusion coefficients of molecules in granules are often measured with methods based on mass balances or on microelectrodes. The diffusion coefficients that are reported in literature vary greatly. We demonstrated in Chapter 5 that this variability is at least partially caused by the inaccuracy of the methods that are used. We simulated diffusion experiments for six common methods and found that the relative standard deviation of these methods ranged from 5-61%. Furthermore, the diffusion coefficient was underestimated by 37% as a result of six sources of bias. The main reason for the limited accuracy was that the diffusion coefficient is an insensitive parameter in each experiment. At the same time, granule models do not require precise diffusion coefficients as input, since the output of granule models has limited sensitivity toward the diffusion coefficient.

In Chapter 6, we explored the limit of diffusion in aerobic granules. We measured the diffusion coefficients of polyethylene glycols with molecular weights between 61 and 10,000 Da. All molecules up to 4000 Da penetrated the entire granule and the diffusion coefficients in the granule were not significantly different from that in water. The 10,000 Da polyethylene glycol did not penetrate the entire granule, as it was excluded from the micropores. Fractionation of three Dutch wastewaters revealed that a large part (61-69%) of the influent soluble COD was smaller than 1 kDa. As molecules smaller than 1 kDa diffuse easily, the majority of the influent soluble COD can be considered diffusible COD and therefore as a possible substrate for nutrient removal.

Overall, this dissertation shows that diffusion in granules can be simplified with ease. Diffusion in granules is a complex subject, because of the complexity of the granule

matrix. However, the diffusion coefficient is an insensitive parameter that only has a limited impact on the flux of substrate into a granule. This allows granule models to ignore heterogeneous diffusion and to use inaccurate diffusion coefficients. A further study of diffusion in granular sludge is not directly needed to improve the understanding of the conversion processes, but it holds great value for understanding the complex matrix that constitutes the granules.

Samenvatting

Een groot deel van het wereldwijd geproduceerde afvalwater wordt ongezuiverd geloosd. Dit heeft verschillende negatieve gevolgen, zoals de verspreiding van ziektes en vervuiling van het milieu. Eén methode om afvalwater te zuiveren is aeroob korrelslib, een geavanceerde en compacte technologie die gebruik maakt van korrels. Korrels zijn bolvormige aggregaten van micro-organismen en biopolymeren. Diverse micro-organismen breken diverse vervuilende stoffen af binnen in de korrels. De micro-organismen zijn afhankelijk van het stoftransport van vervuilende stoffen de korrel in. Dit gebeurt via diffusie, een passieve manier van transport die wordt gedreven door een concentratieverschil.

Diffusie is een essentieel aspect van aeroob korrelslib en andere biofilmprocessen. De meeste eerdere onderzoeken hebben aangetoond dat diffusie in korrels en biofilms een complex proces is. Het diffusiegedrag varieert tussen biofilms, binnen in de biofilm en tussen verschillende moleculen. Tegelijkertijd gebruiken korrel- en biofilmmodellen een eenvoudige benadering om diffusie te beschrijven. Deze modellen gebruiken vaak één enkele diffusiecoëfficiënt voor de hele korrel of biofilm. Het is onduidelijk hoe steekhoudend deze vereenvoudigingen zijn en in hoeverre ze de nauwkeurigheid van de modeluitkomsten beïnvloeden. In dit proefschrift hebben we verschillende aspecten van diffusie in korrels bestudeerd om eerder onderzoek naar de complexiteit van diffusie te verifiëren en uit te breiden. De resulterende informatie werd vervolgens gebruikt om de impact op korrelmodellen te evalueren.

Het is bekend dat diffusie in korrels wordt beïnvloed door de korreldichtheid. De dichtheid kan eenvoudig worden gemeten en wordt vaak gebruikt om diffusiecoëfficiënten in een korrel te voorspellen. Er bestaan echter meerdere methoden om de korreldichtheid te meten. In Hoofdstuk 2 hebben we vier veelgebruikte methoden geëvalueerd: de pyknometermethode, de Percoll-dichtheidsgradiëntmethode, de dextranblauwmethode en de bezinkingssnelheids-methode. We ontdekten dat alle methoden vergelijkbare en betrouwbare resultaten opleverden, behalve de methode gebaseerd op de bezinkingssnelheid.

De korrels zijn heterogene structuren, met een dichtheid die varieert binnen in de korrels. In Hoofdstuk 3 hebben we de heterogene structuren van verschillende korrels gevisualiseerd met magnetische resonantie beeldvorming, een unieke en niet-invasieve methode. De korrels vertoonden heterogene structuren, gebieden met hoge en lage dichtheid, holtes met vrij water en ingesloten deeltjes. Grote en aaneengesloten

kanalen werden echter niet waargenomen. Dit is in tegenstelling tot eerdere studies die gebruik maakten van beeldvormende methoden met uitgebreide verwerking van de proefstukken. Onze bevindingen suggereren dat de grotere kanalen die in eerdere onderzoeken zijn waargenomen, een artefact zijn van de verwerking van de proefstukken en geen structureel kenmerk van de korrels.

Het effect van de waargenomen heterogene structuren op de kinetische eigenschappen van aeroob korrelslib wordt geëvalueerd in Hoofdstuk 4. Magnetic resonance imaging werd gebruikt om de zelfdiffusiecoëfficiënten van water in korrels van verschillende oorsprong te meten. De zelfdiffusiecoëfficiënten in de korrels waren ongeveer 70% van de zelfdiffusiecoëfficiënten van vrij water, voor de korrels van alle oorsprongen. Er was echter geen duidelijke correlatie tussen de structuur van de korrels en de lokale diffusiecoëfficiënten. Een reactie-diffusiemodel werd gebruikt om het effect van zes verschillende heterogene diffusiescenario's op de flux van substraat in een korrel te evalueren. Uit het model bleek dat er slechts kleine verschillen (< 5%) waren tussen de verschillende scenario's, wat aangeeft dat heterogene diffusie geen significante invloed heeft op het korrelslib proces.

De diffusiecoëfficiënten van moleculen in korrels worden vaak gemeten met methoden die gebaseerd zijn op massabalansen of op micro-elektroden. De diffusiecoëfficiënten die in de literatuur worden vermeld, variëren sterk. In Hoofdstuk 5 hebben we aangetoond dat deze variabiliteit op zijn minst gedeeltelijk wordt veroorzaakt door de onnauwkeurigheid van de gebruikte methoden. We simuleerden diffusie-experimenten voor zes veelgebruikte methoden en ontdekten dat de relatieve standaarddeviatie van deze methoden varieerde van 5-61%. Bovendien werd de diffusiecoëfficiënt met 37% onderschat als gevolg van zes bronnen van bias. De belangrijkste reden voor de beperkte nauwkeurigheid was dat de diffusiecoëfficiënt in elk experiment een ongevoelige parameter is. Tegelijkertijd vereisen korrelmodellen geen nauwkeurige diffusiecoëfficiënten als invoer, aangezien de uitkomst van korrelmodellen een beperkte gevoeligheid heeft voor de diffusiecoëfficiënt.

In Hoofdstuk 6 hebben we de limiet van diffusie in aerobe korrels onderzocht. We hebben de diffusiecoëfficiënten van polyethyleenglycolen met molecuulgewichten tussen 61 en 10.000 Da gemeten. Alle moleculen tot 4000 Da drongen de gehele korrel in en de diffusiecoëfficiënten in de korrel waren niet significant verschillend van die in water. De 10.000 Da polyethyleenglycol drong niet de gehele korrel in, omdat het uit de microporiën was uitgesloten. Fractionering van drie Nederlandse afvalwaters bracht aan het licht dat een groot deel (61-69%) van het influent opgeloste CZV kleiner was dan 1 kDa. Aangezien moleculen kleiner dan 1 kDa gemakkelijk diffunderen, kan het grootste

deel van het influent opgeloste CZV als diffundeerbaar CZV worden beschouwd en daarmee als potentieel substraat voor nutriëntenverwijdering.

In het geheel laat dit proefschrift zien dat diffusie in korrels gemakkelijk kan worden vereenvoudigd. Diffusie in korrels is een complex onderwerp vanwege de complexiteit van de korrelmatrix. De diffusiecoëfficiënt is echter een ongevoelige parameter die slechts een beperkte invloed heeft op de flux van substraat een korrel in. Hierdoor kunnen korrelmodellen heterogene diffusie negeren en onnauwkeurige diffusiecoëfficiënten gebruiken. Een verdere studie van diffusie in korrelslib is niet direct nodig om het begrip van de omzettingsprocessen te verbeteren, maar het is van grote waarde voor het begrijpen van de complexe matrix waaruit de korrels bestaan.

A granule with a large protozoa stalk

1

Introduction

1.1 | WASTEWATER

The average human produces 134 L of wastewater per day (Jones et al., 2021). A large part of this wastewater (around 50%) is released directly to the environment (Jones et al., 2021). The discharge of untreated wastewater leads to diseases, contamination of surface waters, and emission of greenhouse gasses. Therefore, one of the sustainable development goals of the United Nations is to halve the proportion of untreated wastewater (UN Habitat & WHO, 2021). Wastewater is often treated with biological processes, like activated sludge. Biological processes use bacteria and other (micro)organisms to break down the pollutants in the wastewater. Biological wastewater treatment has proven itself as an efficient and reliable process.

1.2 | AEROBIC GRANULAR SLUDGE

The activated sludge process was developed more than a century ago, and it requires large clarifiers to operate (Jenkins & Wanner, 2014). The need for process intensification has led to the development of more compact processes. One of these compact processes is called aerobic granular sludge (AGS) (Morgenroth et al., 1997). The name derives from the granular microbial aggregates that are a key part of this technology. The granules consist of a layered structure of microorganisms embedded in extracellular polymeric substances (EPS). The microorganisms are responsible for the degradation of wastewater pollutants and the EPS forms the matrix that holds the microorganisms together. The granules are spherical and typically 1-2 mm in diameter (van Dijk et al., 2020). The AGS technology is applied at an ever-growing number of wastewater treatment plants, under the trade name Nereda® (Royal HaskoningDHV, 2021). The Nereda® technology reduces the required land area by 25-75% and the energy demand by 20-50% compared to conventional wastewater treatment (Pronk et al., 2017).

The AGS process is usually carried out in a sequencing batch reactor (SBR), with three distinct phases (see Figure 1.1):

- **Anaerobic feeding:** In the first phase, untreated wastewater (influent) is fed gently into the reactor from the bottom. At the same time, treated wastewater (effluent) is pushed out at the top of the reactor. The influent flows through the granular sludge bed, where soluble COD diffuses into the granules. Within the granules, the soluble COD can be converted to volatile fatty acids (VFA) through hydrolysis and fermentation (Layer et al., 2019). The VFAs can be taken up by phosphate accumulating organisms (PAOs), which store the VFAs inside

the cell in the form of polyhydroxyalkanoates (de Kreuk & Van Loosdrecht, 2004).

- **Aerobic reaction:** In the second phase, the reactor is aerated to provide mixing of the granules and the wastewater. At the same time, oxygen is transported from the air bubbles via the liquid into the granules. The presence of oxygen allows the microorganisms in the granules to oxidise several wastewater pollutants. For example, nitrifying microorganisms convert ammonium to nitrate and PAOs use the stored PHA to remove phosphorus from the liquid (de Kreuk et al., 2005). These reactions consume oxygen and as a result, the core of the granule remains without oxygen. In the absence of oxygen other microorganisms can treat the wastewater pollutants, such as denitrifying organisms that convert nitrate into harmless nitrogen gas (de Kreuk et al., 2005).
- **Settling:** In the third phase, the aeration is switched off and the granules settle to the bottom of the reactor. A granular sludge bed forms and the cycle starts again.

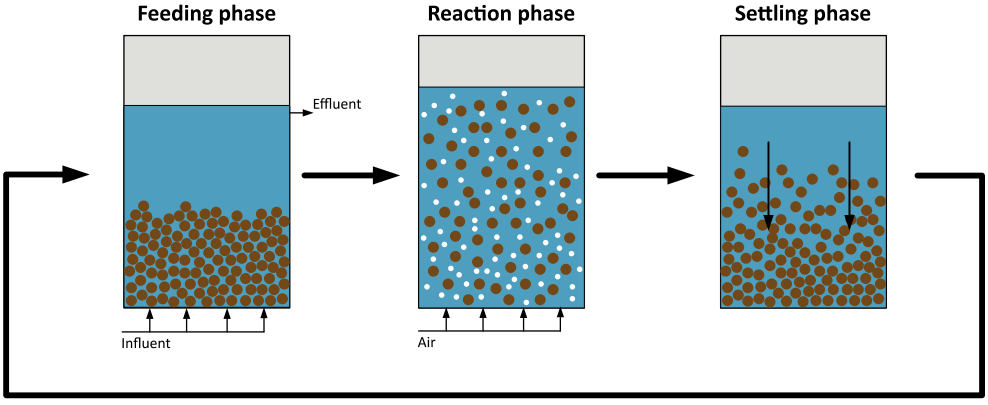

Figure 1.1. A typical AGS cycle with a feeding phase, reaction phase, and settling phase.

In the different conversions within the granule, substrates are consumed and products are formed. For example, during nitrification ammonium and oxygen are consumed and nitrate is formed. These substrates and products are transported into and out of the granules through diffusion. The rate of diffusion of substrates partly determines the overall reaction rate. If diffusion is quick, the substrates can penetrate deeper into the granule and more microorganisms can convert them into products. If diffusion is slow, the substrates penetrate less and the reaction rate is lower. Therefore, diffusion is a key

process of the AGS technology. A thorough understanding of diffusion of different molecules within the granules is important for optimization of the conversion processes.

1.3 | BASIC CONCEPTS OF DIFFUSION

Diffusion describes the thermal movement of molecules through a medium (e.g., air, water, granules). Through diffusion, molecules are transported from a region with a high concentration to a region of lower concentration. In the case of AGS, the concentration of substrates in the granules is initially low. As a result, substrates are transferred from the bulk liquid into the granules. This movement of molecules is generally referred to as flux. As long as there is a difference in concentration between two regions, there will be a diffusive flux.

1.3.1 | Fick's 1st law

The magnitude of the flux is related to the magnitude of the concentration gradient and to the diffusion coefficient through Fick's 1st law (Fick, 1855):

$$J = -D\frac{dC}{dx} \qquad (1.1)$$

Here, J is the diffusive flux (g m^{-2} s^{-1}), D is the diffusion coefficient of a specific molecule in a specific medium (m^2 s^{-1}), C is the concentration of a specific molecule (g m^{-3}), and x is the distance between two regions (m). This relation highlights that the diffusive flux not only depends on the difference in concentration between two regions (dC), but also on the distance between these two regions (dx). As a result, the impact of diffusive mass transfer is only significant over short distances (Stewart, 2003). On the scale of a granule (millimetres) diffusion is an important process to get the electron donor (substrates) and acceptors (oxygen, nitrate, nitrate) to the bacteria in the granules. However on a scale of the entire reactor (meters) the diffusion plays a negligible role, as mass transfer is dominated by convective transport. Therefore, the bulk liquid is generally considered to be completely mixed and the diffusive process only concerns the immediate vicinity of the granules.

1.3.2 | Fick's 2nd law

Fick's 1st law (Equation 1.1) is only relevant when the concentration gradient is known. In a granule the concentration gradient is generally not known, but it can be described with the reaction-diffusion equation, which is based on Fick's 2nd law (Fick, 1855):

$$\frac{dC}{dt} = D\left(\frac{d^2C}{dr^2} + \frac{2}{r}\frac{dC}{dr}\right) - R \qquad (1.2)$$

Here, *C* is the concentration of substrate (g m^{-3}), *D* is the diffusion coefficient of a specific molecule in a specific medium (m^2 s^{-1}), *r* is the granule radius (m), and R is the reaction rate (g m^{-3} s^{-1}). This equation is a partial differential equation and therefore it requires initial conditions and boundary conditions. Under steady-state conditions, the *dC/dt* term vanishes and there will be a balance between the diffusive supply of substrate through diffusion and the consumption of substrate through reaction. The relative rates of both processes will determine the steady-state concentration profile of a substrate.

For a typical substrate in aerobic granular sludge, the concentration profile is determined by several factors: (1) the concentration of the substrate in the bulk liquid, (2) the thickness of the mass transfer boundary layer (MTBL), (3) the diffusion coefficient of the substrate in water, (4) the diffusion coefficient of the substrate in the granule, and (5) the consumption rate of the substrate. An example concentration profile that highlight these factors is indicated in Figure 1.2.

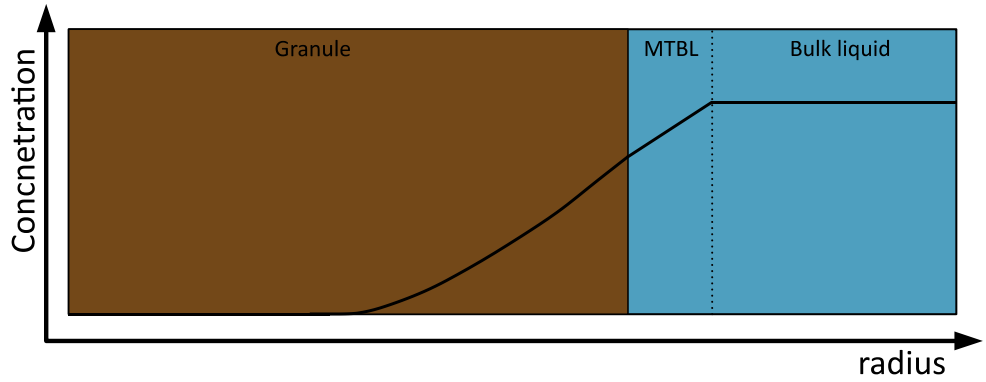

Figure 1.2. Mass transfer in a granular sludge system and resulting concentration gradients in the granule and mass transfer boundary layer.

1.3.3 | Effective diffusion coefficient

Fick's laws have been developed for diffusion in homogeneous media. This means that the diffusion coefficient is constant throughout the entire medium. Granules are not homogeneous and the diffusion coefficient is not constant throughout the granule (Hinson & Kocher, 1996). Granules contain microbial cells, which are generally impermeable objects for diffusing molecules (Beuling, 1998). Thus, granules are often considered as a porous medium and diffusing molecules can only penetrate the pore space. As a result, the concentration in a granule can be defined based on the pore volume and based on the total volume. This leads to a concentration in the pores (C_P) and a concentration in the total granule (C_T). These concentrations differ by a factor that is based on the fraction of microbial cells and EPS (φ):

$$C_T = (1 - \phi) \cdot C_P \qquad (1.3)$$

Usually, the concentration C_P is more easily quantifiable than the concentration C_T. After all, at the granule surface, C_P is equal to the concentration in the bulk liquid. Microelectrodes also measure C_P directly. However, Fick's 1st law evaluates the flux based on the total granule area and is therefore most conveniently expressed based on the total granule volume:

$$J = D\frac{dC_T}{dx} \qquad (1.4)$$

By combining equations 1.3 and 1.4, a new expression of Fick's 1st law is obtained:

$$J = D(1 - \phi)\frac{dC_P}{dx} \qquad (1.5)$$

This expression is simplified by the introduction of an effective diffusion coefficient D_{eff}:

$$D_{eff} = D(1 - \phi) \qquad (1.6)$$

This D_{eff} is closely related to the diffusion coefficient. It illustrates the effect of the impermeable cells (as well as the EPS) on the diffusion through a granule. A higher fraction of cells leads to a lower D_{eff} and thus a lower flux. Even though this relation is intuitively clear, the distinction between both parameters is not always made. Both parameters are used interchangeably, despite efforts to distinguish them more clearly (Axelsson & Persson, 1988; Libicki et al., 1988; Stewart, 1998). To reiterate: D_{eff} is used

to calculate the flux of a solute into the granule with Fick's 1st law (see Equation 1.5), while *D* is used to calculate the transient concentration profiles in the granule with Fick's 2nd law (see Equation 1.2). Fick's 2nd law is not affected by the fraction of impermeable cells, as the impermeable cells have two counteracting effects. On the one hand, the mass flux into the granule is reduced by the impermeable cells, as described in Equation 1.5. On the other hand, less mass of a solute is needed to change the concentration in the granule, if there are more impermeable cells. The solute only accesses the pore volume in the granule, not the total volume. A higher fraction of impermeable cells leads to a lower pore volume, and thus, less mass of a solute is needed to change the concentration. If a mass balance is made over a certain granule volume, the effect of impermeable cells on the flux is cancelled out by its effect on the concentration change.

This dissertation will primarily deal with the actual diffusion coefficient. The D_{eff} is a lumped parameter that is affected both by the diffusion coefficient and by the porosity. The goal of this dissertation is to improve our understanding of diffusive mass transfer and therefore, it is beneficial to separate both effects.

1.4 | FACTORS AFFECTING THE DIFFUSION COEFFICIENT

Fundamentally, the diffusion coefficient is a measure of mobility of a molecule in a certain medium. It is therefore a property of both the diffusing molecule and the medium through which the molecule diffuses. Without a mention of the medium, any diffusion coefficient is meaningless. For most molecules, the diffusion coefficient in the gas phase is much greater than the diffusion coefficient in the liquid phase. For example, carbon dioxide in air has a diffusion coefficient of $1.6 \cdot 10^{-5}$ m^2/s (Engineering Toolbox, 2018), while its diffusion coefficient in water is only $1.7 \cdot 10^{-9}$ m^2/s (Engineering Toolbox, 2008). Diffusion coefficients of molecules in water have generally been determined precisely and can readily be found in literature or estimated with the Wilke-Chang correlation (Wilke & Chang, 1955).

Diffusion coefficients in aerobic granular sludge and other biofilm systems have only been measured sporadically. The values that are reported in literature are not universally applicable, due to the complexity of granular sludge and other biofilms (Stewart, 1998). The diffusion coefficient of a molecule is influenced by the properties of the granule matrix, like density (Horn & Morgenroth, 2006). The diffusion coefficient is also influenced by the properties of the diffusing solute, such as charge (Stewart, 1998). This paragraph will focus on the factors that influence the diffusion coefficient

that are most important for granular sludge.

1.4.1 | Matrix effects

A granule is composed of water, EPS, and microbial cells. Typically around 20% of the granule volume consists of microbial cells and EPS and the remaining 80% of the volume is occupied by free, extracellular water (T.C. Zhang & Bishop, 1994a, 1994b). Diffusion occurs mainly within the extracellular water. A molecule that diffuses in water only interacts with water molecules and with other diffusing molecules. When the same molecule diffuses in aerobic granules, it will also encounter EPS and microbial cells. Since EPS and cells obstruct diffusing molecules, diffusion coefficients in granules are lower than in water (Stewart, 1998). The obstruction effect of the granule matrix plays a role at two different scales: the microscale and the mesoscale (see Figure 1.3).

Obstruction

At the microscale, the diffusion coefficient is reduced through an increased diffusive path length. Most diffusing molecules are blocked by microbial cells and biopolymers (Beuling, 1998). As a result, a molecule that diffuses from point A to point B has to travel a greater distance. The increase of the diffusive path length is described by the tortuosity. A high tortuosity indicates a very long and twisted path between two points, whereas a low tortuosity indicates a short and straight path. Microbial cells and other impermeable objects in a granule increase the tortuosity. The effect of tortuosity on the effective diffusion coefficient is as follows (Epstein, 1989):

$$D_{eff} = \frac{1}{\tau^2} D_{aq} \qquad (1.7)$$

Here, D_{eff} is the effective diffusion coefficient ($m^2\ s^{-1}$), τ is the tortuosity, and D_{aq} is the diffusion coefficient in water ($m^2\ s^{-1}$). The tortuosity of a granule is proportional to the fraction of cells and EPS in a granule (T.C. Zhang & Bishop, 1994b). Thus, a higher content of cells and EPS leads to a higher tortuosity and thereby a reduced diffusion coefficient.

In practice, the content of cells and EPS in a granule is not known directly, but only approximated by the granule density. The granule density represents the mass of dry matter per granule volume. Most aerobic granules have a density of 50-100 g/L (Cassidy & Belia, 2005; de Kreuk & Van Loosdrecht, 2004; Di Iaconi et al., 2004). Previous research has shown that there is a distinct correlation between the biofilm density and the

diffusive permeability in the biofilm (Fan et al., 1990; Horn & Morgenroth, 2006; Stewart, 1998). Thus, the relatively high density of aerobic granules suggests that the diffusive permeability in these granules is probably quite low.

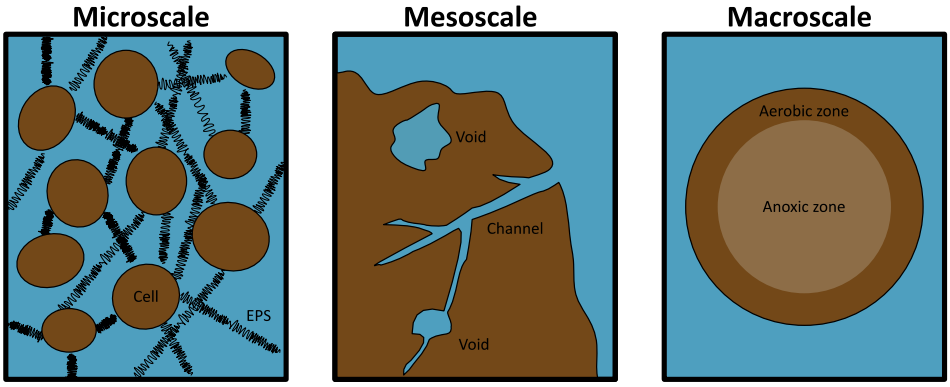

Figure 1.3. Schematic representation of the granule structure at different spatial scales.

Heterogeneity

At the mesoscale, granules are heterogeneous structures. The concentration of cells and EPS is not constant throughout the granule. As a result, the obstruction by the cells and EPS is also not constant. Understanding the heterogeneity of granules and biofilms has been a major research theme in the past decades (Chen et al., 2007; Gonzalez-Gil & Holliger, 2014; Lemaire et al., 2008; Stewart et al., 1995; Stoodley et al., 1999). Many researchers have attempted to quantify the heterogeneity of the diffusion coefficient in biofilms. There are different techniques available to measure local diffusion coefficients, including fluorescence recovery after photobleaching (FRAP) and magnetic resonance imaging (MRI). These techniques make it possible to measure the diffusivity in small regions of a biofilm. For example, Bryers and Drummond (1998) have shown that a biofilm can consist of channels and cell clusters. Diffusion in the cell clusters was much slower than diffusion in water, due to the presence of cells and EPS. In contrast, diffusion in the biofilms channels was comparable to diffusion in water. Similar results have been found in a myriad of studies (de Beer et al., 1994; Gonzalez-Gil et al., 2001; Sankaran et al., 2019; Van Schadewijk et al., 2018; Wieland et al., 2001; Yang & Lewandowski, 1995). Other studies found a layered structure, with a diffusion coefficient that decreased linearly towards the bottom of the biofilm (Beyenal & Lewandowski, 2002; Renslow et al., 2010).

Convective diffusion

Biofilm researchers have observed liquid flowing through biofilm channels (Lewandowski et al., 1994; Stoodley et al., 1994; Wilking et al., 2013). This mass transfer mechanisms is also referred to as convective diffusion (Afridi et al., 2017). Convective diffusion has the potential to increase mass transfer rates significantly. In anaerobic granular sludge, the presence of channels has been linked to gas bubble formation inside the granule (Henze & Harremoës, 1983). If the production rate of gasses (e.g., methane) exceeds the diffusive transport out of the granule, supersaturation occurs, and a gas bubble forms. The flow of gas bubbles out of the granule is believed to create microcurrents that enable liquid flow. Research by Van den Heuvel et al. (1996); Van den Heuvel et al. (1997) showed that a gas bubble inside a granule can enhance mass transfer even more, if the granule circulates through the reactor. The pressure difference between the top and bottom of the reactor causes the gas bubble inside the granule to grow and shrink. This pumping effect allows liquid to flow into and out of the granule.

Channels have been observed in aerobic granules as well (Gonzalez-Gil & Holliger, 2014; Ivanov et al., 2005; Lemaire et al., 2008). However, most observations were made after extensive processing of the granule (i.e., dehydration). It is therefore questionable if the observed channels are really present or if they are an artefact of the sample processing. Furthermore, studies on the effect of the channels on overall mass transfer rate have shown diffusion to be the predominant process for soluble substrates (Eberl et al., 2000; Gonzalez-Gil et al., 2001; Huisman et al., 1990; Lens et al., 2003).

1.4.2 | Solute effects

Diffusion in aerobic granules also depends on the properties of the diffusing molecule. Different molecules are affected differently by the granule matrix. The two most important properties are the molecular weight and the charge of the solutes (Stewart, 1998).

Molecular weight

The diffusion coefficient of solutes in water is described by the Stokes-Einstein equation:

$$D = \frac{k_B T}{6\pi\eta r} \qquad (1.8)$$

Here, k_B is the Boltzmann constant (J K^{-1}), T is the temperature (K), η is the viscosity of water (Pa s), and r is the hydrodynamic radius of the solute (m). This equation shows that the diffusion coefficient in water is inversely proportional to the hydrodynamic radius of the diffusing solute. Larger molecules will therefore diffuse slower than smaller molecules. In aerobic granules, the molecular weight has an even bigger influence on the diffusion coefficient of a solute. The granules consist of EPS that form a porous network (see Figure 1.4). Small molecules can diffuse freely through the pores, while larger molecules are blocked by the pores. Since granules have a pore size distribution, some molecules are able to diffuse in certain parts of the granule, while they are blocked in other parts (Witten & Ribbeck, 2017).

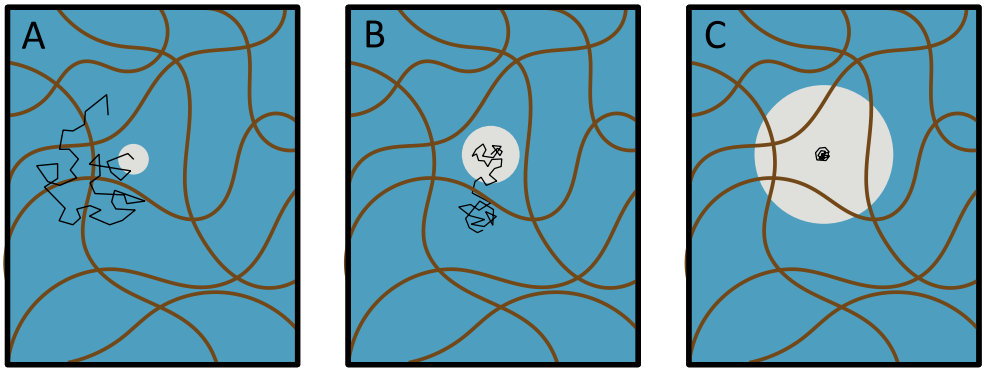

Figure 1.4. Steric effects on diffusion in granules. (A) Particles smaller than the mesh size diffuse freely. (B) Particles on the order of the mesh size have significant steric hindrance but eventually penetrate the granule. (C) Large particles cannot penetrate the granule. Adapted from Witten and Ribbeck (2017).

The theory of diffusion of molecules with different molecular weight is straightforward, but the experimental observations are conflicting. Stewart (1998) reviewed a wide range of diffusion coefficient measurements. He found that the relative diffusion coefficient was not significantly different for small solutes up to 44 Da (D/D_{aq} = 0.46) compared to large solutes with molecular weight of 44-342 Da (D/D_{aq} = 0.39). It could be that all solutes up to 342 Da are smaller than the pore size of the biofilms and therefore, that none of the solutes are obstructed by the pores of the biofilm. However, if all solutes diffuse unobstructed, the relative diffusion coefficient would be expected closer to 1. Even more conflicting results have been obtained for molecules of 1-900 kDa. Most authors found that the relative diffusion coefficient decreased with molecular weight (Bryers & Drummond, 1998; de Beer & Stoodley, 1995; Takenaka et al., 2009; Thurnheer

et al., 2003). However, other authors found that the relative diffusion coefficient actually decreased for larger molecules (Birmingham et al., 1995; Lawrence et al., 1994; Marcotte et al., 2004). Thus, the effect of solute molecular weight on diffusion in granules and biofilms is still poorly understood. It is unclear how the granule matrix affects diffusing molecules of different size and what molecules are still able to penetrate into the granules.

Charge

Many molecules that are relevant for wastewater treatment are charged, including ammonium, phosphate, nitrate, and nitrite. The charge of these ionic solutes affects their diffusion in the granules. There are three main differences between ionic and neutral solutes. The first difference is that ionic solutes never diffuse as single ion. Electroneutrality dictates that diffusion of a single ion is always paired with either co-diffusion of an ion of opposite charge or counter-diffusion of an ion of the same charge. The second difference is that ionic solutes are attracted or repelled by the charged groups on the EPS in the granule. The EPS is generally negatively charged and therefore, diffusion of cations is faster than diffusion of anions. This charge effect is described by the Donnan equilibrium theory (Golmohamadi & Wilkinson, 2013). The final difference is that ionic solutes can adsorb to the EPS. It is well-documented that cations such as ammonium and heavy metals can bind to the negatively charged groups of the EPS (Bassin et al., 2011; Karim & Gupta, 2002; W. Wang et al., 2002). The diffusive penetration of adsorbing molecules will be slower until all binding sites are occupied (Stewart, 1996). The exact impact of solute charge on its diffusion coefficient is poorly understood. Siegrist and Gujer (1985) argued that for wastewater and tap water, the ionic strength is high enough that the influence of solute charge is negligible. However, the review of Stewart (1998) revealed that there were significant differences between diffusion of neutral and ionic solutes.

1.5 | MODELLING THE DIFFUSION PROCESS

Research and development of AGS is often based on mathematical models that simulate the conversion processes in an AGS reactor. A wide range of mathematical models exist, but the most commonly used models are relatively simple. The focus of these models is to predict the flux of substrates into the granules as well as the resulting effluent concentrations. As described above, the flux of substrates is a function of diffusion

coefficient and as a result, diffusion is an important part of the mathematical models. However, different models use different approaches to include diffusion.

The standard approach is very straightforward. Diffusion is described according to Fick's laws, with a single diffusion coefficient for each solute in the granules. For each solute, the diffusion coefficient in the granule is set to 80% of D_{aq} (Boltz et al., 2011; Morgenroth, 2008; Nicolella et al., 1998; Wanner et al., 2006). The variability of the diffusion coefficient and the properties of the solute are not considered in this approach. The use of the 80% value reduces the complexity of the model, while the model is supposedly still reasonable accurate. Some models only use an implicit description of diffusion, with apparent kinetic coefficients (Baeten et al., 2018). These models are even less complex, but satisfactory results for the macroscopic description of the process have been obtained.

There are many authors that suggest biofilm and granule models should include heterogeneous diffusion (de Beer et al., 1994; Gonzalez-Gil & Holliger, 2014; Lemaire et al., 2008). However, there are only a handful of biofilm models that have done so (Shanahan et al., 2005; Siegrist & Gujer, 1985). Apparently, most model developers feel that the increased model complexity outweighs the supposed improved performance.

1.6 | OUTLINE OF THE THESIS

So far, AGS research has assumed a simplified view of diffusion. The granule is treated as a perfect homogeneous sphere and a single diffusion coefficient is used for all diffusible compounds. At the same time, fundamental research has shown the complex nature of the granule (in terms of structure and chemical composition) and the potential implications for diffusion. Therefore, the main goal of this study was to **gain mechanistic understanding of solute diffusion in aerobic granular sludge** and its impact on process engineering.

The research was divided into two parts:

1. Matrix effects
    - It was already well-established that the granule density has a major influence on diffusion in granules. There are different **methods to measure the granule density.** However, the methods have not been tested and compared properly. Therefore, a comparison was made between four

methods to measure granule density, including the pycnometer method and the dextran blue method. The results are discussed in **Chapter 2**.

- Many studies of the granule structure were carried out with invasive methods. Artefacts may arise and observed granule structures (e.g., channels) might not be representative of undisturbed granules. Magnetic resonance imaging (MRI) is a non-invasive method that can be used to visualize the granule structure non-invasively. Here, the granule structure was studied with high-field strength MRI. The **heterogeneous structure** of different granular sludges and the absence of channels is described in **Chapter 3**;
- Based on the observations of heterogeneous granule structures, many researchers have postulated that mass transfer is heterogeneous as well. However, validation of this hypothesis was lacking. Therefore, the diffusive properties of aerobic granules were studied with nuclear magnetic resonance (NMR) methods and a mathematical model was set up to evaluate the impact of **heterogeneous diffusion** on mass transfer (flux) into the granule. These findings are described in **Chapter 4**;

2. Solute effects
   - In order to study the impact of solute properties on diffusion through a granule, the diffusion coefficient of different solutes should be measured. However, all common **methods** that are used **to measure diffusion coefficient**s in granules are inaccurate and suffer from significant bias. The exact impact and the implications are discussed in **Chapter 5**;
   - The diffusion behaviour of larger molecules has only been studied sporadically. Therefore, the relation between the **molecular weight** and he **diffusion coefficient** of several model solutes was determined. These results were linked with the molecular weight distribution in influent wastewater. This is described in detail in **Chapter 6**.

Finally, **Chapter 7** gives an evaluation of the overall results of this thesis and highlights recommendations for future research.

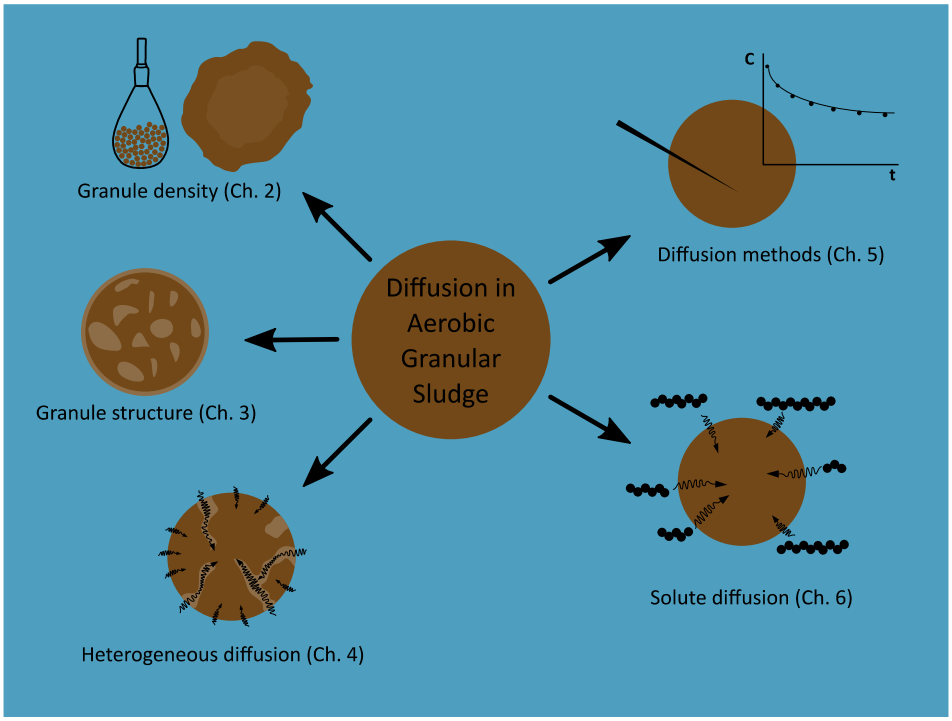

Figure 1.5. Schematic overview of the main chapters of this dissertation.

Granules inside a pycnometer

2

Density measurements of aerobic granular sludge

Published as: Van den Berg, L., Pronk, M., Van Loosdrecht, M.C.M. & De Kreuk, M.K. (2021). Density measurements of aerobic granular sludge. *Environmental Technology*. DOI: 10.1080/09593330.2021.2017492

ABSTRACT

Background

Granular sludge processes are frequently used in domestic and industrial wastewater treatment. The granule buoyant density and biomass density are important parameters for the design and operation of granular sludge reactors. Different methods to measure the granule density include the pycnometer method, the Percoll density gradient method, the dextran blue method, and the settling velocity method.

Methods

In this study, a comparison was made between these four methods to measure granule density for granules from a full-scale granular sludge plant treating domestic sewage. The effect of salinity on granule density was assessed as well.

Results

Three out of the four evaluated methods yielded comparable results, with granule buoyant densities between 1025.7 and 1028.1 kg/m^3 and granule biomass densities between 71.1 and 71.5 g/L (based on volatile suspended solids (VSS)). The settling velocity method clearly underestimated the granule density, due to the complex relation between granule properties and settling velocity. The pycnometer method was the most precise method, but it was also quite susceptible to bias. The granule buoyant density increased proportionally with salinity, to 1049.2 kg/m^3 at 36 g/L salinity. However, the granule biomass density, based on VSS, remained constant. This showed that the granule volume was not affected by salinity and that the buoyant density increase was the result of diffusion of salts into the granule pores.

Conclusions

Overall, the granule density can be measured reliably with most methods, as long as the effect of salinity is considered. The results are discussed in light of operational aspects for full-scale granular sludge plants.

2.1 | INTRODUCTION

Granular sludge processes are popular technologies for domestic and industrial wastewater treatment. The granules that are used in these technologies are compact microbial aggregates with excellent settling properties (Y. Liu et al., 2005; Winkler et al., 2012). Aerobic granular sludge (AGS) is a recently introduced technology for the removal of organic carbon and nutrients from domestic and industrial wastewaters (Pronk et al., 2015b). The biomass concentration in granular sludge reactors is very high (8-15 g/L), made possible by the high biomass density and excellent settling properties of the granules (de Kreuk & Van Loosdrecht, 2004). As a result, AGS has a small footprint and a low energy demand compared to conventional municipal wastewater treatment technologies (Bengtsson et al., 2019).

An important parameter for the AGS process is the density of the granules. In fact, there are two related parameters which are both referred to as *granule density*. The first parameter is the buoyant granule density, also called the wet granule density. It is defined as the granule mass per unit volume, where the mass includes all components that make up the granule (microbial cells, extracellular polymeric substances (EPS), water, precipitates, etc.). The buoyant density of granules is reported in the range of 1005-1070 kg/m3 (Etterer & Wilderer, 2001; Quoc et al., 2021; Winkler et al., 2013). The buoyant density of a granule relates to the hydrodynamics in the granular sludge reactor. The settling velocity of a granule can be estimated from its size and density through a force balance (Nicolella et al., 1999). Thus, the buoyant density is an important parameter for the design of reactor hydrodynamics, for the granule bed settling and stratification, and for the selection of granular biomass over flocculent biomass.

The second parameter which is referred to as *granule density* is the granule biomass density, also referred to as dry granule density. This parameter is defined as the mass of dry solids (total or volatile) per granule volume. The biomass density is reported in the range of 50-100 gVSS/L (Cassidy & Belia, 2005; de Kreuk & Van Loosdrecht, 2004; Di Iaconi et al., 2004). The biomass density influences the diffusion of substrates into the granules, as a higher fraction of cells and EPS limits the diffusing molecules more (Beuling et al., 1998; Horn & Morgenroth, 2006; Stewart, 1998). Furthermore, models of the granular sludge process generally require the maximum biomass density as an input (de Kreuk et al., 2007; Hao et al., 2002; Takács et al., 2007). This maximum density leads to competition for space between different organisms and it determines the maximum conversion rates per granule volume. Thus, an accurate determination of the biomass density is an important step in the study of conversions in AGS.

The granule density can be measured with several methods: the pycnometer method (Torfs et al., 2016), the Percoll density gradient method (Etterer & Wilderer, 2001; Pertoft et al., 1978), the dextran blue method (Beun et al., 2002), and a method based on settling velocity measurements (Trego et al., 2018). All four methods yield the buoyant density, but only the pycnometer method and the dextran blue method determine the biomass density. It is not clear to what extent these methods are comparable and there is no standard method available for the measurement of granular sludge density. This makes it difficult to compare the outcomes of studies that used different methods. Furthermore, the granule density is commonly measured in a physiological saline solution with the Percoll density gradient method, but in freshwater with the other methods. The effect of salinity on the granule density is not reported or discussed. In practice salinity can vary over time, for example, due to seawater intrusion in coastal wastewater treatment plants. This could play a role in the settling properties of granules and the design of these installations. Therefore, the goal of this study was to compare the granule density methods and to quantify the effect of salinity on the granule density.

2.2 | MATERIALS & METHODS

2.2.1 | Source of granules

Aerobic granules were harvested from the municipal wastewater treatment plant in Utrecht, The Netherlands. The treatment plant was designed by Royal HaskoningDHV under the trade name Nereda®. The granules were sieved with tap water to retain granules with a diameter between 1600 and 2500 µm. This fraction was used due to its abundance in the reactor. The granules were stored in tap water at 4°C for up to two weeks. No changes in granule density were observed during this period.

2.2.2 | Comparison of methods

All density measurements were carried out at room temperature (20.0 ± 0.5 °C).

Pycnometer method

The pycnometer method was carried out as described by Torfs et al. (2016). Briefly, excess water was removed from a granule sample by spreading out the granules over a sieve with 200µm mesh and briefly dabbing from underneath the sieve with a paper towel. Next, the granules were transferred into a calibrated pycnometer with a volume

of 100mL ($V_{pycnometer}$) and a certain empty weight ($W_{pycnometer,empty}$). The weight of the pycnometer with added granules was recorded ($W_{pycnometer,withgranules}$). Typically, 20-25g of granules (wet weight) was used in each pycnometer experiment. The pycnometer was filled with tap water and the weight of the full pycnometer was determined ($W_{pycnometer,full}$). The buoyant density was calculated based on the density of tap water (ρ_{H2O}):

$$\rho_{buoyant} = \frac{W_{granules}}{V_{pycnometer} - \frac{W_{pycnometer,full} - W_{granules}}{\rho_{H2O}}} \quad (2.1)$$

Subsequently, the entire granule sample was subjected to total suspended solids (W_{TSS}) and volatile suspended solids (W_{VSS}) determination according to Standard Methods (APHA, 2005). The biomass densities were calculated as follows:

$$\rho_{biomass,TSS} = \frac{W_{TSS}}{V_{pycnometer} - \frac{W_{pycnometer,full} - W_{granules}}{\rho_{H2O}}} \quad (2.2)$$

$$\rho_{biomass,VSS} = \frac{W_{VSS}}{V_{pycnometer} - \frac{W_{pycnometer,full} - W_{granules}}{\rho_{H2O}}} \quad (2.3)$$

The pycnometer method was carried out in triplicate. An additional experiment was performed, in which the step to remove excess water from the granules was changed. Instead of spreading granules on a sieve and dabbing them from underneath, excess water was removed by (1) placing the granules directly on a paper towel or (2) placing the granule sample in a beaker and pouring off excess water. The remaining procedure was unaltered.

Percoll density gradient method

The Percoll density gradient method was carried out as described in Etterer and Wilderer (2001). Briefly, a number of granules (15-25) were placed in a 10 mL plastic tube containing 3 mL Percoll solution (GE Healthcare) and 7mL tapwater. Marker beads (Cospheric LLC) were added with densities of 1020 kg/m^3 and 1040 kg/m^3. The plastic tubes were subjected to centrifugation at 15,000 x g in a Sorvall ST 16R centrifuge (Thermo Fisher Scientific) for 120 min in a non-swing out rotor (25° pitch angle). A slow deceleration (requiring approximately 20 min) was applied to preserve the density gradient and the position of the granules. The density gradient was photographed together with a ruler to determine the position of the density markers beads and the granules with ImageJ software (Schneider et al., 2012). The measurement was repeated

6 times to determine two descriptors of the precision of this method: the standard deviation of the density of all granules individually (n ≈ 120) and the standard deviation of the average density in each tube (n ≈ 6).

Modified dextran blue method

The modified dextran blue method is based on Beun et al. (2002). The method uses a molecule that is called 'blue dextran 2000', which has a molecular weight of 2 MDa. It is excluded from the granules due to its large size (Jimenez et al., 1988a; Jimenez et al., 1988b). If a solution of dextran blue with known volume and known concentration is added to a granule sample, the dextran blue will be diluted by the liquid between the granules. The liquid volume in the granule sample can thus be estimated by measuring the dextran blue concentration after dilution. The granule volume follows if the total volume is known as well. The procedure, with modifications, consisted of the following steps:

1) A granule sample was poured with water into a 200 mL beaker to obtain a settled bed volume of roughly 125 mL. Next, the granule sample was transferred to a pre-weighted 200 mL volumetric flask ($W_{flask,empty}$). The flask was filled completely with tap water and the full weight was recorded ($W_{flask,full}$). Subsequently, the granules were transferred to a 500 mL beaker for the dextran blue volume measurement. The weight of the emptied volumetric flask ($W_{flask,emptied}$) was used to correct for the small volume of liquid remaining in the volumetric flask after transferring the granules.
2) The 500 mL beaker with granule sample was placed on a scale and its weight was recorded at each of the following steps. First, the initial weight was recorded. Next, approximately 50 mL of water was removed from the beaker. Then, approximately 150 mL of a dextran blue solution (2 g/L) was added to the beaker. The beaker contents were mixed gently with a stir rod, left for 10 min, and mixed again. After the granules had settled, approximately 100 mL of liquid was removed, from which a fraction was stored for analysis (sample 1). The volume removed was replaced by tap water. After mixing, waiting 10 min, mixing, and settling, again approximately 100 mL of liquid were removed (sample 2) and replaced by tap water. This step was repeated once more to obtain a total of three samples, each at a different dilution. The dextran blue stock solution and the samples were filtered with 0.45 µm PVDF filters and their absorbance was determined with a spectrophotometer (Genesys 6, Thermo Fisher Scientific) at 620 nm, in triplicate.

3) The granules were washed with tap water to remove the dextran blue. The entire granule sample was subject to determination of total suspended solids (W_{TSS}) and volatile suspended solids (W_{VSS}) according to Standard Methods (APHA, 2005).

The first step was added to the original method to allow the determination of the buoyant granule density. Furthermore, four main modifications were made to improve the precision. First, the concentration of the stock dextran blue solution was increased from 1 to 2 g/L. This avoids measurements in the lower detection range of the spectrophotometer (<0.2 absorbance). Second, the volumes of dextran blue stock, sample, etc. were determined precisely by recording the weight of the beaker at each step. Third, a 10 min waiting period was introduced to allow dextran blue to diffuse into any boundary layers or granule macropores. Lastly, the samples were all filtered prior to the absorbance measurement to remove any particulates that might interfere with the measurement.

The dextran blue was diluted in three steps. Therefore, three mass balances could be made, based on the concentrations of dextran blue and the total volume (liquid and granules) for each dilution step:

$$V_{DextranBlue} \cdot C_{DextranBlue} = \left(V_{Total,1} - V_{granules}\right) \cdot C_1 \quad (2.4)$$

$$\left(V_{Total,1} - V_{granules}\right) \cdot C_1 = \left(V_{Total,2} - V_{granules}\right) \cdot C_2 \quad (2.5)$$

$$\left(V_{Total,2} - V_{granules}\right) \cdot C_2 = \left(V_{Total,3} - V_{granules}\right) \cdot C_3 \quad (2.6)$$

Here, $V_{DextranBlue}$ = volume of dextran blue stock added, $C_{DextranBlue}$ = concentration of dextran blue in the stock solution, $V_{Total,i}$ = total volume (liquid and granules) at step *i* (*i* = 1, 2, 3), and C_i = concentration of dextran blue in sample *i*. The total volume at each step was deduced from the initial volume (200 mL in a volumetric flask) and the volumes of liquid added and removed (measured by weight and converted to volume with the liquid density). The only unknown in each mass balance was the granule volume and thus, three estimates of the granule volume were obtained.

The final granule volume was taken as the average of the three measurements. The wet weight of the granules was determined based on the weight of the granules and water inside the 200 mL volumetric flask (step 1 of the protocol) and the weight of the water inside the flask:

$$W_{granules} = W_{granules+water} - W_{water} \quad (2.7)$$

The weight of the water was not measured directly, but it can be deduced from the total volume of the volumetric flask (200 mL), the volume of the granules in the flask ($V_{granules}$, determined from the dextran blue dilution), and the density of tap water (ρ_{H2O}):

$$W_{granules} = W_{granules+water} - \rho_{H2O} \cdot \left(V_{flask} - V_{granules}\right) \quad (2.8)$$

The weight of the granules and the volume of the granules can subsequently be combined to yield the buoyant density:

$$\rho_{buoyant} = \frac{W_{granules}}{V_{granules}} \quad (2.9)$$

The biomass densities can be determined straight-forward from the total or volatile suspended solids and the granule volume:

$$\rho_{biomass,TSS} = \frac{W_{TSS}}{V_{granules}} \quad (2.10)$$

$$\rho_{biomass,VSS} = \frac{W_{VSS}}{V_{granules}} \quad (2.11)$$

The modified dextran blue method was carried out in triplicate.

Settling velocity method

The terminal settling velocity of individual granules was measured by placing a single granule in the middle of a measuring cylinder with an internal diameter of 7.94 cm and a height of 42.1 cm. A camera (GoPro Hero Session 4) was used to record the settling and extract settling velocities. The settling on the boundaries of the camera image was ignored to reduce distortion effects and to ensure the granule had reached its terminal settling velocity. The experiment was carried out at room temperature with 150 granules from the 1600-2500 µm fraction. Approximately 500 granules from this size fraction were also analysed with a digital microscope (Keyence VHX-700F) and ImageJ software (Schneider et al., 2012). The circular equivalent diameter derived from the microscope images was used to obtain a granule size distribution and an average granule diameter. From the measurement of terminal settling velocity and diameter of the granules, the particle Reynolds number (*Re*) can be calculated:

$$Re = \frac{\rho_l v_t d_{avg}}{\mu} \quad (2.12)$$

Here, μ = dynamic viscosity of the fluid ($1.002 \cdot 10^{-3}$ kg m^{-1} s^{-1}), v_t = terminal settling velocity of the granule (m s^{-1}), ρ_l = density of the liquid (998.23 kg m^{-3}), and d_{avg} = average granule diameter (m). Since the particle Reynolds numbers were in the transitional regime (Reynolds numbers of 0.01-1000), the correlation of Khan and Richardson (1987) was used to calculate the drag coefficient (C_d):

$$C_d = \left(\frac{2.25}{Re^{0.31}} + 0.36\, Re^{0.06}\right)^{3.45} \quad (2.13)$$

A force balance on a settling granule leads to the following expression of the terminal settling velocity:

$$v_t = \sqrt{\frac{4g}{3C_d}\left(\frac{\rho_g - \rho_l}{\rho_l}\right) d_{avg}} \quad (2.14)$$

Here, g = gravitational acceleration (m s^{-2}) and ρ_g = granule density (kg m^{-3}). Since the granule density is the only remaining unknown, this parameter can be estimated directly.

2.2.3 | Effect of salinity

Granule samples were acclimatized for 24 hours in NaCl solutions and Instant Ocean® artificial seawater (Atkinson & Bingman, 1997) with concentrations of 9 , 18, and 36 g/L. For each experiment, approximately 22 g of granules were placed in 500 mL of saline solutions. The liquid was refreshed three times during acclimatization, to account for the drop in salinity through diffusion of the salt ions into the granules. After acclimatization, the granule density was measured with the pycnometer method. All liquid volumes used in the density measurement were of the same composition as the liquid used for acclimatization. The liquid density of the saline solutions was measured with the pycnometer as well.

2.3 | RESULTS

2.3.1 | Comparison of methods

The granule buoyant density was measured with four different methods: the pycnometer method, the Percoll density gradient method, the modified dextran blue method, and the settling velocity method. The measured granule densities are shown in

Table 2.1. The buoyant granule density values obtained with three out of the four methods were quite comparable, with minimum and maximum values of 1025.7 and 1028.1 kg/m^3. This density difference translates to a settling velocity relative difference of 3.7%, according to Equation 14 and assuming a fixed drag coefficient. The buoyant granule density obtained with the settling velocity method (1012.4 kg/m^3) deviated clearly from the densities found with the three other methods. The good congruence of the other methods suggests that it is the settling velocity method that is inaccurate. However, since there is no standard method, it cannot be excluded that actually the other three methods are the ones that have to be considered inaccurate. Furthermore, it should be noted that the Percoll density gradient method was carried out with tap water, while 0.15 M NaCl is commonly used for density gradients (Etterer & Wilderer, 2001). When the method was carried out with 0.15 M NaCl, the measured buoyant density (1034.9 kg/m^3) deviated clearly compared to the other methods. The higher salinity in the Percoll density gradient method leads to an overestimation of the buoyant density in freshwater (see also Figure 2.2). The Percoll method will thus overestimate the settling velocities of granules in a wastewater treatment plant.

Table 2.1. Buoyant and biomass granule density as measured by the different methods

Method	Units	Value	Standard deviation
Buoyant density			
Pycnometer	kg/m^3	1027.4	0.7
Percoll (n = 119)	kg/m^3	1027.8	9.2
Modified dextran blue	kg/m^3	1025.7	1.3
Settling velocity (n = 150)	kg/m^3	1026.6	-
Biomass density			
Pycnometer	gTSS/L	90.5	2.7
	gVSS/L	71.5	2.0
Modified dextran blue	gTSS/L	90.2	2.5
	gVSS/L	71.1	2.6

The obtained standard deviation of the methods was relatively small for the pycnometer method (0.7 kg/m^3) and the modified dextran blue method (1.3 kg/m^3). The standard deviation between all individual granules for the Percoll density gradient method was much larger (9.5 kg/m^3), which was expected. This higher standard deviation does not only reflect the precision of the method, but also the degree of heterogeneity within the granule sample. The standard deviation of the Percoll density gradient method between the six tubes was markedly lower (0.9 kg/m^3). The standard deviation of the settling

velocity method reflects the heterogeneity within the sample as well and was therefore relatively high (7.2 kg/m^3).

The granule biomass density was only quantified by two methods: the pycnometer method and the modified dextran blue method. The difference between both methods was only minor, both for TSS-density and VSS-density (Table 2.1). However, the pycnometer method was influenced by the way the granules were dried. The measured biomass density was 55.8 g VSS/L when the granules were dried by pouring off excess water, 71.5 g VSS/L when the granules were dried from underneath a sieve, and 84.2 g VSS/L when the granules were dried directly on a paper towel (see Figure 2.1). The relative difference between the lowest and the highest value is 40.5%, indicating that the granule drying step has a major impact on the pycnometer method. Most likely, excess water remained between the granules when water was only poured off, leading to an overestimation of the granule volume and an underestimation of the biomass density. For the granule dried directly on a paper towel, the opposite is most likely true. Drying the granules with a paper towel from underneath a sieve resulted in similar values as the modified dextran blue method, suggesting it adequately removed excess water.

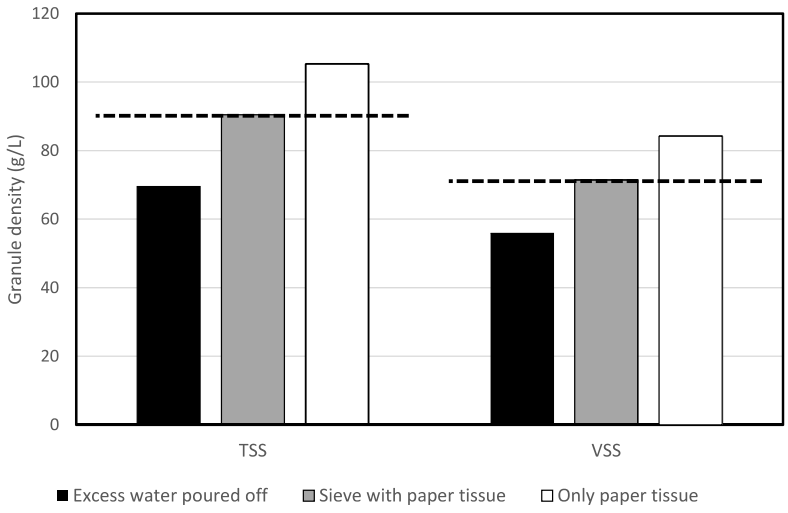

Figure 2.1. Granule biomass density determined with the pycnometer method with different drying approaches. The dashed lines are added as reference, and represent the granule biomass density determined with the modified dextran blue method.

The granule biomass density was only quantified by two methods: the pycnometer method and the modified dextran blue method. The difference between both methods was only minor, both for TSS-density and VSS-density (Table 2.1). However, the pycnometer method was influenced by the way the granules were dried. The measured biomass density was 55.8 g VSS/L when the granules were dried by pouring off excess water, 71.5 g VSS/L when the granules were dried from underneath a sieve, and 84.2 g VSS/L when the granules were dried directly on a paper towel (see Figure 2.1). The relative difference between the lowest and the highest value is 40.5%, indicating that the granule drying step has a major impact on the pycnometer method. Most likely, excess water remained between the granules when water was only poured off, leading to an overestimation of the granule volume and an underestimation of the biomass density. For the granule dried directly on a paper towel, the opposite is most likely true. Drying the granules with a paper towel from underneath a sieve resulted in similar values as the modified dextran blue method, suggesting it adequately removed excess water.

2.3.2 | Effect of salinity

The effect of salinity on the granule density was evaluated with the pycnometer method. The liquid density of NaCl and artificial seawater solutions was measured with the pycnometer as well. The liquid density increased linearly with increasing salinity, as is expected (see Figure 2.2). The artificial seawater had a slightly lower density than the NaCl solutions at the same salt content, but the trend was similar. The granule buoyant density increased with increasing salinity as well. The granule buoyant density followed a slope that was comparable to that of the liquid density, at least over the range of 3-36 g/L. For NaCl, the slopes were 0.77 and 0.69 $(kg/m^3)/(g/L)$ for granule buoyant density and liquid density, respectively. For the artificial seawater, the slopes were 0.76 and 0.63 $(kg/m^3)/(g/L)$ for granule buoyant density and liquid density, respectively. The density difference between granules and liquid is therefore relatively independent of salinity. This could indicate that the settling behaviour of the granules will not be affected by salinity. Based on the relative density difference, the settling velocity at higher salinity is expected to be 10-20% lower than in freshwater (see equation 12).

The biomass density was only partly affected by the increase in salinity (Figure 2.3). The TSS-density showed a clear linear increase with salinity, but the VSS-density remained constant. The dashed line in Figure 2.3 indicates the TSS-density if 80% of the granule volume would contain liquid with the same salinity as outside the granules. The experimental results fall along this dashed line, suggesting that the salts have diffused

in the granule pore volume until equilibrium. The remaining 20% of the granule volume is most likely occupied by bacterial cells, EPS, and inorganic material. The constant VSS-density and the proportional increase of the TSS-density suggest that the granule volume does not change during short-term (24 h) saline exposure. There was no clear difference between the effect of sodium chloride salt and artificial seawater. Since sodium chloride is the major constituent of the artificial seawater (Atkinson & Bingman, 1997), this result is not entirely surprising.

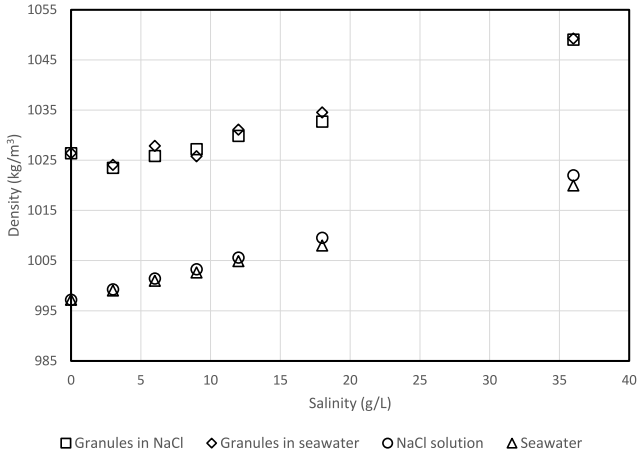

Figure 2.2. Granule buoyant density as function of NaCl concentration. The buoyant density increases with salinity with a similar slope as the liquid density.

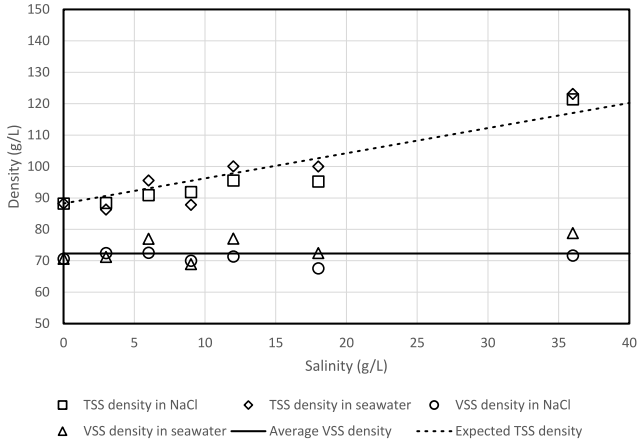

Figure 2.3. Granule biomass density as gTSS/L and gVSS/L as function of the NaCl concentration. The TSS- density increases with salinity, while the VSS-density stays in the same range, indicating that the granule volume is not affected by the salinity. The solid line indicates the average VSS-density of all measurements shown in this graph. The dashed line indicates the expected TSS-density if 80% of the granule volume is occupied by saline liquid.

2.4 | DISCUSSION

2.4.1 | Comparison of methods

A comparison was made between four different methods that were previously used in literature to measure granule buoyant density and granule biomass density: the pycnometer method, the Percoll density gradient method, the modified dextran blue method, and the settling velocity method. Three out of the four methods yielded comparable granule densities. It is not completely surprising that the settling velocity method deviated from the other methods, as it is the most indirect approach to measure granule density. The settling velocity of a granule is not only determined by its density, but also by its drag coefficient (see equation 14). In this study, we used a general correlation between Reynolds number and drag coefficient (see equation 13). This correlation was developed for smooth, solid spheres, not for spheroidal granules with a rough surface. The lower density found with the settling velocity method suggests that the drag coefficient of the granules was higher than that of spheres of equivalent size. Typically, a unique correlation between the Reynolds number and drag coefficient is determined for different granule samples (Nicolella et al., 1999; van Dijk et al., 2020) This highlights that the granule density cannot be determined accurately with simple approaches, such as Stokes' law (Trego et al., 2018) or the Khan & Richardson equation (Khan & Richardson, 1987).

Even though the three other methods were comparable in terms of results, there are still advantages and drawbacks of each method. For example, the Percoll density gradient method provides the granule density of the individual granules, while the pycnometer and extended dextran blue method only yield an average density. The Percoll method is therefore especially useful for determining the density distribution within a granular sludge sample. However, it is important to consider the salinity in the Percoll method. The method is normally carried out with a NaCl concentration of 0.15 M (Pertoft et al., 1978). The granule density found at this salinity is not representative of the density in freshwater. However, our results show that the Percoll method can provide reliable results in freshwater as well.

The pycnometer method is generally used to determine the granule buoyant density (Alphenaar et al., 1993; Bueno et al., 2020; Herrling et al., 2017; X. Li et al., 2017; Quoc et al., 2021; Tassew et al., 2019; S.P. Wei et al., 2021; Xu et al., 2021; Xu et al., 2019) and the dextran blue method is generally used to measure the granule biomass density (Arrojo et al., 2006; Beun et al., 2002; Cassidy & Belia, 2005; Corsino et al., 2016; de Kreuk et al., 2005; Di Iaconi et al., 2004; Isanta et al., 2012; Lemaire et al., 2008; López-

Palau et al., 2011; Mu et al., 2006; Nor-Anuar et al., 2012; Tijhuis et al., 1994b; Yuan et al., 2017). However, as shown here, both methods can determine the buoyant density as well as the biomass density. The two methods were mostly comparable in terms of accuracy and bias (see Table 2.1). Still, the pycnometer method is more precise regarding the buoyant density. The standard deviation of the pycnometer method was 0.7 kg/m^3, while that of the modified dextran blue method was 1.3 kg/m^3 (see Table 2.1). This precision is a small advantage of the pycnometer method for the granule buoyant density measurement. A disadvantage of the pycnometer method is the potential bias from the removal of excess water. If the granule is not dried properly and too much or too little water is removed, a substantial bias is introduced (see Figure 2.1). Our results show that good results are possible with the right drying procedure, as long as the biomass is not flocculent. However, our results are only valid for one granule type. We did not consider the impact of granule properties (e.g., presence of filamentous outgrowth, hydrophobicity) on the drying step of the pycnometer method. Operator error could play a significant role as well. Therefore, we recommend comparing the pycnometer method and the modified dextran blue method in future studies, to further clarify the effect of the drying step. The Percoll density gradient method can be used to study the variation of granule density within a granule sample.

There are many literature reports of density measurements of granules grown at lab-scale and full-scale conditions. However, most studies focused on specific substrates or operating conditions and the resulting densities are not directly comparable (Bueno et al., 2020; Cassidy & Belia, 2005; Lemaire et al., 2008; X. Li et al., 2017; López-Palau et al., 2011). An extensive review of the impact of these conditions on the granule density is beyond the scope of this study. Still, the densities for granules from a full-scale Nereda plant found in this study (1020-1030 kg/m^3 and 50-70 gVSS/L) are comparable to the densities reported for granules grown on acetate as sole carbon source (de Kreuk et al., 2005; Winkler et al., 2012). The buoyant granule densities reported by Etterer and Wilderer (2001) are higher (1037-1052 kg/m^3), but they measured the density with the Percoll density gradient method in 0.15 M NaCl. The higher salinity in these experiments could explain the higher reported granule densities (see also Section 2.4.2).

2.4.2 | Effect of salinity

Municipal wastewater treatment plants in coastal areas and industrial wastewater treatment plants often have to deal with fluctuating salinity of the influent (Lefebvre & Moletta, 2006). As the salinity influences the liquid density, the fluctuating salinity could have an effect on settling of the granular sludge. Our results show that the granule

density increases with salinity as well. Both the absolute and relative density difference between the granule density and the liquid density change only marginally with increasing salt concentration. Winkler et al. (2012) reported that the settling velocity of lab-grown freshwater granules decreased by only 10% after exposure to 40 g/L NaCl for 24 h. This minor difference in settling velocity matches with the change in relative density difference that we observed.

As a result, seawater only has a minor effect on granule settling and fluidisation. This aspect simplifies the design of WWTPs that receive wastewater with high or fluctuating salinity. It should be noted that we did not consider the short-term response of granules to a saline shock in this study. Diffusion of salts into the granule requires time, around 15-20 min (Winkler et al., 2012). At the start of a saline shock, the granule density is still around 1026 kg/m^3, while the liquid density is already that of the saline liquid (1020 kg/m^3 for 36 g/L seawater). The granules will still settle, but with a much lower velocity. The influent salinity will most likely not fluctuate from 0 to 36 g/L in 15-20 min, but the batch-wise operation of AGS could mean that the influent of one batch contains 36 g/L salt while the effluent of the previous cycle contains almost no salt. In the worst-case, this could lead to fluidization of the granules during feeding and effluent withdrawal. Therefore, the short-term effects of fluctuating salinity require further study.

Saline exposure also has the potential to change the granule volume. Several authors have observed a volume decrease after saline exposure, for hydrogels (Golmohamadi & Wilkinson, 2013; Saitoh et al., 2000), biofilms (N. Liu et al., 2020; Yan et al., 2017), and aerobic granules (Seviour et al., 2009). A decrease of granule volume was suggested as explanation for a decrease in settling velocity at higher salinity (Winkler et al., 2012) and for an increase in granule strength at higher salinity (de Graaff et al., 2018). However, clear evidence of granule shrinking at higher salinities is lacking. Seviour et al. (2009) studied granule swelling and deswelling based on the equilibrium water content (EWC). The EWC is based on the dry weight (W_{TSS}) and wet weight ($W_{granules}$) of the granules:

$$EWC = 1 - \frac{W_{TSS}}{W_{granules}} \quad (2.15)$$

Seviour et al. (2009) reported a decrease in EWC with increasing salinity. This decrease can be caused by a decrease in wet weight, which would indeed indicate shrinking of the granules. However, the decrease can also be caused by an increase in the dry weight (measured as TSS), which would indicate diffusion of salt into the granules. Our findings regarding the granule biomass density show that the latter explanation is correct. A change in granule volume would have affected both the TSS-density and the VSS-

density, which is clearly not the case (see Figure 2.3). Diffusion of salts into the granule will not affect the VSS-density, but only the TSS-density and the granule buoyant density. This is exactly what we observed, showing that the granule volume is unaffected by the salinity. It is therefore likely that the granule volume was also unaffected by salinity in the study of Seviour et al. (2009).

The question remains why the granules did not shrink at higher salinities. One possible explanation relates to the EPS composition of the granules. It is well known that ionic hydrogels (e.g., alginate gels) swell or shrink as a result of difference in mobile ion concentration within the gel and outside the gel (Flory, 1953; Saitoh et al., 2000). The difference in concentration of mobile ions arises from the Donnan equilibrium and depends on the density of negatively-charged functional groups in the gel (Golmohamadi & Wilkinson, 2013; Pfaff et al., 2021). However, non-ionic hydrogels (e.g., collagen gels) do not swell or shrink as a function of salinity (Lai et al., 2016; Voutouri et al., 2016). It is likely that the aerobic granules contain such non-ionic structural components (Felz et al., 2020a), besides the more widely reported ionic components (Felz et al., 2020b; Lin et al., 2009). For example, amyloid proteins have been found in AGS (Lin et al., 2018) and are known to form a fibrilar network (Erskine et al., 2018; Romero et al., 2010). The fibrilar network can be strong enough to limit or prevent shrinking of the granules (Lai et al., 2016; Voutouri et al., 2016). This explanation is speculative and needs further investigation. An in-depth analysis of the Donnan equilibrium, EPS composition, and granule rheology can reveal how the granule structure is affected by environmental conditions like salinity (see also Pfaff et al. (2021)).

2.5 | CONCLUSION

In this study, a comparison was made between four methods to measure granule density. Three out of the four methods yielded comparable results, both for the buoyant and biomass granule density. The settling velocity method clearly underestimated the granule density, due to the complex relation between granule properties and settling velocity. The pycnometer was the most precise method, but it was also susceptible to bias; removal of excess water from a granule sample was a critical step in the pycnometer method. Higher salinities led to increased granule densities, but the granule volume did not change. The increased granule densities were mainly caused by the diffusion of salt ions into the granules and the granule volume was not affected by salinity.

Granules inside an NMR tube

3

Characterizing the structure of aerobic granular sludge using ultra-high field magnetic resonance

Published with minor modifications as: Kirkland, C.M., Krug, J.R., Vergeldt, F. J., van den Berg, L., Velders, A.H., Seymour, J.D., Codd, S.L., Van As, H. & de Kreuk, M.K. (2020). Characterizing the structure of aerobic granular sludge using ultra-high field magnetic resonance. *Water Science and Technology*, 82(4), 627-639.

ABSTRACT

Background

Despite aerobic granular sludge wastewater treatment plants operating around the world, our understanding of internal granule structure and its relation to treatment efficiency remains limited. This can be attributed in part to the drawbacks of time-consuming, labour-intensive, and invasive microscopy protocols which effectively restrict samples sizes and may introduce artefacts. Time-domain nuclear magnetic resonance (NMR) allows non-invasive measurements which describe internal structural features of opaque, complex materials like biofilms.

Methods

NMR was used to image aerobic granules collected from five full-scale wastewater treatment plants in the Netherlands and United States, as well as laboratory granules and control beads.

Results

T_1 and T_2 relaxation-weighted images reveal heterogeneous structures that include high- and low-density biofilm regions, water-like voids, and solid-like inclusions. Channels larger than approximately 50 µm and connected to the bulk fluid were not visible. Both cluster and ring-like structures were observed with each granule source having a characteristic structural type. These structures, and their NMR relaxation behaviour, were stable over several months of storage.

Conclusions

These observations reveal the complex structures within aerobic granules from a range of sources and highlight the need for non-invasive characterization methods like NMR to be applied in the ongoing effort to correlate structure and function.

3.1 | INTRODUCTION

Compared to conventional activated sludge systems, aerobic granular sludge (AGS) offers numerous benefits for wastewater treatment including compact design, lower energy costs, and excellent biomass retention (de Bruin et al., 2004). In the last two decades, research into the formation, structure, and metabolism of granular sludge has flourished (Beun et al., 2002; de Kreuk & van Loosdrecht, 2006; Tay et al., 2001; Wilén et al., 2018) and numerical models have been developed to simulate substrate removal, the distribution of microbial populations, and biochemical processes within the biofilm granule (Kagawa et al., 2015; Xavier et al., 2007). Today, full-scale reactors are in operation around the world (Pronk et al., 2017).

Numerous studies have reported heterogeneous internal structures in aerobic granules from various sources (Chen et al., 2007; Gonzalez-Gil & Holliger, 2014; Lemaire et al., 2008; L. Liu et al., 2010; Mcswain et al., 2005; Weissbrodt et al., 2013). Typical methods of analysis include use of fixatives, fluorescent in-situ hybridization (FISH) probes, or staining with fluorophores followed by cryo-sectioning and imaging with confocal microscopy to identify the spatial arrangement of cells and biopolymers like proteins and polysaccharides within the granules. These types of studies have revealed microbial communities occupying niche environments within the granule architecture as well as the presence of voids and channels in the granule interior. This study, for the first time, applied ultra-high field nuclear magnetic resonance (NMR) to explore the structural heterogeneity of aerobic granular sludge from full-scale municipal wastewater treatment reactors, as well as from lab scale reactors.

Time-domain NMR can provide spatially-resolved data on the structure and water diffusivity present in intact granules under various hydrodynamic conditions (Codd et al., 2006; Van As & Lens, 2001). Early NMR experiments on anaerobic granules provided evidence of a cluster structure (Gonzalez-Gil et al., 2001), while NMR imaging of methanogenic granules showed that the matrix of extracellular polymeric substances (EPS) is organized in concentric layers and the granules appear to have hollow centres (Lens et al., 2003). While the achievable spatial resolution is less than that typically obtained with optical methods, magnetic resonance is non-destructive and non-invasive. It can be used to image opaque and heterogeneous samples by exploiting the contrasts between the NMR signal intensity and decay rates associated with various granule components. In this research paper, the additional use of state-of-the-art ultra-high magnetic field strength (22.3 Tesla (T) or 950 MHz where MHz = Tγ and γ is 2.675 x 10^8 rad/(s*T) for protons) allows for enhanced contrast between various biochemical macromolecules and fast, high-resolution imaging. Moreover, the sensitivity of NMR to

molecular motion provides an opportunity to observe the inherent transport characteristics of a system *in-situ* in relation to structure (Van As & Lens, 2001). These capabilities represent significant advantages compared to conventional methods like microscopy and micro-electrode studies which are necessarily invasive or destructive. Thus, because NMR is sensitive to a different array of physical and chemical parameters than traditional microscopy methods and can be used to screen larger sample sizes non-invasively, NMR imaging has the potential to highlight structural features that might otherwise not be visible, providing complementary data to inspire new research questions.

The primary research questions addressed here are related to the internal granule structure. To what extent does the internal structure of aerobic granules used in practice for wastewater treatment conform to a layered (Lens et al., 2003) or cluster (Gonzalez-Gil et al., 2001) conceptual model? How consistent are the observed structures between samples from the same treatment plant, from different treatment plants, over time as the granules age, and between laboratory granules and those treating municipal wastewater? NMR imaging experiments and T_1-T_2 relaxation correlation experiments (see Materials & Methods section) give insight to these structural questions.

3.2 | MATERIALS & METHODS

3.2.1 | Sample collection and preparation

Samples of aerobic granular sludge were collected during the aeration phase of the treatment cycle from the following sequencing batch reactors (SBR): full-scale Garmerwolde (the Netherlands), full-scale Vroomshoop (the Netherlands), prototype Utrecht (PNU) (the Netherlands), and demonstration-scale Rockford (IL, United States). In addition, granules were sampled from the full-scale Utrecht wastewater treatment plant during the start-up phase, after seeding the reactor with Garmerwolde granules. Table 3.1 provides data regarding average influent characteristics for the treatment plants sampled. These granules will be collectively called 'full-scale' granules hereafter, unless otherwise noted.

Two types of granules were compared with the full-scale granules. Control beads were prepared by extracting structural EPS components from aerobic granules with acid and re-gelling them with $CaCl_2$ solution (Felz et al., 2016). The control EPS beads originate from AGS, but do not contain cells or the full suite of extracellular polymers present in full-scale granules. Second, saline laboratory granules, grown in synthetic wastewater

with an added 5 g/L NaCl were collected from a 3 L sequencing batch reactor at TU Delft (de Graaff et al., 2018). The saline granules contain microbes that would be expected to exist within the AGS samples from municipal wastewater reactors but were not exposed to complex substrates.

Table 3.1. Average influent characteristics for sources of full-scale granules. PE: Population Equivalents, COD: Chemical Oxygen Demand, TSS: Total Suspended Solids, TN: Total Nitrogen, TP: Total Phosphorus.

Source	COD (mg/L)	BOD_5 (mg/L)	TSS (mg/L)	TN (mg/L)	TP (mg/L)	Reference
Garmerwolde, NL	506	224	236	49.4	6.7	(Pronk et al., 2015b)
Vroomshoop, NL	720	263	317	-	9	(Pronk et al., 2017)
Utrecht, NL	660	247	300	58	8.2	-
Utrecht (PNU), NL	732	289	385	74	13.4	-
Rockford, USA	142		111	19.4	1.8	-

All samples, which ranged in volume from several hundred millilitres to several litres, were stored in airtight plastic containers in the refrigerator at 4°C without substrate addition until the NMR measurements were performed. For the NMR imaging experiments, several granules (~5-10) were added to water in a 5 mm NMR sample tube. For the multi-dimensional correlation measurements, numerous granules (>>10) were added to the 5 mm NMR sample tube without excess water to maximize the signal obtained from the granules relative to bulk water signal. Granules selected for NMR measurements were typically 2 – 4 mm in diameter to provide sufficient image pixels within the granule relative to the imaging field of view.

3.2.2 | NMR measurements

^{1}H NMR is sensitive to hydrogen protons. In most biological systems, the dominant source of the NMR signal is water, though protons found in organic matter and extracellular polymers also contribute to the total signal. NMR image contrast depends on signal intensity and the signal relaxation rates of sample constituents (Van As & Lens, 2001). Signal intensity is a function of the position r dependent proton density, ρ(r), within a sample and applied magnetic field strength. The T_1 (or longitudinal) relaxation time and the T_2 (or transverse) relaxation time provide information on the physico-chemical environments in which different water populations exist (Callaghan, 1993). T_1 relaxation is related to the timescale for the sample's net magnetization to return to thermal equilibrium following an excitation pulse. T_2 relaxation is related to molecular interactions that occur in the local magnetic field during the measurement. T_1 and T_2

relaxation occur on the order of seconds in bulk liquids and tens to hundreds of milliseconds in biofilms. Chemical exchange of protons between water and hydroxyl groups on polymer chains (Hills, 1992) as well as the presence of rotationally restricted water in cells and the EPS matrix enhance T_2 relaxation in biofilms relative to bulk water. Controlling the timing of the radiofrequency (rf) pulses which make up magnetic resonance measurements can accentuate contrast between the various water populations without addition of chemical tracers. Further discussion of NMR theory is provided in Callaghan (2011) and (Gjersing et al., 2005).

T_1 relaxation-weighted images show signal intensity at a single time, while $T_{2,\,eff}$ maps, which are derived from a series of T_2 relaxation-weighted images, show rates of signal relaxation over a period of time. T_1 relaxation-weighted images will look different for the same granule depending on when the image was acquired during the measurement and are considered qualitative images. $T_{2,eff}$ maps capture the entire signal decay quantitatively and are therefore more representative of the structure than any single T_1 relaxation-weighted image. T_1 relaxation- and T_2 relaxation-weighted ($T_{2,eff}$) images were collected on a NMR spectrometer operating at 22.3 T (950 MHz) using an Avance III HD console, with a Micro5 imaging probe, maximum gradients 3 T/m, and a 5 mm birdcage coil (Bruker Biospin, Ettlingen, Germany) at the uNMR-NL national facility (Utrecht, the Netherlands) using parameters found in Table 3.2 for AGS samples from PNU and Garmerwolde, as well as the EPS and saline control granules. The matrix size was 128 x 128 and receiver bandwidth was 50 kHz. Note that parameters used for NMR images of Utrecht start-up granules, acquired at a later time on the 22.3 T system and shown in Figure 3.3, are different and are given in the caption to Figure 3.3. The NMR images of PNU granules were collected on both fresh granules (several days after sampling) and on aged samples (approximately 2 months after sampling). Granules from the Vroomshoop and Rockford treatment plants were not available at the time of image acquisition on the 22.3 T system. Measurement parameters for images of Vroomshoop, Garmerwolde, and Rockford AGS samples made on a Bruker Avance III system with a 5.9 T (250 MHz for protons) superconducting magnet are found in Table 3.2. The matrix size was 128 x 64 and receiver bandwidth was 50 kHz.

Multidimensional NMR experiments combine two pulse sequences such that the induced signal is encoded in multiple independent dimensions to explore how two parameters are related. In the T_1-T_2 relaxation correlation experiment, T_2 relaxation is measured for protons experiencing a given T_1 relaxation rate over a range of T_1 relaxation times. The measurement can be used to separate signal which overlaps in one domain or, as in this case, can provide insight into the mechanism behind enhanced

signal relaxation. T_1-T_2 relaxation correlation experiments were performed on a 5.9 T superconducting magnet networked to a Bruker Avance III spectrometer and using a high rf power probe, a 5 mm rf coil, and a 5 mm sample tube. The correlation measurements were performed using an inversion recovery- CPMG sequence at 20°C with a dwell time of 10 µs, an echo time, t_E, of 100 µs, 30,000 echoes, 32 inversion times between 1 ms - 50 s, and 16 averages.

Table 3.2. NMR measurement parameters for multi-slice multi-echo (MSME) images. Samples imaged at 22.3 T included AGS samples from PNU and Garmerwolde, as well as control EPS beads and saline granules. Samples imaged at 5.9 T included AGS samples from Vroomshoop and Rockford treatment plants, as well as control EPS beads.

	T_1-weighted	T_2-weighted	$T_{2,eff}$ map	
Field strength (T)	22.3	22.3	22.3	5.9
Repetition time, T_r (ms)	550	5000	5000	5000
Echo time, t_E (ms)	5.3	5.3	5.3	5.6
Number of echoes	16	16	32	8
X-Y resolution (µm)	47 x 47	47 x 47	47 x 47	94 x 94
Z-slice thickness (µm)	100	100	100	500
Number of averages	8	1	4	32
Duration	9 min 23 s	10 min 40 s	42 min	2 h 50 min

3.2.3 | Other microscopy

Aged granules from Garmerwolde were also imaged using transmission electron microscopy (TEM). Granules were fixed in 3% glutaraldehyde for 24 hours, cut into quarters, then returned to the glutaraldehyde solution. The granule quarters were subsequently treated according to (Brumfield et al., 2009). Images were made using a LEO 912AB TEM (Zeiss) operated at 100KV accelerating voltage and a 2,048 X 2,048 Proscan CCD camera.

3.2.4 | Data analysis

$T_{2,eff}$ Maps

Multi-slice multi-echo (MSME) imaging produces 2D T_2 relaxation-weighted images showing the signal echo amplitude per voxel, or volume element, in each sample slice for a given echo time, t_E. An image is collected at times equal to n*t_E, where n is the echo number, such that the stack of images for each slice shows the attenuation of signal in each voxel with time. Fitting the echo attenuation in each voxel as an exponential decay produces a 2D relaxation map of the sample where the pixel intensity corresponds to

the effective relaxation rate, $R_{2,eff}$, or the effective relaxation time, $T_{2,eff}$. Since signal from protons experiencing restricted rotational mobility or chemical exchange will experience enhanced relaxation, $T_{2,eff}$ maps are used to identify regions of varying cell and EPS densities (Edzes et al., 1998; Gjersing et al., 2005; Gonzalez-Gil et al., 2001). $T_{2,eff}$ relaxation times are significantly shorter than T_2 relaxation times measured without spatial resolution due, in part, to the influence of water diffusion across magnetic field gradients applied for imaging. Higher resolution images produce shorter $T_{2,eff}$ relaxation times. In addition, higher magnetic field strength and longer t_E also enhance relaxation (Edzes et al., 1998). Thus, $T_{2,eff}$ values are only comparable between images when the same magnetic field strength and measurement parameters are used across samples. $T_{2,eff}$ map data was analysed using Prospa ((v3.13) Magritek Ltd, Wellington, NZ).

T_1-T_2 Relaxation Correlation Experiments

When data is collected from a sample exhibiting multi-exponential signal decay due to a range of relaxation domains, the data can be analysed by an Inverse Laplace Transform (ILT) in both dimensions. The 2D ILT was implemented in MATLAB (R2018a, MathWorks, Natick, MA, USA) using a non-negative least squares fitting function with a regularization parameter, α, to minimize the error in the solution (Callaghan et al., 2003; Hürlimann et al., 2002)

3.3 | RESULTS AND DISCUSSION

The goal of this study was to identify internal structural features within aerobic granules from full-scale municipal wastewater treatment plants and determine how consistent those features are across granule sources and over time. T_1 and T_2 relaxation-weighted images of granules from wastewater treatment plants reveal heterogeneous internal structures where water molecules and biopolymers experience different degrees of rotational mobility and variable opportunities for chemical exchange as reflected in the T_1 and T_2 relaxation behaviour. The NMR images presented here show an axial 'image slice' through a 5 mm NMR sample tube with water surrounding the intact granule. The NMR parameters, as defined in Table 3.2, are identical in all T_1-weighted images presented in Figure 3.1.

3.3.1 | T_1 (relaxation)-weighted images

EPS beads (Figure 3.1A) and saline laboratory granules (Figure 3.1B) showed significantly different degrees of heterogeneity compared to the aerobic granules treating municipal wastewater (Figure 3.1C and D). The EPS beads were uniform and showed no discernible internal structure. This is attributable, in part, to the extraction method which is selective for specific biopolymers. Saline granules showed a radial distribution of signal intensity with faster relaxation and more apparently dense regions on the outer surface and higher intensity, less dense regions in the centre of the granules.

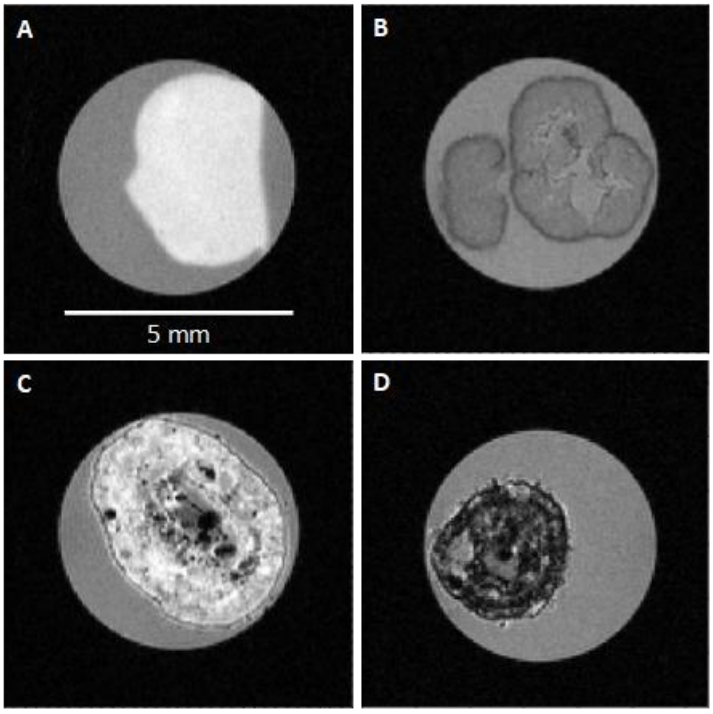

Figure 3.1. T_1-weighted images. Compared to the control EPS bead (A) and saline laboratory granule (B), aerobic granules collected from the PNU reactor (C) and Garmerwolde treatment plant (D) show a heterogeneous internal structure. Lighter regions correspond to regions with diffuse EPS while darker areas suggest denser or highly cross-linked EPS and cell clusters. Black regions indicate a lack of signal due to either a solid inclusion, or signal relaxation on the timescale of the measurement, i.e., faster than 5.3 ms. (950 MHz, 47 µm x 47 µm x 100 µm, t_E = 5.3 ms, T_r = 550 ms, 1st echo)

Images of granules from the prototype Utrecht (PNU) reactor and Garmerwolde treatment plant reflected spatially heterogeneous NMR signal intensity and relaxation behaviour, though the AGS samples from PNU appeared to have a higher relative volume of brighter regions with slower T_2 relaxation than the Garmerwolde granules. It

was significantly more difficult to collect high quality images from the Garmerwolde granules at 22.3 T due to their rapid signal decay at the ultra-high magnetic field, suggesting a denser structure overall in the EPS matrix or greater abundance of relaxation-enhancing components like paramagnetic ions (e.g. Fe(III)) and biopolymers with a high proportion of exchangeable protons. Granules from Vroomshoop and Rockford were not imaged at 22.3 T, though imaging at lower magnetic field strength (5.9 T, see Figure 3.5) suggests that their internal structural properties are more similar to Garmerwolde granules than to PNU granules (Figure 3.2).

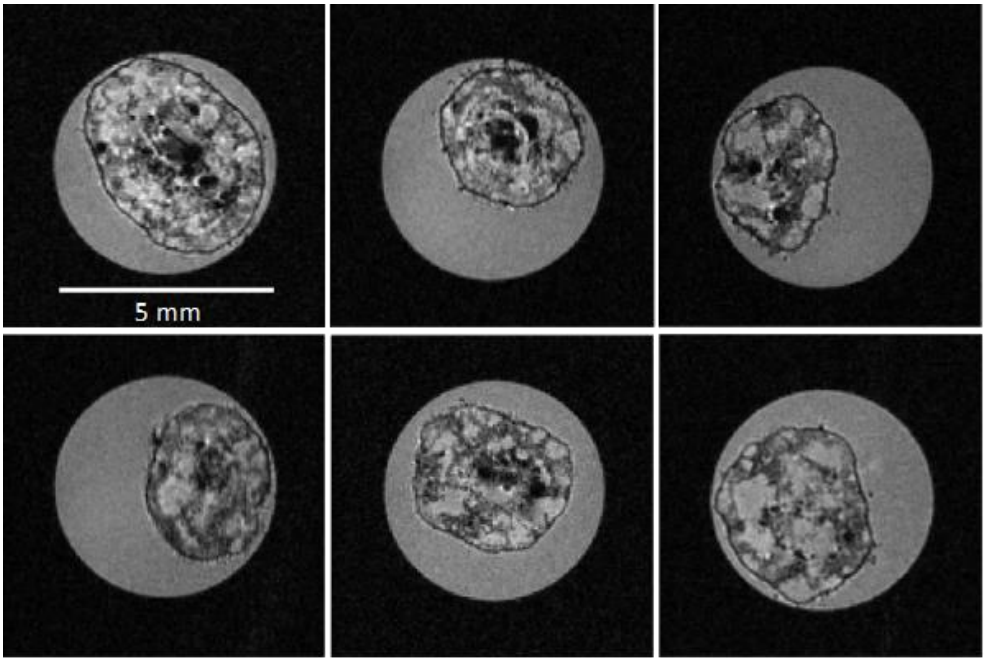

Figure 3.2. Fresh granules from the Utrecht prototype SBR (PNU) with characteristic darker, dense EPS regions and brighter less dense EPS regions. Relatively bright bulk water is visible outside the granule in the 5mm sample tube. (950 MHz, 47 µm x 47 µm x 100 µm, t_E = 15.9 ms, T_r = 550 ms, 3rd echo)

Figure 3.2 shows an assortment of fresh granules from the PNU reactor with characteristic dark, dense regions and brighter, less dense regions. Like Figure 3.1, these images are T_1-weighted with a short repetition time of 550 ms to enhance signal from the gel-like regions of the granule with shorter T_1 times. They are also T_2-weighted since these images were collected with a t_E of 15.9 ms (third echo image) rather than the 5.3 ms (first echo image) shown in Figure 3.1. The granule pictured in the upper left corner is the same PNU granule shown in Figure 3.1C. The combination of T_1- and T_2-weighting

provides excellent contrast between regions with differing relaxation behaviour. While these images show some variation between the individual granules with respect to size, shape, and spatial arrangement of more and less dense biopolymer and cell mass regions, the general form of internal structures (i.e., clusters) in the granules show similarity indicating consistency in NMR-visible properties among granules from the same reactor. Consistency in structural forms was also observed in granules imaged at 5.9 T. These structural similarities among granules from the same reactor (Figure 3.2), in conjunction with larger variation across different reactors (Figure 3.1), raise questions about the operational conditions under which these structures form and the range of function they support.

Research on NMR relaxation in the presence of proteins and polysaccharides shows that the bound water mechanism for T_2 relaxation enhancement is small compared to the influence of chemical exchange of protons between water molecules and functional groups in biopolymer solutions (Hills, 1992). Macromolecules like proteins and polysaccharides provide more abundant exchangeable protons than cell membranes, making T_2 relaxation more sensitive to EPS density than to cell concentration (Beuling et al., 1998). Thus, lighter regions are interpreted as lower-density EPS regions while darker areas suggest more concentrated or more tightly cross-linked EPS, with the caveat that EPS components are complex and various constituents may provide more or fewer exchangeable proton sites. The EPS comprising the control bead has not been analysed to characterize the number of exchangeable protons but comparison of structures published for the extracted EPS (Lin et al., 2010) and Granulan (Seviour et al., 2012), another gel-forming component of structural EPS, suggests that there may be fewer exchangeable protons on the extracted EPS in the control bead than on other biopolymers known to exist in AGS. Moreover, since EPS is produced by active microbes, it can be surmised that the darker regions also indicate cell clusters. Lemaire et al. (2008) reported evidence suggesting that different bacterial populations produce different types of EPS and are associated with a range of cell densities. Black regions in the images indicate a lack of signal due to solid-like inclusions, gas bubbles, or signal relaxation, $T_{2,\mathrm{eff}}$, on the timescale of the measurement (i.e. faster than 5.3 ms).

Images of granules from the new full-scale reactor at the Utrecht wastewater treatment facility sampled during the reactor start-up phase show what appears to be a core with fast T_2 relaxation typical of Garmerwolde structure overgrown by biomass (i.e., cells and EPS matrix) with relaxation characteristics and internal structures typical of PNU granules (Figure 3.3). Harvested Garmerwolde granules were used as seed sludge to inoculate the system at start-up while the influent wastewater comes from the same

municipal source as the PNU reactor. Verawaty et al. (2012) observed that flocs labelled with fluorescent microbeads aggregated around crushed seed granules labelled with contrasting fluorescent microbeads in both batch and SBR systems. After 80 days of SBR operation, Verawaty's experimental granules reflected a distribution where granule-labelled beads were located near the core and floc-labelled beads were located near the surface of the aggregates. Figure 3.3 appears to support the finding that seed granules can act as a template for new growth and suggests that the seed granules may retain their structural form while new biomass develops under the influence of current operating conditions. The NMR images of these granules therefore confirm that influent wastewater characteristics and reactor operations govern the formation of the internal structures observed within AGS. However, the controlling parameter(s) cannot be identified with these NMR images.

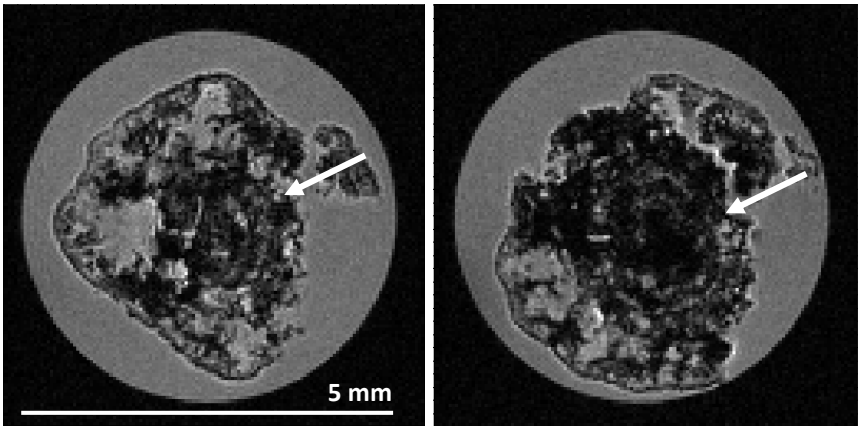

Figure 3.3. T_1-weighted MSME images of two granules from the start-up phase of the full-scale Utrecht wastewater treatment plant. The faster relaxation in the center is characteristic of the seed granules from Garmerwolde wastewater treatment plant, while the outer shell (~700 µm) resembles the internal structure of a prototype Utrecht (PNU) granule. The white arrows indicate the apparent boundary between the old and the new growth. Bulk water visible outside the granule in the 5 mm sample tube provides a reference for the NMR parameter signal intensity weighting of free water. (950 MHz, 35 µm x 35 µm x 100 µm, t_E = 3.19 ms, T_r = 550 ms, 2nd echo)

3.3.2 | $T_{2,eff}$ maps

$T_{2,eff}$ maps of a control EPS bead and two granules from the PNU reactor are shown in Figure 3.4. One of the PNU granules was from a fresh, 4-day old sample (Figure 3.4B) while the other was 2 months old (Figure 3.4C), with both stored at 4°C. Both PNU granules show the same heterogeneous internal structure observed in Figure 3.1 and

Figure 3.2. The $T_{2,eff}$ maps also show that neither the structure nor the $T_{2,eff}$ relaxation behaviour changes significantly over the timescale of approximately 2 months. In both PNU $T_{2,\,eff}$ maps, the bulk water $T_{2,eff}$ relaxation time is 18 ms, which is approximately equal to the maximum internal $T_{2,eff}$ time in the granule voids. In the dense regions of the granules, the minimum $T_{2,eff}$ times are approximately 6 ms with the apparent transition between voids and dense EPS occurring around an $T_{2,eff}$ time of 12 ms.

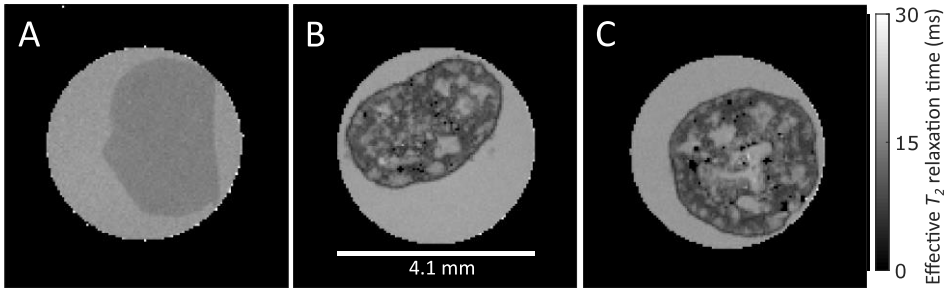

Figure 3.4. $T_{2,eff}$ relaxation maps of a control EPS bead (A) and two granules from the PNU reactor. A 4-day old PNU granule (B) and a 2-month old PNU granule (C) show the same heterogeneous internal structure observed in Figure 3.1 and Figure 3.2 and the same range of $T_{2,eff}$ values. The EPS bead (A) displays a homogeneous $T_{2,eff}$ time of approximately 14.7 ms which is within the range of that found in the voids of both PNU granules (B, C). The maps were produced from MSME images (32 echoes) made on the 22.3 T system in the national ultra-high field NMR lab in Utrecht, NL. Spatial resolution is 47 x 47 x 100 microns.

$T_{2,eff}$ maps of EPS beads collected with the same measurement parameters (Figure 3.4A) show low contrast between the effective relaxation times of bulk water and the EPS bead. The $T_{2,eff}$ maps produced the same bulk water relaxation time as the PNU maps, as expected, and a relatively uniform effective relaxation time within the bead of approximately 14.7 ms. This $T_{2,eff}$ is within the range of relaxation times found in the apparent voids in the PNU granules. The longer $T_{2,eff}$ relaxation times observed in the EPS beads, compared to the dense regions of the full-scale granules, may be due to the absence of other exopolymers that enhance relaxation. Because of the sensitivity to biopolymer structure with respect to exchangeable protons, time-domain NMR may be useful in identifying differences in EPS components that are not apparent in confocal micrographs of granules stained with FITC for proteins, Con-A for α-polysaccharides, or calcofluor white for β-polysaccharides. Within the field of NMR spectroscopy, characterization of protein structure is well established (Banci et al., 2010), while characterization of polysaccharides remains a challenge. Thus, time-domain NMR imaging alone is not sufficient to identify and elucidate details of EPS content and

structure but may be a useful guide to motivate further investigation with other methods, including NMR spectroscopy.

Several researchers (Stoodley et al., 1994; Wilking et al., 2013) have reported the possibility of liquid flow within a biofilm. Channels within the biofilm would permit convection and could potentially increase the penetration of a substrate into the biofilm. Ultra-high field NMR imaging with a spatial resolution of 19.5x19.5x100 μm^3 revealed the presence of fluid channels in extra-large (1500-2500 µm diameter) algal colonies (Van Schadewijk et al., 2018). Observations of channels in aerobic granules have been made as well, albeit after extensive sample treatment (Gonzalez-Gil & Holliger, 2014; Ivanov et al., 2005; Lemaire et al., 2008) in preparation for light microscopy and TEM. Both of these microscopy methods involve sectioning and dehydration of the granule or granule slice. It can therefore be questioned if the observed channels are an artefact of the sample preparation or if they are truly present in the intact granules. NMR imaging has potential to identify channel morphologies in intact and representative granules, since the method is non-invasive and non-destructive, provided the achievable spatial resolution is greater than the channel diameter.

The $T_{2,eff}$ relaxation maps of PNU granules in Figure 3.4 (B, C) reveal the presence of a large number of voids, distributed throughout the granule and a large cavity in the centre of the aged granule (Figure 3.4C). The similarity of $T_{2,eff}$ times in Figure 3.4A (bulk liquid and EPS) and granule voids in Figure 3.4B and C suggests that the voids are in fact filled with water and a small fraction of EPS or EPS with few exchangeable proton sites. In these images, the voids do not appear to be connected to the outside bulk liquid but instead are separated by biomass (cells and EPS) with distinctively different relaxation behaviour. It should be noted that the spatial resolution of NMR images presented here (47 x 47 x 100 µm) is relatively low compared to traditional microscopy and is lower than that applied in the algal colonies where channels were observed (Van Schadewijk et al., 2018). A channel with a diameter smaller than the spatial resolution will be hard to detect with NMR, though ultra-high field magnetic resonance has potential to further improve resolution limits. The channels reported by Gonzalez-Gil and Holliger (2014) are estimated to be roughly 50 µm in diameter, approximately the detection limit in this study. These NMR results suggest that channels with a diameter larger than 50 µm and connected to the bulk fluid are not present in aerobic granules imaged here and that convection may play a limited role in substrate transport in the granule interior.

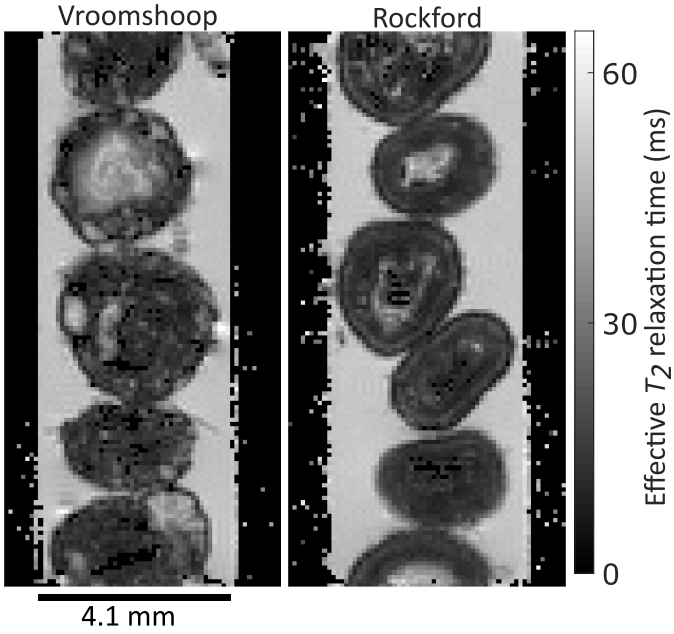

Figure 3.5. $T_{2,eff}$ maps of granules from the Vroomshoop (left) and Rockford (right) treatment plants show a longitudinal slice through a stack of granules in water in the 5 mm NMR sample tube. The two samples contain a similar range of relaxation times and provide an example of the variability of relaxation times within granules from the same reactor and between treatment plants. The maps were produced from MSME images (8 echoes) made on the 5.9 T system. Spatial resolution is 94 x 94 x 500 microns.

$T_{2,eff}$ maps of granules from Vroomshoop and Rockford were made using the 5.9 T (250 MHz) system. Figure 3.5 shows a representative longitudinal slice through a stack of granules in water in the 5 mm NMR sample tube and highlights the variability observed both within and across granule sources. These granules again show heterogeneous internal structure and appear to be more similar to Garmerwolde granules than to granules from the PNU reactor. In the Rockford granules there appears to be more of a concentric ring structure than is apparent in PNU granules, and the less dense EPS regions appear to be less numerous but larger in volume. There are few locations in both samples with relaxation times equal to the bulk water value. The Vroomshoop granules exhibit more of a cluster structure than concentric rings and most closely resemble Garmerwolde granules of all the granules imaged in this study. Despite the internal structural differences between the granule sources, a similar range of relaxation times is apparent in Vroomshoop and Rockford granules, ranging from less than 10 ms in the dense biomass to more than 40 ms in the less dense EPS regions. The bulk water relaxation in both cases is approximately 50 ms. Since the magnetic field strength, imaging gradient strengths, and spatial resolution are different between Figure 3.4 and

Figure 3.5, the values of $T_{2,eff}$ are not directly comparable. The lower spatial resolution and lower magnetic field strength on the 5.9 T system produce a wider range of $T_{2,eff}$ times within the biofilm, while the ultra-high field 22.3 T system provides high contrast and resolution of chemical exchange between biopolymer species in the NMR imaging experiments shown in Figure 3.1-Figure 3.3.

3.3.3 | T_1-T_2 relaxation correlations

In addition to imaging experiments, 2D T_1-T_2 relaxation correlation measurements were collected. These measurements confirm the presence of multiple T_2 populations and a distribution of T_1 populations within the granules. Since these data were collected without spatial resolution, the resulting distributions reflect the range and relative proportion of relaxation times inherent in the sample and are not subject to enhanced relaxation related to imaging.

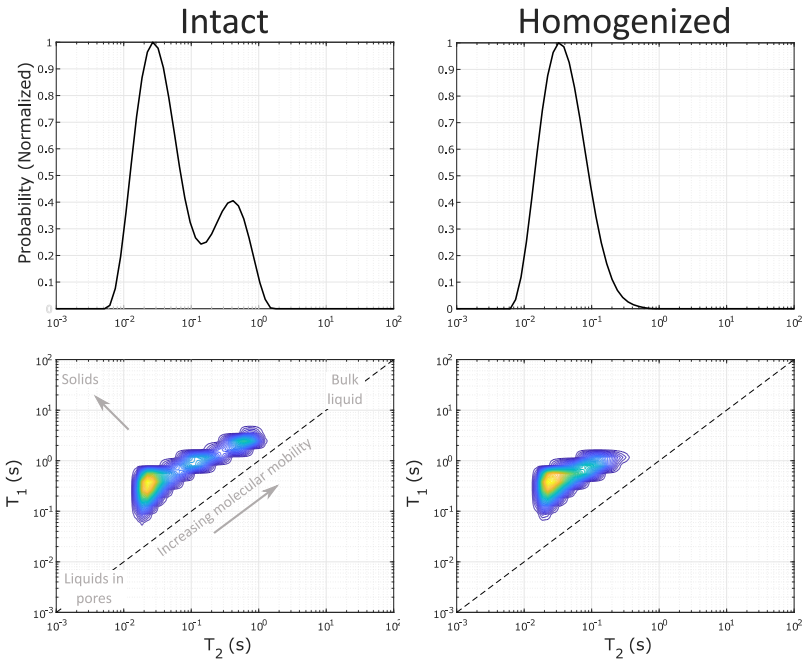

Figure 3.6. The T_1-T_2 correlation measured on the 5.9 T system on a stack of 1 month old Vroomshoop granules (left), and the same sample after homogenization inside the NMR sample tube (right). The loss of the population with the longer T_1 and T_2 times, corresponding to water populations in the granule voids, confirms that the internal granule structures are responsible for the distribution of relaxation times observed.

T_1-T_2 relaxation correlations were measured for 1-month-old Vroomshoop granules without bulk water using the 250 MHz (5.9 T) system (Figure 3.6). The measurements were made using intact granules (left) and the same sample after crushing the granules in the sample tube (right). The broad T_1-T_2 correlation for the intact granules reflects the presence of spatial heterogeneities that exist across length scales many orders of magnitude larger than the length scale of molecular interactions between water and biopolymers. The distribution approaches the T_1-T_2 parity line at longer relaxation times, indicating highly mobile water populations in the voids, and diverges from the parity line at shorter relaxation times. The short relaxation times indicate water in the pores of a highly cross-linked EPS matrix where the biopolymer signal may exhibit more solid-like behaviour. Because of the spatial heterogeneity of the internal structural features, even highly mobile water in a void would not experience the dense EPS of a cluster over the timescale of the measurement, resulting in the broad T_1-T_2 correlation observed. After crushing the granules, the T_1-T_2 correlation shows the loss of the population with larger T_1 and T_2 relaxation times, corresponding to the very diffuse EPS regions in the granules where molecular interactions are limited on the timescale of the measurement. Homogenization of the biofilm minimizes the length scale of heterogeneity, allowing interactions between hydrogen-bearing species previously separated in space. Water molecules previously in the void regions can undergo chemical exchange of protons with EPS after homogenization, leading to a decrease in the maximum T_2 relaxation time. Physically breaking the structure of the granules may also have entangled polymers that were spatially separated, increasing the rotational correlation time of the biopolymers previously in the voids. This would also lead to a decrease in the maximum T_1 relaxation time, as was observed. These measurements provide further confirmation that the structure of the granule is responsible for the distribution of relaxation times observed in the NMR measurements. Thus, the observed relaxation times in the NMR images are a clear indicator of different local physical and chemical environments and point to the importance of chemical exchange of protons in the relaxation response.

3.3.4 | Apparent ‘boundary layer’

An apparent ‘boundary layer’ was observed as a thin dark layer on the surface of the municipal AGS samples imaged at 22.3 T but was not observed on the EPS beads. The layer was approximately 1 pixel wide (~50 µm) in the NMR data. The darkness of the layer in the image could be attributed to a lack of signal (fewer protons), or very fast signal relaxation. To eliminate the possibility that the ‘boundary layer’ was simply an artefact of the measurement at the ultra-high magnetic field, a granule from PNU was

cut in half with a razor blade and imaged in the 22.3 T system (Figure 3.7A). The layer is visible on the undisturbed outer surface of the granule but not on the cut edge, suggesting that the physico-chemical properties of the surface are indeed different from the centre of the granule. An NMR artefact would be expected to be visible on the cut edge as well.

As part of the effort to identify the cause of the apparent boundary layer observed with NMR, images were also made using transmission electron microscopy (TEM) to more directly observe the surface layer of aerobic granules from the Garmerwolde treatment plant. Inorganic debris and solid particulates that might be present in municipal wastewater would be visible under TEM. Figure 3.7B shows dense cell clusters at the surface of a granule in the top of the image, with the embedding resin outside of the granule at the bottom. There was no precipitate or solid particulate debris visible on any granule surface examined with TEM. Research is ongoing to determine the source of the apparent boundary layer and to determine if the same mechanism is responsible for the apparent ring structure that can be seen in the $T_{2,\text{eff}}$ relaxation maps of Rockford granules shown in Figure 3.5 or in the Garmerwolde granule in Figure 3.1.

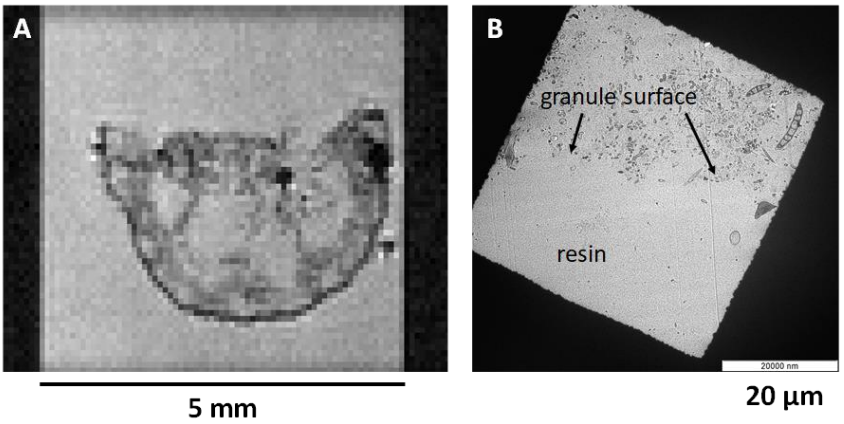

Figure 3.7. A PNU granule cut in half and imaged at 22.3 T (950 MHz) (A) shows the dark apparent 'boundary layer' on the outer surface of the granule, but no such layer on the cut edge, suggesting that the layer is not an artefact of the measurement. A TEM image of the outer surface of an aged Garmerwolde granule (B), shows a dense cell layer but not inorganic material that might explain the 'boundary layer.'

3.4 | CONCLUSIONS

Even though the structure of aerobic granular sludge is directly linked to mass transport and conversion processes in the granules, our understanding of the granule structure and the mechanisms by which it forms are still quite limited. In this paper, state-of-the-art ultra-high field and non-invasive magnetic resonance methods were used to explore the structural characteristics of full-scale and lab-scale granules. NMR provides the ability to screen larger samples sizes of intact granules and can, therefore, help to provoke and answer questions related to structure and function, as well as the reliability and representativeness of data collected via more labour-intensive and destructive microscopy methods. NMR results indicated that aerobic granules from municipal treatment plants exhibit a heterogeneous structure comprised of variable density EPS and cell clusters, and water-like voids. The structures observed were either similar to the cluster structure observed in some anaerobic granules (Gonzalez-Gil et al., 2001) or similar to a concentric ring structure with each granule source having a characteristic type. The structures in all granules were stable over a storage period of several months. The NMR data further revealed an apparent boundary layer, which appeared to be of organic origin and cannot be attributed to measurement artefact or accumulation of inorganic material on the granule surface. The granules did not contain channels larger than 50 µm, but rather apparent voids containing water and diffuse EPS or exopolymers with few exchangeable protons. These observations highlight the complex structure of aerobic granules and the need for non-invasive characterization methods such as NMR that can provide unique data on the granule structure.

A microscope image of a sliced granule

4

Heterogeneous diffusion in aerobic granular sludge

Published as: Van den Berg, L., Kirkland, C. M., Seymour, J. D., Codd, S. L., van Loosdrecht, M. C. M., & de Kreuk, M. K. (2020). Heterogeneous diffusion in aerobic granular sludge. *Biotechnology and bioengineering*, 117(12), 3809-3819. https://doi.org/10.1002/bit.27522

ABSTRACT

Background

Aerobic granular sludge (AGS) technology allows simultaneous nitrogen, phosphorus, and carbon removal in compact wastewater treatment processes. To operate, design, and model AGS reactors, it is essential to properly understand the diffusive transport within the granules. In this study, diffusive mass transfer within full-scale and lab-scale AGS was characterized with nuclear magnetic resonance (NMR) methods.

Methods

Self-diffusion coefficients of water inside the granules were determined with pulsed field gradient NMR, while the granule structure was visualised with NMR imaging. A reaction-diffusion granule-scale model was set-up to evaluate the impact of heterogeneous diffusion on granule performance.

Results

The self-diffusion coefficient of water in aerobic granular sludge was approximately 70% of the self-diffusion coefficient of free water. There was no significant difference between self-diffusion in AGS from full-scale treatment plants and from lab-scale reactors. The results of the model showed that diffusional heterogeneity did not lead to a major change of flux into the granule (< 5%).

Conclusions

This work shows that differences between granular sludges and heterogeneity within granules have little impact on the kinetic properties of AGS. Thus, a relatively simple approach is sufficient to describe mass transport by diffusion into the granules.

4.1 | INTRODUCTION

Aerobic granular sludge (AGS) is an advanced technology for the treatment of wastewater. Aerobic granules are compact microbial aggregates, which allow simultaneous removal of COD, nitrogen and phosphate, and have excellent settling properties (Adav et al., 2008; de Kreuk et al., 2005; Kishida et al., 2009). Aerobic granular sludge technology has a reduced footprint and energy requirement compared to conventional activated sludge processes (de Bruin, de Kreuk, van der Roest, Uijterlinde, & van Loosdrecht, 2004). Since the first full-scale application of AGS in 2005, many AGS installations have been built (Pronk et al., 2017; van der Roest et al., 2011).

To treat the wastewater in AGS installations, contaminants have to be transferred from the bulk liquid to the microorganisms that are located within the granules. Due to the compact and dense nature of the granules (Nor-Anuar et al., 2012), diffusion is generally the predominant mass transfer mechanism. Diffusion of different solutes in granules can be relatively slow compared to the volumetric reaction rates. A variety of chemical gradients within the granule (e.g., substrate concentration, oxygen concentration, and pH) arise as a result. These gradients directly impact the conversion processes in the granular sludge reactors. The simultaneous nitrification and denitrification requires a careful balance between the aerobic and the anoxic volume of the granules (Di Bella & Torregrossa, 2013; Mosquera-Corral et al., 2005; Yilmaz et al., 2008). These processes can only occur at the same time within a granule if the nitrification reaction is diffusion limited (Daigger & Littleton, 2014). On the other hand, mass transfer limitation can lead to filamentous outgrowth or hollow cores in the granule. Both phenomena have been shown to notably reduce reactor performance (de Kreuk et al., 2010; Zheng et al., 2006). Therefore, understanding of the diffusive transport within granules is essential to operate, design and model AGS reactors.

Diffusion has been extensively studied in biofilm systems, with methods such as the diffusion cell (Horn & Morgenroth, 2006; Pu & Yang, 1988) and microelectrodes (Chiu et al., 2006; Chiu et al., 2007a). However, neither of these methods can detect heterogeneities of diffusion coefficients from the surface to the inner parts of a biofilm. Pulsed-field gradient nuclear magnetic resonance (PFG-NMR) is an alternative method that overcomes these disadvantages. It can determine the displacement of hydrogen-bearing molecules in a sample. This displacement can be related to the self-diffusion of water molecules, since water is the most abundant hydrogen-bearing molecule in biofilms. Furthermore, with PFG-NMR one can distinguish water molecules based on their local physical and chemical environment in a biofilm. The self-diffusion coefficient of water in biofilms has been found to be a good indicator of the diffusion coefficient of

glucose (Beuling et al., 1998) and oxygen (Wieland et al., 2001). Previous work with PFG-NMR has focused on artificial and natural biofilms (Beuling et al., 1998; Hornemann et al., 2008; Renslow et al., 2010) and various types of anaerobic granular sludge (Gonzalez-Gil et al., 2001; Lens et al., 2003; Lens et al., 1997). It was observed that both biofilms and anaerobic granules were not homogeneous and contained a distribution of diffusion coefficients. Lens et al. (2003) reported that the type of wastewater and operational conditions influenced the diffusional properties of the granular sludge. However, it is unclear to what extent diffusivity in biofilms and anaerobic granules is similar to that in aerobic granules.

The aim of this study was to characterize the diffusional properties of aerobic granular sludge. We used PFG-NMR to measure effective diffusion coefficients in granular sludges from full-scale and lab-scale AGS reactors. Furthermore, we investigated the presence of heterogeneous diffusion within the granules and its impact on process engineering of granular sludge processes. Lastly, we provided a recommendation on how to include diffusion in the analysis of AGS kinetic properties and in AGS modelling.

4.2 | MATERIALS & METHODS

4.2.1 | Source of biomass

Aerobic granular sludge was collected from full-scale aerobic granular sludge plants in Garmerwolde, Vroomshoop and Simpelveld, all located in the Netherlands. The plants were designed by Royal HaskoningDHV under the trade name Nereda®. The plants treat domestic wastewater with influent concentrations as shown in Table 4.1. They are operated with biological phosphate removal and an average solids retention time of 20–50 days. Laboratory-scale aerobic granular sludge was taken from a fresh-water reactor and a sea-water reactor, both fed with acetate as sole carbon source. Reactor operation is described elsewhere (de Graaff et al., 2018). All samples were rinsed with tap water to remove the majority of flocculent biomass. The granules were stored in tap water at 4 °C for up to two months. No changes in self-diffusion coefficients were observed during this period. For the NMR measurements, the granules were poured onto a petri-dish and granules with a size of roughly 1-3mm in diameter were manually selected.

Table 4.1. Average sludge loading and influent concentrations of the reactors from which the aerobic granular sludge was harvested. TSS: Total Suspended Solids, COD: Chemical Oxygen Demand, BOD5: Biochemical Oxygen Demand in five days, SS: Suspended Solids.

	Sludge Loading (kg/kgTSS/d)		Influent (mg/L)			Reference
	COD	BOD5	COD	BOD5	SS	
Lab-scale reactors						
Fresh water	0.18	0.18	366	366	-	de Graaff et al. (2018)
Saline water	0.18	0.18	366	366	-	de Graaff et al. (2018)
Full-scale reactors						
Nereda	0.10	0.04	506	224	236	Pronk et al. (2015b)
Garmerwolde						
Nereda Vroomshoop	0.09	0.03	720	263	317	Pronk et al. (2017)
Nereda Simpelveld	0.04	0.01	300	124	169	-

4.2.2 | NMR measurements of diffusion coefficients

Self-diffusion coefficients of water molecules within granules and within bulk water were measured using the pulsed-field gradient stimulated echo (PFG-STE) sequence (Stejskal & Tanner, 1965). The PFG-STE measurements were carried out at room temperature (20 ± 1°C) with a 250 MHz superconducting magnet (Bruker Avance III, Bruker BioSpin GmbH, Rheinstetten, Germany). The magnet was equipped with a Diff30 probe (17 T/m maximum gradient). For the diffusion measurement, granules were stacked in a 5 mm NMR tube without excess water to maximize the signal obtained from the granules relative to bulk water signal. Roughly 20-30 granules were within the sensitive region of the NMR spectrometer, and thus contributed to the NMR signal. Typical acquisition parameters were as follows: 5,000 Hz spectral width, 1 ms gradient pulse duration (δ), 40 ms gradient pulse separation (diffusion time Δ), 1 s repetition time, 0–2.65 T/m diffusion gradient amplitude (g, linear in 128 steps), and 32 averages.

Fitting of the normalized NMR signal S/S_0 with a mono-exponential or bi-exponential model will yield the diffusion coefficient(s) of the diffusing population(s) within the sample. Here, a bi-exponential model was used to fit the signal of the granular sludge samples:

$$\frac{S}{S_0} = A_1 \exp\left(-\gamma^2 g^2 \delta^2 D_1 \left(\Delta - \frac{\delta}{3}\right)\right) + A_2 \exp\left(-\gamma^2 g^2 \delta^2 D_2 \left(\Delta - \frac{\delta}{3}\right)\right) \quad (4.1)$$

Here, A_1 and A_2 correspond to the relative size of two diffusing populations, D_1 and D_2 their respective diffusion coefficient (m^2/s), γ the gyromagnetic ratio (MHz/T), g the gradient amplitude (T/m), δ the gradient pulse duration (ms), and Δ the diffusion time (ms). A plot of a typical normalized NMR signal with mono-exponential and bi-exponential fits is shown in the Supplementary Information A.

The normalized NMR signal was also processed with the 1D Inverse Laplace Transform, which uses a non-negative least squares fitting function with a regularization parameter to minimize the error in the solution (Callaghan et al., 2003). Here, the data were transformed with a regularization parameter α of $1 \cdot 10^8$and 64 steps. The regularization parameter was chosen based on the approach of Provencher (1982). This process yields a one-dimensional diffusion coefficient distribution. However, due to the ill-posed nature of the Inverse Laplace Transform, the distribution is only an approximation and should be interpreted accordingly.

Self-diffusion coefficients of fresh and saline water without granules present were measured with the same acquisition parameters, but a mono-exponential model was used for data analysis. These self-diffusion coefficients of water without granules were used to quantify the impact of the granule matrix on the mobility of water molecules.

4.2.3 | MRI measurements of granule structure

The granule structure was characterized with Magnetic Resonance Imaging (MRI) experiments. The goal of this experiment was to obtain transverse relaxation times (T_2) at different locations throughout the granule. The T_2 time is a measure of how fast the NMR signal loses phase coherence after an excitation pulse. The relaxation time depends on the local physical-chemical environment in which different water populations exist (Callaghan, 1993). Since water molecules in a granule are generally less mobile, they will have a shorter T_2 time than water molecules in bulk liquid (Hoskins et al., 1999). Different locations in the granule can have different local environments (e.g., cell density, EPS density, paramagnetic ions) and therefore different T_2 values. Visualizing these differences in a T_2 map can be used to characterize the granule structure (Kirkland et al., 2020; Seymour et al., 2004).

The MRI experiments were performed with a 250 MHz superconducting magnet (Bruker Avance III, Bruker BioSpin GmbH, Rheinstetten, Germany). The magnet was equipped with a high-power probe, micro5 gradient set (2.81 T/m maximum gradient), and a 5 mm radio-frequency coil. A stack of 5–10 granules was placed in a 5 mm NMR tube filled

with tap water. A multi-slice multi-echo (MSME) imaging sequence was used to acquire T_2-weighted images. Typical acquisition parameters were as follows: 5 s repetition time, 5.04 ms echo time, 8 echoes, 16 averages, 50 kHz spectral width, 39 x 39 x 200 µm resolution, and 5 x 5 mm field-of-view. The MSME produces a stack of 2D images showing the NMR signal amplitude per pixel at each image acquisition time. Because the NMR signal amplitude decays with time, fitting the signal attenuation in each pixel ultimately yields the effective T_2 relaxation time in each pixel (Edzes et al., 1998). Here, 2D maps of the T_2 relaxation times were obtained with Prospa v3.13 (Magritek).

4.2.4 | NMR measurements to correlate diffusion with structure

A two-dimensional correlation experiment was conducted to relate diffusion to T_2 relaxation. During the experiment, each water molecule in the granular sludge sample will diffuse at a certain rate. Simultaneously, each water molecule will experience a T_2 relaxation that is indicative of its local environment. With a correlation experiment the diffusion and relaxation rate are measured for each water molecule. It should be noted that, unlike in the MRI experiment, the T_2 values are not spatially resolved. Correlation of the diffusion and T_2 relaxation rate can give valuable insight into the relationship between structure (by T_2 relaxation) and diffusion in the granular sludge sample. The correlation experiment was carried out with a PFG-STE sequence, followed by a Carr-Purcell-Meiboom-Gill (CPMG) sequence (Callaghan, 2011). The data was processed in Matlab with the 2D Inverse Laplace Transform, which is similar to the aforementioned 1D Inverse Laplace Transform (Callaghan et al., 2003). Here, the data were transformed with a regularization parameter α of $1 \cdot 10^8$and 64 steps. The regularization parameter was chosen based on the approach of Provencher (1982).

4.2.5 | Granule-scale reaction-diffusion model

A 2D axisymmetric, steady-state, reaction-diffusion granule model was set up in COMSOL Multiphysics. Heterotrophic oxidation of organic matter was used as model reaction, with Monod kinetics and oxygen as single limiting substrate. Model parameters were derived from the first biofilm benchmark problem (Morgenroth et al., 2004) and are as follows: q_{max} = 3.54 gO_2 $gCOD^{-1}$ d^{-1}, C_X = 10,000 gCOD m^{-3}, K = 0.2 gO_2 m^{-3}. The granule radius was set to 0.55 mm, with a bulk oxygen concentration of 2 g m^{-3}. Six different scenarios were created with respect to the heterogeneous distribution of the diffusion coefficient (see Figure 4.1). The flux of oxygen into the granule for each case was calculated in COMSOL with an integration of the diffusive flux over the granule

surface. The flux deviation was calculated as the relative difference between the flux for each case and flux obtained in a scenario with a homogeneous diffusion coefficient. In all scenarios, the diffusion coefficient was normally distributed, with a mean of $1.4 \cdot 10^{-9}$ m^2 s^{-1} (based on the result of this study, see Table 4.2) and a relative standard deviation of 10%. Convective mass transfer was not included. The granules were discretized with 600,000 grid points based on equal volumes. A sensitivity analysis was carried out with discretisation with 60 and 6,000 grid points.

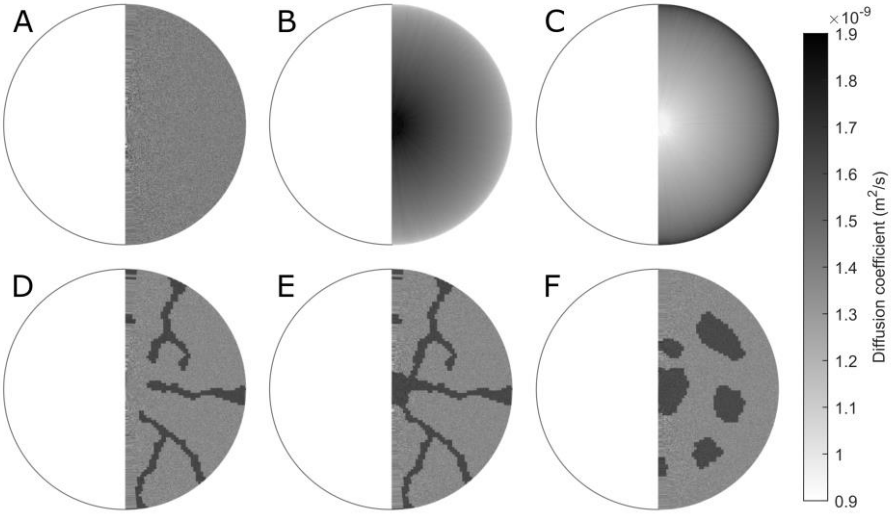

Figure 4.1. Spatial distribution of diffusion coefficients of oxygen for six different scenarios (all with 600,000 grid points). The colour bar indicates the diffusion coefficient of oxygen. An axisymmetric granule model was used for simplicity, meaning that the granule was assumed to be rotationally symmetric around the vertical axis through the granule centre.

4.3 | RESULTS

4.3.1 | Self-diffusion of water in granular sludge

The self-diffusion coefficients of the granular sludges were analysed with a bi-exponential model. For all sludges, the NMR signal originated from a large amount of mobile water (approximately 95% of the signal) and a smaller amount of less mobile water (roughly 5% of the signal). The mobile water had an average diffusion coefficient between $1.3 \cdot 10^{-9}$ and $1.5 \cdot 10^{-9}$ m^2 s^{-1}. The diffusivity of the less mobile water was around $1.0 \cdot 10^{-10}$ m^2 s^{-1}. The diffusion coefficient distributions determined with the Inverse Laplace Transform can be found in Supplementary Information B.

The diffusional properties of the granular sludges were determined in triplicate (that is, three NMR tubes with 20-30 granules each). The average diffusion coefficients can be found in Table 4.2. The standard deviation within the triplicates was small and exceeded 5% only for the Simpelveld granules. The diffusional properties of the granular sludges did not depend on their origin, based on a one-way Analysis of Variance ($F(4,10) = 2.57$, $p = .10$).

Table 4.2. Overview of the water self-diffusion coefficient of the granular sludges. The relative diffusivity (D/D_{aq}) was based on the self-diffusion coefficient of fresh water (D_{aq}). For the granules grown in saline water, the self-diffusion coefficient of saline water was used instead. NMR measurements revealed the self-diffusion coefficient of fresh-water to be $2.03 \cdot 10^{-9}$ m^2 s^{-1} and of saline water to be $1.91 \cdot 10^{-9}$ m^2 s^{-1}. Diffusivity values are given as mean ± standard deviations from triplicate experiments.

	D (10^{-9} m^2 s^{-1})	D/D_{aq}
Lab-scale reactors		
Fresh water	1.44 ± 0.01	0.71
Saline water	1.32 ± 0.03	0.69
Full-scale reactors		
Nereda Garmerwolde	1.39 ± 0.04	0.69
Nereda Vroomshoop	1.33 ± 0.05	0.66
Nereda Simpelveld	1.32 ± 0.10	0.65

4.3.2 | Granule structure

A T_2 map reveals the granule structure, by showing the local T_2 values throughout the granule. Roughly six granules were imaged per sludge source. Overall structural features were constant between different granules of the same origin (data not shown), similar to what was found by Kirkland et al. (2020). In Figure 4.2, only two T_2 maps are presented: one typical of full-scale granules and one typical of lab-scale granules. Maps for other granules can be found in the Supplementary Information C.

The T_2 map of a full-scale granule shows that there is a range of T_2 values within a single granule, confirming that water is present in different environments (see Figure 4.2a). The full-scale granule has a heterogeneous structure, with regions that have a T_2 close to that of bulk water, and with regions in which water is either not present or strongly restricted in mobility. No apparent ultrastructure could be observed (e.g., concentric, cluster-like structure). The surface of the granule is not smooth, possibly due to the presence of protozoa clusters or filamentous outgrowths (Pronk et al., 2015b). The T_2 map of lab-scale granules reveals much less heterogeneity (see Figure 4.2b). The

variation in T_2 values in the granules showed a concentric pattern. The core of the granules has a T_2 close to that of the bulk water, which suggests that the granules are filled with water and effectively hollow.

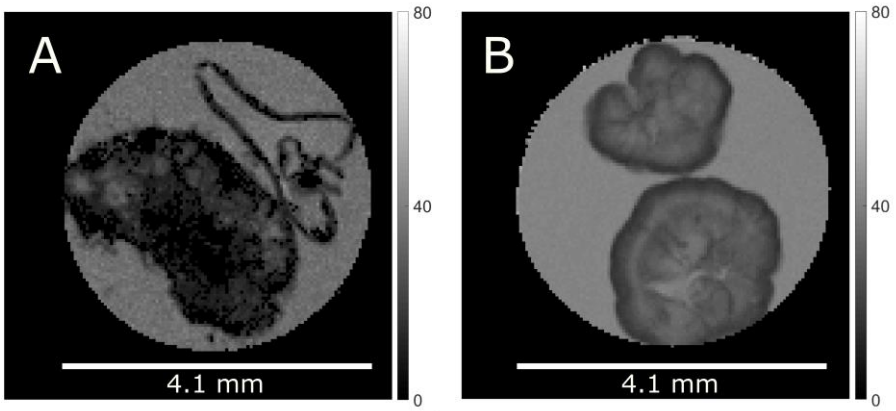

Figure 4.2. Typical effective T_2 map for a Garmerwolde full- scale granule (A) and a saline lab-scale (B) granule. The scale bar indicates effective T_2 in ms. The spatial resolution is 39 x 39 x 100 µm. Lighter regions correspond to a higher T_2 (more water-like), while darker regions correspond to a lower T_2 (more solid-like).

The heterogeneity of the T_2 maps can be related to diffusional properties with a D-T_2 correlation experiment. This experiment correlates the T_2 of water molecules to the diffusion coefficient of those molecules. It includes all the observable water molecules in a granular sludge sample. In Figure 4.3, typical D-T_2 correlations are shown for full-scale and lab-scale granular sludge. It should be noted that the T_2 values in the D-T_2 correlation experiment are almost an order of magnitude smaller than the T_2 values in the T_2 maps (compare Figure 4.2 and Figure 4.3). This is not unexpected, since the T_2 maps represent effective T_2, while the D-T_2 correlation represents true T_2. The effective T_2 is reduced due to the imaging gradients required for the T_2 maps (Edzes et al., 1998). Therefore, direct comparison of the different T_2 values is not possible.

A range of T_2 values were present in the granular sludge, again revealing the presence of a range of physical and chemical environments. The T_2 values of the full-scale granular sludge were lower than those of lab-scale granular sludge, indicating that water was more restricted in the full-scale sludge. Note that neither free water (the NMR tube did not contain excess water during these measurements) nor intracellular water (which has

a relatively small signal) contributed to the correlation. The correlation also showed a range of diffusivity values, although with a narrower distribution. Clearly, water within granular sludge did not have a single, discrete diffusion coefficient, but rather a diffusion coefficient distribution. However, there was no clear correlation between T_2 and diffusivity.

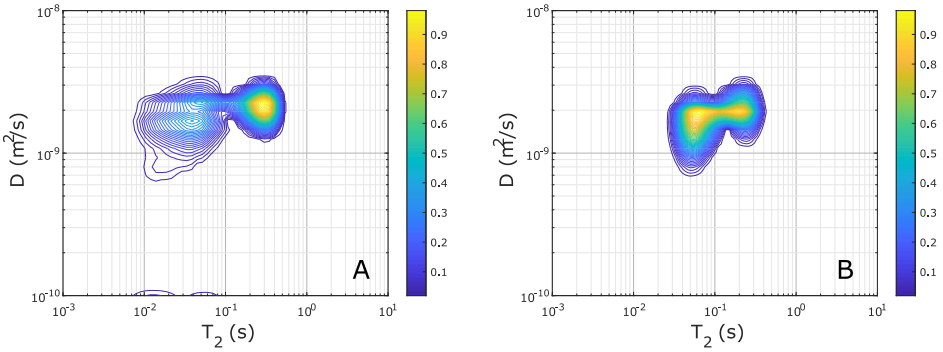

Figure 4.3. Typical D-T_2 correlation for Garmerwolde full- scale granular sludge (A) and saline lab-scale (B) granular sludge. The colour bar represent signal intensity in arbitrary units.

4.3.3 | Granule heterogeneity model

The impact of different models of heterogeneous diffusion on the flux of a model substrate into a granule was evaluated with a reaction-diffusion model. In all six diffusion models, oxygen penetrated only the outer part of the granule, as can be seen in the 1D oxygen profile of Figure 4.4B. The full spatial oxygen profiles for each diffusion model showed no discernible difference and therefore only the spatial profile for the channels-scenario is shown (insert of Figure 4.4B). For the six heterogeneous diffusion models shown in Figure 4.1, the deviations in flux (compared to the flux for homogeneous diffusion) was always smaller than 5% (see Figure 4.4A). Channels or voids with a higher diffusivity apparently only slightly enhance diffusive mass transfer into the granule. When the diffusion coefficient varied with the granule radius (cases B and C), the largest deviation in flux was observed. A low diffusivity near the granule surface resulted in a reduced flux (case B), while a higher diffusivity near the surface resulted in an increased flux (case C). In these simulations the substrate only partially penetrated the granule, as can be seen in Figure 4.4B. To see the impact of penetration depth, we calculated the average diffusion coefficient of the penetrated volume (here defined as the volume where the local concentration was at least 1% of the bulk

concentration) for the heterogeneous diffusion scenarios. There was a strong correlation (R^2 = 0.97) between the diffusion coefficient of the penetrated volume and the flux deviation (see Supplementary Information D). It appears that the change in flux for heterogeneous diffusion is almost entirely caused by the change in average diffusion coefficient of the outer layer. The number of grid points only had a minor influence, as the differences between the simulations with 60, 6,000 and 600,000 grid points was maximally 0.2%.

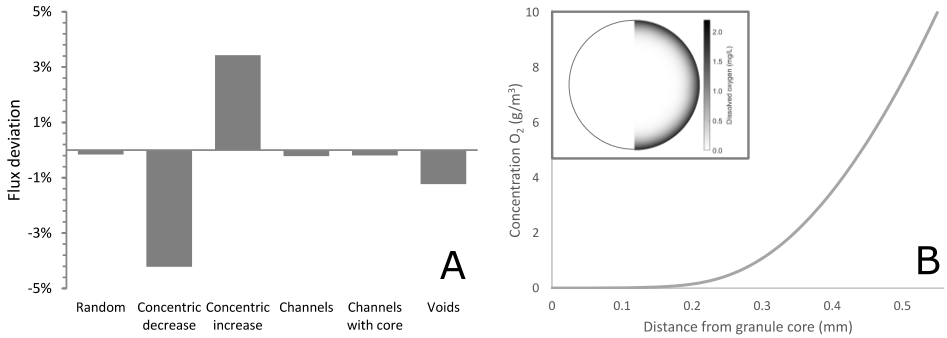

Figure 4.4. Deviation of steady-state flux of solute into the granule for the six different heterogeneous diffusion scenarios compared to homogeneous diffusion as defined in Figure 4.1. (A). Typical steady-state concentration profile in a scenario with homogeneous diffusion, showing the limited penetration in these simulations (B).

4.4 | DISCUSSION

4.4.1 | Self-diffusion coefficient of granular sludges

The PFG-NMR experiments yielded two diffusing populations in each granular sludge. Previously, two similar populations have been reported as well in anaerobic granular sludges and a biofilm (Beuling et al., 1998; Hornemann et al., 2008; Lens et al., 2003). They identified the less mobile population as cell-internal water. The T_2 for the less mobile population that was obtained in our study, was similar to the intracellular water in anaerobic granular sludge (10–30 ms). A quantitative analysis of the intracellular volume is complex, due to the small signal size, short T_2 value, and the permeability of the bacterial cell wall to water (Beuling et al., 1998). Therefore, in our study the small population of less mobile protons is excluded from all analyses.

For the mobile population, self-diffusivity of water in the granules is reduced compared to the self-diffusivity of free water. The diffusion coefficients that were found in this study for aerobic granular sludge are in the same order of magnitude as the water self-diffusion coefficients determined for different anaerobic and aerobic aggregates and biofilms (Beuling et al., 1998; Herrling et al., 2017; Hornemann et al., 2008; Lens et al., 2003; Lens et al., 1997; Phoenix & Holmes, 2008; Renslow et al., 2013; Renslow et al., 2010; Vogt et al., 2000).

Lens et al. (2003) have shown with PFG-NMR that operational conditions can influence the diffusional properties of anaerobic granular sludge. No such effect was found for the aerobic granular sludge that was analysed in this study. The variation in operating conditions between the granular sludges from the full-scale treatment plants was minimal, since all plants treat domestic wastewater with biological phosphate removal. However, the lab-scale reactors were operated with notably different hydrodynamics, influent characteristics, and loading. The wet density of lab-grown granules is typically reported to be around 1040 kg/m^3 (Etterer & Wilderer, 2001; Herrling et al., 2017; Winkler et al., 2012), although the ash content plays a major role (Winkler et al., 2013). The wet density of granules from the Garmerwolde treatment plant was found to be around 1020 kg/m^3. Considering the observed differences in granule structure and density, it was expected that full-scale and lab-scale granular sludges would have different diffusive properties, but this was not the case.

The diffusivity in a granule depends on its structural properties. Extracellular polymeric substances (EPS) and relatively impermeable cells within the granule hinder diffusing molecules. A molecule has to diffuse around EPS and cells, increasing the diffusive path length. The increase in path-length is generally referred to as tortuosity. The impact of tortuosity on the effective diffusivity in a granule is given by the following relation (Epstein, 1989):

$$\mathfrak{D}_{eff} = \frac{1}{\tau^2} \cdot \mathfrak{D}_{aq}, \qquad (4.2)$$

where $\mathfrak{D}_{eff}$ is the effective diffusivity in the granule, $\mathfrak{D}_{aq}$ is the diffusivity in the bulk water phase, and τ is the tortuosity. The tortuosity is defined here as ratio of the actual path length over the Euclidian distance (shortest linear distance). If the effective diffusivity in a granule is known (e.g., measured with PFG NMR), the tortuosity of the granular sludge can be calculated. For the granular sludges used in this study, the tortuosity is roughly 1.2. This means that the actual path length that a water molecule has moved along is only 20% increased due to the presence of cells, inorganic material, and EPS. Since a

granule consist mostly of water, it is not surprising that the tortuosity is relatively close to 1 (Etterer & Wilderer, 2001; Zheng & Yu, 2007).

The diffusion coefficient that is obtained with PFG NMR is the effective diffusivity (Beuling et al., 1998; Stewart, 1998). The effective diffusivity is generally used to describe transient penetration of a solute into a biofilm. However, for wastewater treatment applications, the (pseudo-)steady-state flux of some solute into a granule is generally more relevant. This flux is not described by the effective diffusivity, but rather by the effective diffusive permeability. Since the terminology can be confusing, we refer to Stewart (1998) for a detailed discussion of both parameters. Here, the emphasis is on the relation between both parameters:

$$D_{eff} = (1 - \phi) \cdot \mathfrak{D}_{eff}, \qquad (4.3)$$

where D_{eff} is the effective diffusive permeability (Libicki et al., 1988) and ϕ is the volume fraction occupied by cells and EPS. The effective diffusive permeability includes another effect of the granule matrix on the diffusivity: the volume exclusion by cells and EPS. Since a molecule cannot diffuse through the non-water phase of a granule, the effective diffusive permeability is reduced.

In order to obtain the effective diffusive permeability, further information on the porosity (1 - ϕ) of the granule is required. However, both the porosity and the tortuosity depend on the fraction of cells and EPS. Knowledge of one parameter can be used to estimate the other. For example, T.C. Zhang and Bishop (1994b) found a tortuosity of 1.15 for biofilms with porosities of 0.84-0.93. Comparable values for porosities of aerobic granular sludge have been found by Etterer and Wilderer (2001) and Zheng and Yu (2007). Since the tortuosity of the granular sludges in this study was around 1.2, the porosities are most likely within this range as well. This indicates that the effective diffusive permeability is roughly 84-93% of the effective diffusivity.

4.4.2 | Structural heterogeneity of granules

A range of T_2 values were present and spatially distributed over the full-scale granule, indicating the structural heterogeneity (Figure 4.2A). These findings are in line with the extensive study of granule structure by Kirkland et al. (2020). The T_2 value measured using the imaging MSME sequence in a biofilm is influenced by the diffusion of the water molecules, presence of relaxation sinks, and magnetic field inhomogeneities (Brownstein & Tarr, 1979; Edzes et al., 1998; Godefroy et al., 2001). Examples of relaxation sinks are bound water, paramagnetic impurities, and EPS. In a detailed study,

Beuling et al. (1998) have shown the importance of the EPS content for the average relaxation time T_2. An increase of the agar concentration from 1.5 to 4% w/w led to a decrease in relaxation time from 100 to 38 ms. The large impact of EPS on the relaxation time can be explained by the exchange of protons between water and EPS functional groups (e.g., -OH, -NH_2, -SH groups). The impact of the EPS is a function of the amount of exchangeable protons, their local chemical environment (chemical shift), and their exchange rate (Hills, 1992). Thus, it can be deduced that the T_2 relaxation time is not only impacted by the concentration of polymers, but also by the type of polymers. A different number of ionisable groups on a polymer will lead to a different T_2 value.

Although many attempts have been made to relate the structure of aerobic granular sludge to mass transport within the granules (Chiu et al., 2007a, 2007b; Y. Li et al., 2008; L. Liu et al., 2010; Meyer et al., 2003; Tay et al., 2002), the exact relationship remains unclear. These authors used (invasive) techniques that can either determine substrate diffusion into the granules (e.g., micro-electrodes) or that can observe the heterogeneity inside the granules (e.g., Confocal Laser Scanning Microscopy methods). In this study, multiple attempts were made to obtain local diffusion coefficients in a granule with an Apparent Diffusion Coefficient (ADC) map. An ADC map visualizes the heterogeneity of diffusion in a granule by displaying the apparent diffusion coefficient for each pixel in an image. However, due to rapid signal loss (short T_2) in the granular sludge matrix, it was not possible to obtain useful ADC maps. As an alternative method to indicate the heterogeneity of diffusivity, T_2 maps and D-T_2 correlations can be used. A T_2 map shows local T_2 values in a granule, while a D-T_2 correlation shows how diffusivity and T_2 are related. A clear correlation implies that the heterogeneity for the diffusivity is similar to any heterogeneity visible in the T_2 map. The D-T_2 correlation is much less impacted by the rapid signal loss since no imaging gradients are required in the experiment.

The D-T_2 correlations of both the full-scale and lab-scale granular sludge do not show a clear correlation between these parameters. A wide range of T_2 values is present, but the range of diffusivities is more narrow. Apparently, the heterogeneity that is visible in the T_2 maps does not translate to heterogeneity in the diffusivity. If the T_2 values are mainly a function of local EPS content, the diffusivity is not correlated with EPS content. There are three possible explanations for the absence of a correlation: firstly, the diffusivity could be more impacted by the presence of microbial cells than by the presence of EPS. Secondly, the T_2 values are influenced by the local amount of exchangeable protons (Hills, 1992). If the EPS properties are heterogeneous throughout the granule, the range of T_2 values does not represent EPS content, but rather EPS properties. Thirdly, the absence of a correlation can be due to the impact of

paramagnetic impurities (e.g., metal ions, iron oxide, iron sulphides, and vivianite). It is known that these impurities have an impact on T_2 (Brownstein & Tarr, 1979) and especially in the granule from full-scale treatment plants inorganic contaminants might be present (Pronk et al., 2015b). Their effect on T_2 was, however, not assessed in this study. Previous researchers have reported a relation between T_2 and diffusivity, although different NMR methods were used. Gonzalez-Gil et al. (2001) found a cluster morphology in methanogenic granules. These clusters could be identified from stereomicroscopy images, T_2 maps, and apparent diffusivity measurements. Similarly, Lens et al. (2003) observed a distribution of T_2 values and diffusion coefficients in methanogenic granules. In neither of these publications, a (quantitative) correlation was reported. In line with the observations in the present study, Phoenix and Holmes (2008) reported relatively little diffusion heterogeneity for a structurally complex phototrophic biofilm. Furthermore, Herrling et al. (2017) found there was no clear relation between diffusion and T_2 based on a D-T_2 experiment. Thus, T_2 maps are of limited use for the characterisation of diffusional properties, despite being relatively easy to obtain.

4.4.3 | Implications for practice

Engineering of aerobic granular sludge reactors is, amongst others, based on conversion rates of different contaminants and on the flux of oxygen into the granules. Ideally, the flux of oxygen is sufficiently high to maintain an aerobic zone for nitrification, but also sufficiently low to maintain an anoxic core for denitrification (Mosquera-Corral et al., 2005). The flux into a granule can be predicted with reaction-diffusion models. In these models, there are two aspects of diffusion that should be considered: (1) using an accurate value for the diffusivity and (2) properly including diffusion heterogeneity. Regarding the first aspect, the question arises what accuracy is required. For most process engineering purposes, the flux into or out of a granule is the parameter of interest. According to half-order kinetics (Harremoës, 1978), the overall substrate flux is proportional to the square root of the diffusion coefficient. This means that an error of 10% in the diffusion coefficient, leads to an error in the flux of roughly 5%. Similar results have been found with the benchmark problem BM1 for different biofilm models (Morgenroth et al., 2004) and a local sensitivity analysis of IFAS and MBBR systems (Boltz et al., 2011). Thus, the uncertainty in the diffusion coefficient is not amplified. However, when the free water diffusion coefficient ($\sim 2.0 \cdot 10^{-9}$ m^2/s) is used instead of the granule diffusion coefficient ($\sim 1.4 \cdot 10^{-9}$ m^2/s) in an AGS model, an error is introduced of 20% in the flux over the granules surface. Incorrect conclusions may be drawn from the model, if this error is not accounted for (e.g., by fitting parameters as in Baeten et al. (2018)).

Regarding the second aspect, multiple authors have argued that heterogeneous diffusion should be incorporated into mathematical models of aerobic granular sludge (Chiu et al., 2007a; L. Liu et al., 2010; Tay et al., 2002). Their argument is generally based on the observation of heterogeneous granule structures with reduced or increased diffusivity, such as channels, layers, clusters, and pores. However, the results from the granule-scale reaction-diffusion model show that heterogeneous diffusion does not lead to a significantly different flux. This is most likely due to the fact that the average diffusion coefficient is maintained in our model. A higher diffusion coefficient in one part of the granule (e.g., channels) leads to a lower diffusion coefficient in the rest of the granule. Thus, the flux into a granule will only increase notably if the average diffusion coefficient over the whole granule increases. Most methods to study the diffusion behaviour of a solute in granules, will yield an average diffusion coefficient (Chiu et al., 2007b; Fan et al., 1990; Horn & Morgenroth, 2006; Yu & Pinder, 1994). This average diffusion coefficient should always be maintained when constructing a biofilm model, to obtain a valid representation of the flux into a granule.

In contrast to our findings, other authors reported a large impact of a heterogeneous diffusion coefficient (Beyenal & Lewandowski, 2005; Morgenroth et al., 2000; Siegrist & Gujer, 1985). The biofilms investigated by these authors, were best described by a stratified diffusion coefficient. However, these biofilms were dense at the bottom and more porous towards the surface. The stratified diffusion coefficient was used to include the effect of advection (eddy diffusion) in the pores of the biofilm. Granules are more dense toward the surface and the surface is smooth (Chiu et al., 2007a; de Kreuk & Van Loosdrecht, 2004). Therefore, the effect of advection is expected to be negligible for granules.

4.5 | CONCLUSION

In this study, diffusive mass transfer within lab-scale and full-scale aerobic granular sludge has been characterized with PFG NMR. The self-diffusion coefficient of water inside the EPS matrix was roughly 70% of the diffusion coefficient in bulk water, for lab-scale as well as for full-scale aerobic granular sludges. Despite the differences in operating conditions and influent characteristics, the differences in diffusion between lab-scale and full-scale granular sludges were only minor. The granules types differed in structure: while lab granules were more homogeneous, full-scale granules were clearly heterogeneous. The latter consistently displayed irregular features such as voids and dense areas. However, no correlation between structural heterogeneity and diffusional

properties was found. Despite the heterogeneous structure, the variation in diffusion coefficient for a single granule source was limited. A granule-scale reaction-diffusion model showed that a small spatial variations in the diffusion coefficient do not lead to a large change (< 5%) of substrate flux into the granule. Therefore, heterogeneity in diffusion does not play a major role in the conversion rates obtained with aerobic granular sludge.

Our study has several implications for modelling of the AGS process and for analysis of AGS kinetic properties. We recommend using a general diffusion coefficient that is 70% of the diffusion coefficient in water. Heterogeneity of diffusion on a granule-scale does not need to be included to evaluate substrate flux into or out of a granule. Thus, a relatively simple approach is sufficient to describe mass transport by diffusion in aerobic granular sludge. Since we did not observe any difference between the different granular sludge types, this approach is most likely valid for all AGS plants that treat domestic wastewater.

SUPPLEMENTARY INFORMATION

Supplementary information A: Stejskal-Tanner plot of a typical diffusion experiment

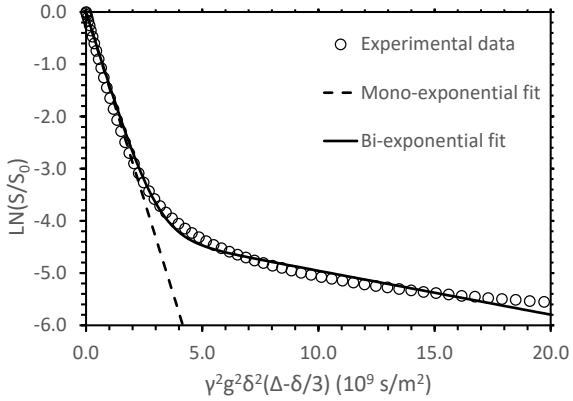

Figure 4.S1. Stejskal-Tanner plot of the normalized NMR signal as function of the b-value, where b is defind as $\gamma^2 g^2 \delta^2 \left(\Delta - \frac{\delta}{3}\right)$. The bi-exponential behaviour of the experimental data is apparent. The experimental data in this plot is from a Garmerwolde granule sample.

Supplementary information B: Probability distributions of the diffusion coefficient

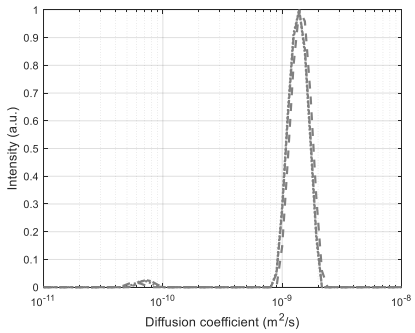

Figure 4.S2. Diffusion coefficient pobability distribution of three Nereda Garmerwolde samples. The small differences between the triplicate samples is clear. Also note the presence of a smaller peak around $5 \cdot 10^{-11}$ m^2/s.

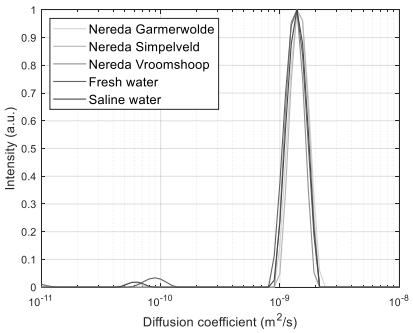

Figure 4.S3. Diffusion coefficient pobability distribution of five different granule samples. The samples are highly comparable on the scale of this figure.

Supplementary information C: Effective T_2 maps and D-T_2 correlations for five different granule types

For all the granular sludge sources investigated, effective T_2 maps and D-T_2 correlations were made. These maps and correlations reveal information on the granule structure and possible relationship with diffusion in the granule (see the main paper for a more detailed explanation). Per granule source, multiple granules were imaged to obtain multiple T_2 maps. Here, only a single T_2 map is reported, which is considered typical of the granule source. For the T_2 maps lighter regions correspond to a higher T_2 (more water-like), while darker regions correspond to a lower T_2 (more solid-like). The D-T_2 correlations are made for a granular sludge sample (test tube packed with >> 10 granules) and only a single D-T_2 correlation was made.

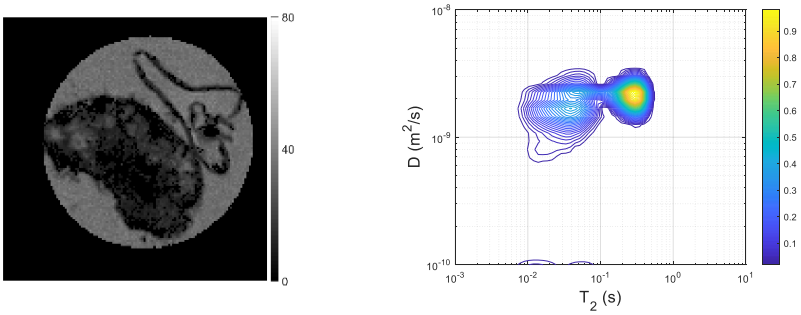

Figure 4.S4. Typical effective T_2 map for a Garmerwolde full-scale granule (left), with the scale bar indicating effective T_2 in ms. The spatial resolution is 39 x 39 x 100 µm. Typical D-T_2 correlation for Garmerwolde full-scale granular sludge (right). The colour bar represents signal intensity in arbitrary units.

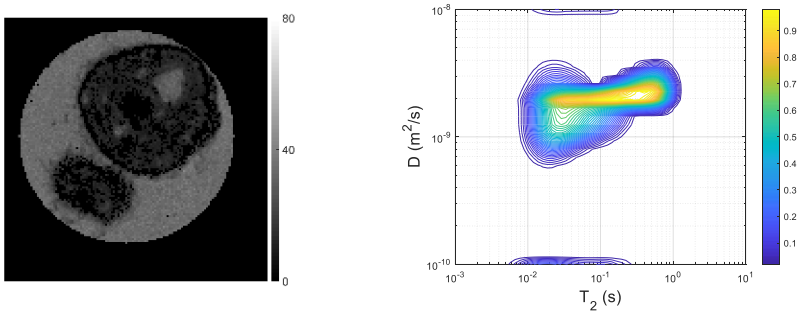

Figure 4.S5. Typical effective T_2 map for a Simpelveld full-scale granule (left), with the scale bar indicating effective T_2 in ms. The spatial resolution is 39 x 39 x 100 µm. Typical D-T_2 correlation for Simpelveld full-scale granular sludge (right). The colour bar represents signal intensity in arbitrary units.

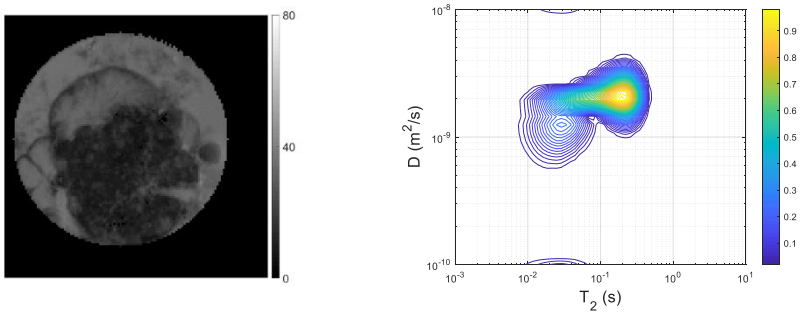

Figure 4.S6. Typical effective T_2 map for a Vroomshoop full-scale granule (left), with the scale bar indicating effective T_2 in ms. The spatial resolution is 39 x 39 x 100 µm. Typical D-T_2 correlation for Vroomshoop full-scale granular sludge (right). The colour bar represents signal intensity in arbitrary units.

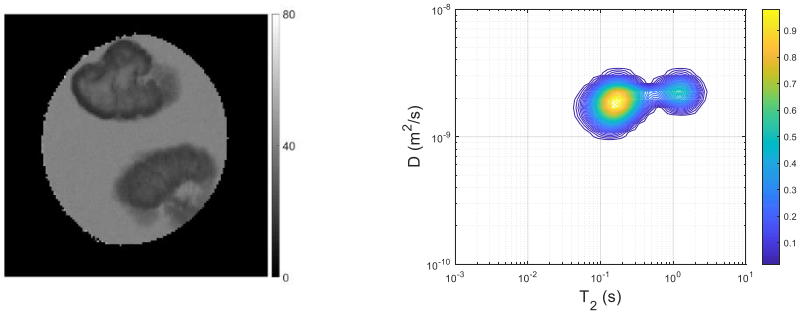

Figure 4.S7. Typical effective T_2 map for a freshwater lab-scale granule (left), with the scale bar indicating effective T_2 in ms. The spatial resolution is 39 x 39 x 100 µm. Typical D-T_2 correlation for freshwater lab-scale granular sludge (right). The colour bar represents signal intensity in arbitrary units.

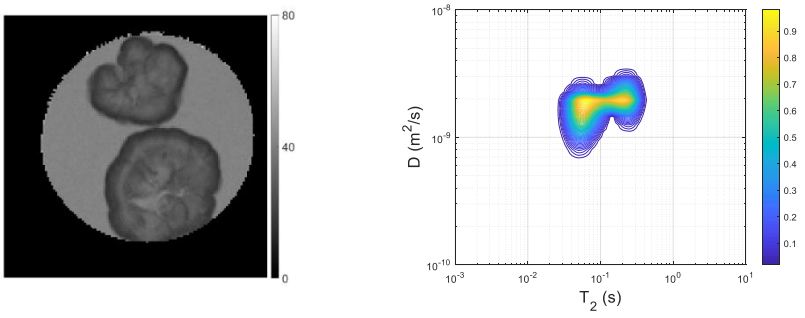

Figure 4.S8. Typical effective T_2 map for a saline lab-scale granule (left), with the scale bar indicating effective T_2 in ms. The spatial resolution is 39 x 39 x 100 µm. Typical D-T_2 correlation for saline lab-scale granular sludge (right). The colour bar represents signal intensity in arbitrary units.

Supplementary information D: Relation between effective diffusion coefficient and simulated flux

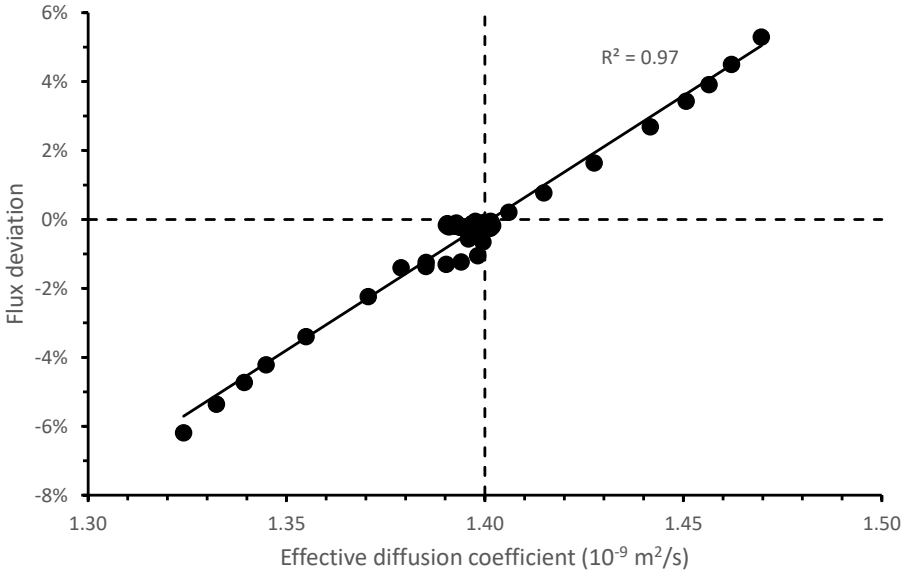

Figure 4.S9. Relation between the diffusion coefficient of the penetrated volume (labeled here as effective diffusion coefficient) and the flux deviation (the difference in flux between a heterogeneous diffusion scenario and homogeneous diffusion). The data points (solid circles) correspond to all six heterogeneity scenarios, with bulk oxygen concentrations of 0.5, 1.0, 1.5, 2.0, 3.0, 5.0, 7.5, and 10.0 mg/L. The good correlation is apparent from the R^2 of the linear trend line (solid line). The dashed lines correspond to the homogeneous diffusion case.

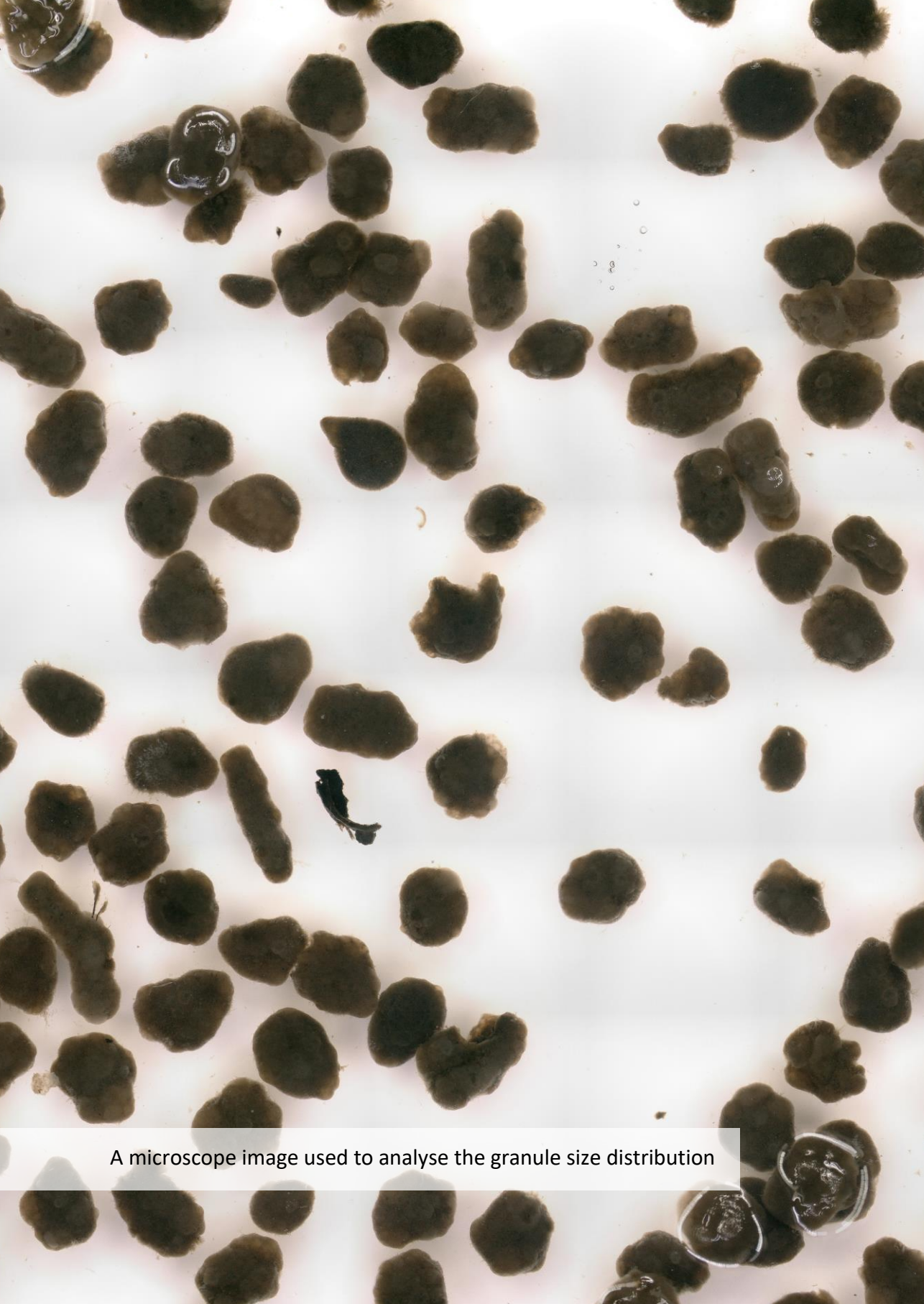

A microscope image used to analyse the granule size distribution

5

How to measure diffusion coefficients in biofilms: A critical analysis

Published with minor modifications as: Van den Berg, L., van Loosdrecht, M. C. M., & de Kreuk, M. K. (2021). How to measure diffusion coefficients in biofilms: A critical analysis. *Biotechnology and bioengineering*, 118(3), 1273-1285. https://doi.org/10.1002/bit.27650

ABSTRACT

Background

Biofilm and granular sludge processes depend on diffusion of substrates. Despite their importance for the kinetic description of biofilm reactors, biofilm diffusion coefficients reported in literature vary greatly. The aim of this simulation study was to determine to what extent the methods that are used to measure diffusion coefficients contribute to the reported variability.

Methods

Granular sludge was used as a case study. Six common methods were selected, based on mass balances and microelectrodes. A Monte Carlo simulation was carried out to determine the theoretical precision of each method, considering the uncertainty of various experimental parameters. A model-based simulation of a diffusion experiment was used to determine the theoretical accuracy as a result of six sources of error: solute sorption, biomass deactivation, mass transfer boundary layer, granule roughness, granule shape, and granule size distribution.

Results

Based on the Monte Carlo analysis, the relative standard deviation of the different methods ranged from 5-61%. In a theoretical experiment, the six error sources led to an 37% underestimation of the diffusion coefficient.

Conclusions

This highlights that diffusion coefficients cannot be determined accurately with existing experimental methods. At the same time, the need for measuring precise diffusion coefficients as input value for biofilm modelling can be questioned, since the output of biofilm models has a limited sensitivity towards the diffusion coefficient.

5.1 | INTRODUCTION

Many biological wastewater treatment technologies use biofilms to immobilize essential microorganisms. Trickling filters have been used for more than a century to treat wastewater (Daigger & Boltz, 2011) and more recently, anaerobic, aerobic, and Anammox granular sludge have been introduced. In essence, granules are a special form of biofilms, where bacteria are immobilised in auto-generating biomass particles instead of growing on a carrier surface. Immobilizing the biomass allows high-rate wastewater treatment because of the efficient separation of granules and treated wastewater. High volumetric conversion rates can be achieved due to the increased liquid/solid mass transfer surface area in granular sludge reactors (Nicolella et al., 2000).

Before a compound can be converted in a biofilm, it has to diffuse into the biofilm. Diffusion has both negative and positive effects on biofilm performance. On the one hand, diffusion will limit the effectiveness of a biofilm. Microorganisms located deeper in the biofilm experience lower substrate concentrations than those located at the biofilm surface. Consequently, the organisms deeper in the biofilm convert substrates at a reduced rate or are inactive. On the other hand, diffusion creates different redox conditions throughout a biofilm. Therefore, multiple biological reactions can take place within a single reactor (de Kreuk et al., 2005; Vlaeminck et al., 2012) and a separate reactor for each conversion is not required. The overall conversion rates can be steered by controlling the diffusion depth of rate-limiting soluble substrates (e.g., oxygen, nitrate, ammonium, carbon sources). Therefore, to optimize the conversion rates in biofilm-based wastewater treatment, a proper understanding of the diffusion process is required.

Extracellular polymeric substances and microbial cells in a biofilm hinder the diffusion of solutes into the biofilm. As a result, the diffusion coefficient for a solute in a biofilm is lower than the diffusion coefficient of the same solute in water (Stewart, 2003). The impact of the biofilm matrix on the diffusion coefficient of a solute depends on the solute properties, which includes size and charge (Hinson & Kocher, 1996; Stewart, 1998), and biofilm properties, such as density (Fan et al., 1990; Horn & Morgenroth, 2006). Many researches have studied diffusion of different solutes in different biofilms, with methods such as steady-state flux measurements (Beyenal & Tanyolac, 1994; Livingston & Chase, 1989; W.T. Tang & Fan, 1987; Williamson & McCarty, 1976), transient uptake measurements (Fan et al., 1990; Westrin & Zacchi, 1991), and microelectrode measurements (Fu et al., 1994; Kühl & Jørgensen, 1992; Lewandowski et al., 1991; Revsbech et al., 1986). A review by Stewart (1998) highlighted the wide range of diffusion coefficients described in literature, even for the same solutes. This

was partially attributed to differences in biofilm density, but very few studies have been done after publication of this review to verify this hypothesis (Guimerà et al., 2016; Horn & Morgenroth, 2006). The wide range of values makes it difficult to know which diffusion coefficients to use in biofilm models or kinetic analyses. Possibly, as suggested by Stewart (1998), the large variation in diffusion coefficients is the result of the variety of biofilms that exist. Another possibility, that has often been overlooked, is the quality of the methods that were used to determine the biofilm diffusion coefficients. The precision or accuracy in the methods might be an important factor in the reported variation. To our knowledge, the methods to determine biofilm diffusion coefficients have never been reviewed comprehensively. Westrin et al. (1994) have given an overview for diffusion coefficient measurements in hydrogels, but several methods commonly used to study biofilms were not included.

The aim of this paper was to illustrate fundamental shortcomings of methods to measure biofilm diffusion coefficients. To limit the scope of this study, aerobic granular biofilms were used as example case. We selected six common methods and used an uncertainty and sensitivity analysis based on Monte Carlo simulations to determine the theoretical precision of each method. Furthermore, we assessed the theoretical accuracy of one method with simulations of six illustrative examples. The examples were solute sorption, granule deactivation, boundary layer, granule roughness, granule shape, and granule size distribution. We found significant method limitations for both precision and accuracy. Furthermore, we discuss the translation of the results to biofilms in general, as well as the implications of our findings for process engineering of biofilm reactors.

5.2 | MATERIALS & METHODS

5.2.1 | Selection of methods

The methods evaluated in this paper were selected based on literature (Stewart, 1998). We chose to exclude light or fluorescence-based methods as they are generally limited to thin or translucent biofilms. Magnetic resonance-based methods are excluded as well, since they only apply to paramagnetic molecules or water. The diaphragm cell was excluded as it does not apply to granular biofilms. Methods 1-3 are based on mass balance calculations, while method 4-6 are based on microelectrode measurements. Note that the steady-state methods (1, 4, and 5) yield the effective diffusive permeability, while the transient methods (2, 3, and 6) yield the effective diffusivity. If the diffusion process is framed in terms of only the biofilm water volume, the effective

diffusivity is the proper parameter. However, if the diffusion process is framed in terms of the whole biofilm volume (including cells and polymeric matrix), the effective diffusive permeability is the right parameter. As a consequence, both parameters typically differ by a factor equal to the porosity. For determination of the steady-state flux into a biofilm, the effective diffusive permeability is required (see Stewart (1998) for a detailed explanation). The theory of six selected methods is briefly described below, with relevant equations given in Supplementary Information A.

Method 1: Steady-state reaction. This method determines the apparent flux of a solute into granules, from the apparent granule area and the concentration change of the solute in the liquid phase. A diffusion-reaction equation (see Supplementary Information A) is then solved iteratively, to match the apparent flux into the granules and the liquid phase concentration. The diffusion coefficient is varied to obtain the best fit, thus kinetic constants should be known *a priori*. This method has been used extensively in the past (Beyenal & Tanyolac, 1994; Livingston & Chase, 1989; W.T. Tang & Fan, 1987; Williamson & McCarty, 1976).

Method 2: Transient uptake of a non-reactive solute. In this method, granules that are free of solute are placed in a well-mixed solution of finite volume and known concentration of a solute. The uptake of the solute into the granules follows Fick's 2nd law of diffusion and the diffusion coefficient is obtained by least-squares fitting of the liquid phase concentration (Crank, 1975, pp. 93-96; Westrin & Zacchi, 1991). This method works with inert molecules or with deactivation of the biomass.

Method 3: Transient release of a non-reactive solute. This method is the reverse of the previous method. The granules are soaked with a solute before being placed in a solution of finite volume that is initially free of solute. The increase in liquid phase concentration can be used to obtain the diffusion coefficient (Crank, 1975, pp. 93-96).

Method 4: Steady-state concentration profiles inside and outside a granule. In this method, microelectrodes are used to measure the concentration profile of many small molecules (e.g., oxygen) within a granule. Under steady-state conditions, the flux into the granule equals the flux through the concentration boundary layer. Both fluxes can be determined from the local concentration gradient and the local diffusion coefficient. If the diffusion coefficient in the boundary layer is known, the diffusion coefficient in the granule can be calculated (Cronenberg & Van Den Heuvel, 1991; Hille et al., 2009; Lewandowski et al., 1991).

Method 5: Steady-state reaction with concentration profile inside a granule. This method is a combination of method 1 and 4 and is useful when the concentration

gradient in the boundary layer is not clearly detectable. The apparent flux into a granule can be estimated from the change in liquid phase concentration, granule area and bulk volume (Hille et al., 2009; Horn & Morgenroth, 2006). This apparent external flux equals the internal flux, which can be calculated from the concentration gradient within a granule and the unknown solute diffusion coefficient. When the concentration gradient within a granule is measured with a microelectrode, the diffusion coefficient is the only unknown parameter.

Method 6: Transient penetration of a solute to the centre of a granule. With a microelectrode tip placed in the centre of a single granule and a step-change in liquid phase concentration, a concentration profile in the centre of the granule can be obtained. This profile follows Fick's 2nd law of diffusion, and a least-squares fitting can be used to obtain the diffusion coefficient (Beuling et al., 2000; Crank, 1975, pp. 90-91; Cronenberg & Van Den Heuvel, 1991; Hille et al., 2009).

5.2.2 | Model experimental system

In order to assess precision and accuracy in an easy and flexible manner, virtual experiments were carried out. These virtual experiments were done with a model system: granules with certain properties and a solute with certain properties. For clarity, the properties of the model system were kept constant throughout all simulations (see Table 5.1). Oxygen was used as the diffusing solute and the reaction kinetics were taken from the first biofilm benchmark problem (Morgenroth et al., 2004). For each of the six methods described in the previous section, an experimental dataset was simulated based on the corresponding model equations and experimental parameters (see Supplementary Information B). The simulated experimental dataset of a method should be similar to a dataset that an experimentalist would obtain with that specific method. We chose to simulate experimental datasets instead of using published datasets, to have full control over the input variables and to have a separate evaluation of precision and accuracy. Still, experimental parameters (e.g., experiment duration, microelectrode step size) were taken from literature when possible. A full overview of the experimental parameters, the governing equations, and the resulting simulated experimental data is given in Supplementary Information A, B, and C.

Table 5.1. Characteristics of the granular sludge and solute, which will be used in all subsequent simulations.

Parameter	Value	Unit	Reference
Granule radius (r_g)	1.5e-3	m	-
Granule diffusion coefficient (D_g)	1.2e-9	$m^2\ s^{-1}$	(Stewart, 2003)
Bulk diffusion coefficient (D_{aq})	2.0e-9	$m^2\ s^{-1}$	(Stewart, 2003)
Biomass concentration (C_X)	10,000	$gCOD\ m^{-3}$	(Morgenroth et al., 2004)
Maximum uptake rate (q_{max})	3.54	$gO_2\ gCOD^{-1}\ d^{-1}$	(Morgenroth et al., 2004)
Half saturation coefficient (K)	0.2	$g\ m^{-3}$	(Morgenroth et al., 2004)

5.2.3 | Simulations to determine precision

The precision of a method refers to the closeness of two or more measured values to each other. Here, the theoretical precision of each method was quantified by the relative standard deviation (RSD) of each method. The RSD was obtained from an uncertainty analysis with Monte Carlo simulations. For each method, typical experimental parameters with corresponding experimental uncertainty were defined. By sampling and propagating this input uncertainty through the measurement methods with Monte Carlo simulations, the theoretical precision of the diffusion coefficient determination could be quantified. The major contributors to the imprecision of the measurements were determined by a sensitivity analysis.

Step 1: Uncertainty analysis

The uncertainty of the parameters that were required as input was estimated based on literature when possible (see Table 5.2). The uncertainty of the remaining five parameters was estimated to our best knowledge: the total volume (sum of liquid and granule volumes), the liquid phase concentration, and the microelectrode concentration were considered quite well known and an RSD of 1% was chosen. The uncertainty in granule volume and granule radius were set to 5% and 10% respectively, according to our own laboratory experience. Lastly, the granule biomass concentration uncertainty was set to 25%. This high value was deemed reasonable, due to the complexity of estimating the microbial cell concentration in the granule. All parameters were assumed to follow a normal distribution and correlation between parameters was not considered. The parameter space of each method was sampled with Latin Hypercube Sampling (LHS) with 1000 samples (McKay et al., 1979; Sin et al., 2009).

Table 5.2. Parameters used in the Monte Carlo simulations including the RSD involved in each parameter and the method, described in Materials & Methods, they are required for. The uncertainty was approximated to be either 1, 5, 10, 25 or 50% RSD, since more accurate estimates could not be made.

Parameter	RSD	Methods	Reference
Granule volume (V_G)	5%	1-3, 5	-
Total volume (V_T)	1%	1-3, 5	-
Granule radius (r)	10%	1-3, 5, 6	-
Bulk concentration (C_B)	1%	1-3, 5, 6	-
Biomass concentration (C_X)	25%	1	-
Half saturation constant (K)`	50%	1	(Sin et al., 2009)
Maximum uptake rate (q_{max})	5%	1	(Sin et al., 2009)
Microelectrode concentration (C_M)	1%	4, 5, 6	(Bryant et al., 2010)
Microelectrode step size (dx)	10%	4, 5	(Cronenberg & Van Den Heuvel, 1991)

Step 2: Model simulation

The Monte Carlo simulations were carried out for each of the six methods (section 5.2.1) separately. For each method, 1000 LHS-sampled datasets were used to fit the simulated experimental datasets of step 1. The procedure to fit the datasets is given in the Supplementary Information A. Due to the changing input parameters, each Monte Carlo simulation step resulted in a slightly different diffusion coefficient. The 1000 combined diffusion coefficients yielded a distribution with a certain standard deviation. The distribution was checked visually for normality, and the RSD was used as the precision of the method. The difference in the diffusion coefficient used to simulate the experimental dataset (Table 5.1) and the mean of the diffusion coefficient distribution, was used as a measure of the inherent accuracy of the method.

Step 3: Sensitivity analysis

A sensitivity analysis was performed to determine the relative importance of the input parameters in the uncertainty in the diffusion coefficient. The analysis consisted of a multivariate linear regression of the model output (diffusion coefficient) on the model inputs (Saltelli et al., 2008). The standardized regression coefficients, β_i, were obtained by mean-centred sigma-scaling (Helton & Davis, 2003). The model was considered sufficiently linear if the coefficient of determination (R^2) was equal to or larger than 0.7 (Sin et al., 2011). An input parameter was considered significant only if its absolute β_i^2 value was greater than 0.01 (Sin et al., 2011). For a concentration profile in time or

space, each data point gave a unique regression coefficient. In that case, the β_i^2 values of each data point were summed together to obtain a β_i^2 that represents the aggregate impact of the uncertainty in concentration measurements.

5.2.4 | Simulations to determine accuracy

Accuracy refers to how close a measured value is to a true value. The accuracy of a method can be limited by simplifications of real conditions, which are often needed to estimate diffusion coefficients in granules. The simplifications that lead to inaccurate measurements are also called systematic errors. The impact of such systematic errors is assessed in this paper. We have selected several potential errors based on prevalence and potential impact, according to our own insight. The potential errors are meant to be illustrative and therefore do not necessarily apply to all the methods described in section 5.2.1. The estimation of the inaccuracy due to solute sorption and biomass deactivation, was based on Stewart (1996) and Stewart (1998), respectively. A detailed description is given in the Supplementary Information D.

The impact of several other errors is estimated with a mathematical model, which compares the experiment with and without the assumptions. The model is based on method *transient uptake of a non-reactive solute*, as described in section 5.2.1. The granule is simulated with a 2D-axisymmetric model. The base model consisted of a single granule in water with an α (the ratio of liquid volume over granule volume) of 4. The initial solute concentration in the liquid was 10 g/L, while the granule was initially free of solute. Other granule characteristics are as described in Table 5.1. The diffusion coefficient in the bulk liquid was set to an artificially high value of $1 \cdot 10^9$ m^2 s^{-1} to simulate a perfectly mixed reservoir. The model simulated the concentration change over time until equilibrium was reached. The concentration data of the bulk liquid were extracted from COMSOL and used as input data to determine the diffusion coefficient (according to the standard procedure for method *transient uptake of a non-reactive solute*, as described in section 5.2.1). The standard procedure did not consider any systematic error and the difference between the diffusion coefficient that was used in COMSOL ($1.2 \cdot 10^{-9}$ m^2 s^{-1}) and the fitted diffusion coefficient therefore equalled the inaccuracy caused by the simplifications of the measurement. The following systematic errors were considered in COMSOL (see Figure 5.1):

- **Mass transfer boundary layer.** A mass transfer boundary layer (MTBL) was added to the model. The MTBL thickness was set to 100 µm (estimated based on Horn and Morgenroth (2006); Rasmussen and Lewandowski (1998)), with a diffusion coefficient of $2 \cdot 10^{-9}$ m^2 s^{-1}.
- **Surface roughness.** The granule surface in the model was changed from smooth to sinusoidal. The amplitude of the sine wave was 50 µm and the period was set to 10 sine waves for the full granule radius (see Figure 5.1b). The average granule radius was kept at 1.5 mm, and therefore the granule volume remained unchanged. The diffusion coefficient in the pores (liquid volume within the maximum granule diameter) was set to $2 \cdot 10^{-9}$ m^2 s^{-1}.
- **Granule shape.** The shape of a granule was changed to an oblate spheroid, with a length of its semi-major axis of 1.80 mm and a length of its semi-minor axis of 1.04 mm. The spheroid had an equivalent spherical diameter of 1.5 mm and a sphericity of 0.95.
- **Granule size distribution.** The model was extended to four differently sized granules to simulate the spread of granule radii present in a sample (Westrin & Zacchi, 1991). Two granules had a radius of 1.5mm, one granule had a smaller radius of (1.5 – δ) mm, and the last granule had a larger radius of (1.5 + δ) mm. Here, δ is the deviation from the mean diameter. It was set to 0.5 mm.

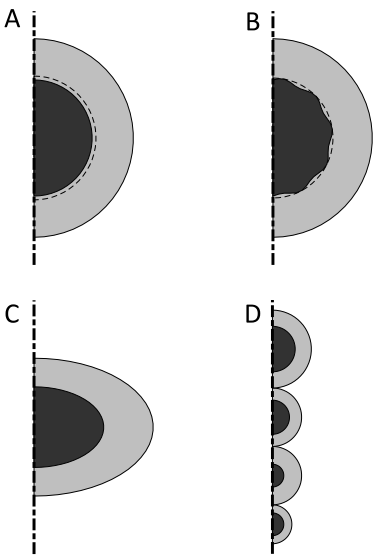

Figure 5.1. Geometry of the four systematic errors that were simulated in COMSOL, based on the typical values. The black area represents the granule, the grey area represents the bulk liquid, and the dash-dotted line represents the axis of symmetry. (A) Concentration boundary layer, with the dashed line indicating the layer thickness. (B) Surface roughness, with the dashed line indicating the liquid volume within the maximum granule diameter where no convection occurs. (C) Granule shape. (D) Granule size distribution, with one bigger, one smaller, and two average granules. Note that figure (D) is drawn to a different scale.

A sensitivity analysis was carried out for each systematic error to investigate the influence of the chosen parameters on the accuracy. The values described here were used as typical values.

5.3 | RESULTS & DISCUSSION

5.3.1 | Precision

A Monte Carlo uncertainty analysis was used to determine the theoretical precision of six common methods to estimate diffusion coefficients. The analysis yielded the precision and the inherent accuracy of each method. The precision was defined as the RSD. The inherent accuracy was defined as the difference between the true diffusion coefficient used to simulate the experimental datasets and the average fitted diffusion coefficient. An example of the output for one method (*transient uptake of a non-reactive solute*) is given in Figure 5.2. The uncertainty analysis to quantify the precision of each method revealed a wide spread among the methods (see Table 5.3). The RSD ranges from 5% (*steady-state concentration profiles inside and outside a granule*) to 61% (*steady-state reaction*). This wide range shows that there are significant differences between the methods. It suggests that the impreciseness of the methods could indeed be a major source of the wide range of diffusion coefficients reported in literature (Stewart, 1998). Strikingly, the *steady-state reaction* method is simultaneously the least precise method and one of the most frequently used methods in past research (Arvin & Kristensen, 1982; Beyenal & Tanyolac, 1994; Herrling et al., 2015; Khlebnikov et al., 1998; Livingston & Chase, 1989; Mulcahy et al., 1981; W.T. Tang & Fan, 1987; Wagner & Hempel, 1988; S.C.P. Wang & Tien, 1984; Williamson & McCarty, 1976; Yano et al., 1961; Yu & Pinder, 1994).

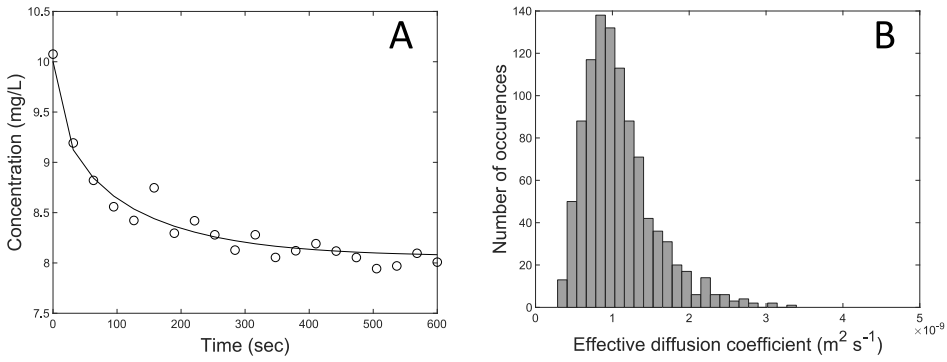

Figure 5.2. Uncertainty analysis output for the transient uptake of a non-reactive solute method. (A) Simulated dataset with simulated experimental data (dots) and example model fit (solid line). (B) Distribution of fitted diffusion coefficient for 1000 Monte Carlo simulations.

Mass balance-based methods

None of the mass balance-based methods (methods 1-3) were precise, with RSD always greater than 33%. A clear comparison between our simulated precision and experimental precisions reported in literature was not possible. Diffusion experiments in a laboratory are often carried out only once, due to the time and effort required per experiment. This also limits the usefulness of replicate measurements. The standard error of the mean of an experiment is given by $\sigma_{\bar{x}} = \frac{\sigma}{\sqrt{n}}$, where σ is the standard deviation of the method and n is the number of replicates. With an RSD of 33%, the relative standard error is 19%, 15%, or 10% for 3, 5, and 10 replicate measurements, respectively.

The uncertainty in the granule volume was a major source of imprecision for the *transient uptake and transient release of a non-reactive solute methods*. The input uncertainty was only 5%, but it accounted for 31% and 57% of the total uncertainty of the *transient uptake* and *transient release* methods, respectively (see Supplementary Information F). The *transient release* and *transient uptake* methods are quite similar, but the *release* method is more precise. This could be expected, since the relative concentration change in the *release* method is greater than in the *uptake* method (see Supplementary Information C). As a result, the concentration uncertainty accounted for less than 1% and 33% of the total uncertainty of the *transient release* and *transient uptake* methods, respectively. For the *steady-state reaction* method, the biomass concentration in the granule was the major source of uncertainty (49% of total uncertainty). This parameter is not easily measured, but it apparently plays a significant role for this method. The granule radius also had a major effect on the precision of the methods (6-37% of total uncertainty).

A substantial inherent inaccuracy was present for the *steady-state reaction* method (19%), which could be caused by non-linearity of the data processing. The distribution of diffusion coefficients of the Monte Carlo analysis is skewed, indicating that input uncertainties are amplified more in one direction than the other (see Supplementary Information E). This inherent inaccuracy is difficult, if not impossible, to identify with conventional experiments. In our analysis, the inherent inaccuracy in the data processing could be identified, because we used virtual experiments. The diffusion coefficient used to design these virtual experiments was known and could directly be compared with the output diffusion coefficient. The inherent inaccuracy of the other methods can be found in Table 5.3.

Table 5.3. Results of Monte Carlo simulation with RSD and inherent inaccuracy per method. A complete overview of the sensitivity analysis results is given in Supplementary Information F.

Method	RSD	Inaccuracy
1 Steady-state reaction	61%	19%
2 Transient uptake of a non-reactive solute	42%	-10%
3 Transient release of a non-reactive solute	33%	5%
4 Steady-state concentration profiles inside and outside a granule	5%	19%
5 Steady-state reaction with concentration profile inside a granule	12%	16%
6 Transient penetration of a solute to the centre of a granule	20%	-1%

Microelectrode based methods

Overall, microelectrode-based methods (methods 4-6) were more precise than mass balance-based methods. The RSD was always 20% or lower, which agrees with Etterer (2006). However, Chiu et al. (2007b) report a higher RSD of 30-40%. Microelectrode measurements are highly localized and rely less on granule parameters, like granule volume, granule area, or granule radius. They are thus less impacted by the relatively large uncertainty in these parameters (see Table 5.2). For microelectrodes, many replicates are done relatively easy (Horn & Morgenroth, 2006). However, these replicates cannot be considered as true repeat measurements. The granules are heterogeneous and multiple granules may have different diffusive properties (Wilén et al., 2004). The repeat measurements in microelectrode studies are required to average spatial heterogeneity. Van Loosdrecht et al. (1995) and Ning et al. (2014) have shown that oxygen profiles at multiple locations can differ significantly and lead to a wide range of calculated flux values.

Similar to the mass balance-based methods, the largest sources of uncertainty for the microelectrode-based methods are the granule volume and granule radius (see Supplementary Information F). Input parameters that are specifically related to microelectrodes are of limited importance. Only for the *steady-state concentration profiles inside and outside a granule* method is the relative impact of microelectrode concentration measurement and microelectrode position significant. However, given the overall high precision of this method (5% RSD), their absolute impact is small. The *steady-state reaction with concentration profile inside a granule* is affected by both the granule radius (74% of total uncertainty) and the granule volume (19% of total uncertainty). The dependence on these uncertain parameters leads to a total uncertainty of 12% RSD. Still, it is significantly more precise than the mass balance-based methods. The *transient penetration of a solute to the centre of a granule* is almost solely

affected by the granule radius, resulting in a lower precision as well (compared to *steady-state concentration profiles inside and outside a granule*).

Recommended method for granular sludge

The ideal method to measure diffusion coefficients can be used for a wide range of solutes, measures diffusion coefficients on a global scale, and combines a high precision with a high accuracy. It is clear that none of the methods analysed meet these requirements. Microelectrodes offer high precision, but they are limited to the molecules for which a microelectrode is readily available, and they only measure locally. We therefore recommend the use of the second method, *transient uptake of a non-reactive solute*, for future experiments. Since its large imprecision makes this method far from ideal, it is an inferior method that is nonetheless the best option. Despite its large imprecision, this method has the potential to determine the order of magnitude of diffusion coefficients for a wide range of solutes. The third method, *transient release of a non-reactive solute*, is more precise, but we expect more practical issues. For example, one major issue is transferring granules soaked with some solute from one solution to another, without transferring excess water that is retained between granules. Note that this recommendation is specific for spherical biofilms, for flat biofilms a diaphragm cell might be the preferred option (see section 5.3.4).

5.3.2 | Accuracy

The impact of six systematic errors was estimated with analytical calculations (solute sorption and deactivation method) and with a COMSOL model (mass transfer boundary layer, surface roughness, shape, and size distribution). The impact of the different systematic errors on the observed diffusion coefficient is shown in Figure 5.3. The figure displays a wide range of under- and overestimations of the true diffusion coefficient. In the most extreme case, the observed diffusion coefficient is more than twice as high as the true diffusion coefficient.

Sorption

Binding of solutes to the granule matrix creates an underestimation of the true diffusion coefficient. A solute that enters a granule has to distribute according to the concentration gradient. If part of the solute binds to the granule matrix, more solute needs to enter the granule before equilibrium is reached. This will require more time and thus lead to an underestimation of the diffusion coefficient. This error only plays a

role with transient methods, since in steady-state the binding of solutes to the matrix is in equilibrium. The nature of the solute will often reveal whether adsorption will be a problem. Hydrophobic molecules (e.g., phenols, phthalates) or charged molecules (e.g., ammonium) are much more likely to adsorb than hydrophilic, neutral molecules. Even though there are some reports that indicate oxygen can adsorb to bacterial cell walls (Beuling et al., 2000; Möller et al., 2005), it is unclear how significant this effect would be for a biofilm. Therefore, no typical error is included.

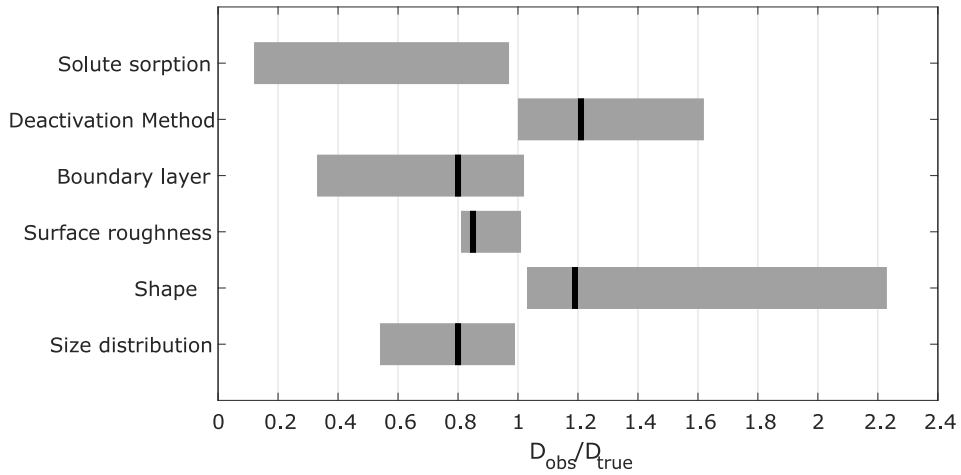

Figure 5.3. Simulated effect of different systematic errors on the observed diffusion coefficient. The bars represent the range of errors that result from the sensitivity analysis (see Supplementary Information G). The black lines indicate the inaccuracy for the typical case.

Deactivation

Permeabilisation of microbial cells leads to an increase in the area available for diffusion, and thereby to a significant overestimation of the diffusion coefficient (up to 60%). Some molecules, such as oxygen, can already diffuse through the cells and will therefore be less impacted (Beuling et al., 2000). Experimental work with nuclear magnetic resonance by Lens et al. (2003) and microelectrodes by Lens et al. (1993) revealed an inaccuracy of similar magnitude due to deactivation of methanogenic granules. Deactivation with glutaraldehyde and mercuric chloride were notable exceptions. Glutaraldehyde caused an underestimation, most likely because it does not permeabilise cells (Azeredo et al., 2003) and even forms cross-links in the EPS matrix (McDonnell & Russell, 1999). Mercuric chloride did not lead to an inaccuracy, but literature reports on its effect are

conflicting (Ames et al., 1986; Fu et al., 1994; Matson & Characklis, 1976; Valko & DuBois, 1944).

Mass transfer boundary layer

Negligence of the mass transfer boundary layer can result in a clear underestimation of the true diffusion coefficient. The layer provides an additional resistance for the diffusing solute, and thus the concentration change will be slower. The error increases with increasing boundary layer thickness. The thickness values tested ranged from 0 to 800 µm, with 100 µm as a typical value (estimated based on Horn and Morgenroth (2006); Rasmussen and Lewandowski (1998)). Reducing the thickness of the boundary layer is not trivial, since it depends on the liquid properties, as well as the slip velocity of the granules (Van Benthum et al., 1999).

Surface roughness

A rough granule surface resulted in a small underestimation of the diffusion coefficient. This may seem counterintuitive since the surface area of a granule increases with its roughness. A higher surface area should lead to an overestimation. However, in the simulation, mass transfer in the liquid volume in the granule valleys was through diffusion only (Picioreanu et al., 2000). The total distance a solute has to diffuse increases with surface roughness, and thus the diffusion coefficient is underestimated. This is in accordance with the findings of Picioreanu et al. (2000), who found that smooth biofilm surfaces allow for maximum mass transfer. Overall, the impact of this error is small, since the roughness amplitude (≤ 100 µm) is small compared to the granule radius (1500 µm).

Shape

Negligence of granule shape can cause a significant overestimation of the diffusion coefficient (up to 120%). A spheroidal granule has a larger surface-to-volume ratio than a perfectly spherical granule. The increase in area leads to a faster change in liquid concentration and thus an overestimation of the diffusion coefficient. Since literature reports of spheroidal granules are common, this is an error that might play a large role (Csikor et al., 1994; Gjaltema et al., 1995; W. Li et al., 2013; Y.-Q. Liu et al., 2006; Schmidt & Ahring, 1996). A correction factor to the measured diffusion coefficient based on observed granule shape might solve this problem partially.

Size distribution

A size distribution of the granular sludge sample can introduce a moderate underestimation of the diffusion coefficient. In the simulation of size distribution, both a smaller granule fraction and a bigger granule fraction are included. Diffusion into the smaller granules proceeds much faster, while diffusion into the larger fraction is much slower. The combined effect is not readily predicted, but the simulation reveals that the larger fraction has a bigger effect. The smaller fraction only impacts the initial concentration change, while the larger fraction increases the time required to reach equilibrium. Therefore, the larger fraction impacts the whole concentration profile, while the smaller fraction only affects the initial part. Our results match with those found by Westrin and Zacchi (1991), who used a similar method to test the impact of the size distribution.

Combined effect

The exact effect of the systematic errors is difficult to quantify since multiple systematic errors might cancel out. However, it seems just as reasonable to expect additive effects of different errors. After all, four out of the six simulated errors lead to underestimations of the diffusion coefficient. If we assume that all errors are multiplicative, we obtain an underestimation of 37% ($D_{observed}/D_{true}$ = 0.63). This highlights the importance of the systematic errors and the need for a thorough analysis of the assumptions that are made. Obviously, other errors, that are not part of this study, can play a role as well. Still, the results highlight that the overall effect can be substantial. We recommend experimentalists to routinely check their diffusion methods for systematic errors in order to maximize accuracy.

5.3.3 | Sensitivity of the diffusion coefficient

At first glance, the simulations of precision and accuracy suggest that the granule surface area is the core parameter that limits the methods. The granule surface area was not included explicitly in the Monte Carlo simulations, but it was implicitly derived from the granule volume and radius. Exactly these two parameters were the biggest contributors to the imprecision of the methods. Furthermore, three out of the six simulated systematic errors (surface roughness, shape, and size distribution) are related to surface area. However, the impact of granule surface area cannot explain all simulation results. For example, the simulation results for method 5 (*Steady-state reaction with concentration profile inside a granule*) suggest that the impact of the granule surface

area is limited. Method 5 depends on granule volume and radius, but it is still quite accurate (12% RSD).

We believe that there is another, more significant reason that limits precision and accuracy. The two most precise methods (methods 4 and 5, see Table 5.3) are based on a direction evaluation of Fick's 1st law. The measurement of the concentration gradient with microelectrodes and a direct measurement of flux allow to directly estimate the diffusion coefficient. In contrast, the four least accurate methods (methods 1, 2, 3, and 6) are based on derivations of Fick's 2nd law. This difference might seem trivial, but that is not the case. We found that all input uncertainties were amplified in methods that depend on Fick's 2nd law. For example, the uncertainty in the granule radius was set to 10% (see Table 5.2). If we carry out a Monte Carlo simulation without considering the uncertainty in other parameters, the precision of method 1, 2, 3, and 6 was always 20% RSD. For other parameters (e.g., granule volume, concentration) the result was amplified by a factor of two as well. This amplification was not observed in methods 4 and 5, which are based on Fick's 1st law. For method 5, a 10% uncertainty in the granule radius led to a precision of 10% RSD.

The aforementioned amplification of uncertainty in Fick's 2nd law suggests that the diffusion coefficient is a parameter with limited sensitivity. Any uncertainty in sensitive parameters (granule volume, radius, etc.) is amplified, leading to imprecise estimates of the diffusion coefficient. This amplification can explain why for some methods, the precision is much worse than the uncertainty of input parameters. For example, method 3 has input uncertainties of 1, 5, and 10%, but the method precision is 33%. Other authors have also found a reduced or limited sensitivity of the diffusion coefficient, at least under certain conditions (Boltz et al., 2011; Harremoës, 1978; Harris & Hansford, 1976; Morgenroth et al., 2004). This reduced sensitivity of the diffusion coefficient is the core reason why diffusion coefficients cannot be measured accurately. Only methods based on Fick's 1st law do not suffer from the reduced sensitivity, but those methods require measurements of the concentration gradient. This means that these methods measure locally and are limited to solutes for which localized measurements are possible.

5.3.4 | Translation to other biofilm types

Even though granular biofilms are an important application of biofilms in wastewater treatment, more biofilm types are being used. Other processes that rely on biofilms are the tricking filter, the moving bed biofilm reactor (MBBR), the membrane biofilm reactor

(MBfR), and the rotating biological contactor (RBC). We believe that the two major reasons that limit diffusion experiments for granular biofilms (biofilm surface area and diffusion sensitivity) apply to flat biofilms as well.

The surface area of biofilm carriers is well-defined, but the actual biofilm surface area is more difficult to estimate. Biofilms growing on carriers can have rough surfaces and the thickness can be non-uniform (for example, see the figures in Gapes and Keller (2009) and Ødegaard (2006)). Furthermore, the relation between biofilm surface area and biofilm volume is not per definition constant with biofilm thickness. Many biofilm carriers have irregular geometries and assuming flat geometry can introduce a systematic error for thicker biofilms. The geometry of typical carriers might also lead to imperfect mixing and mass transfer boundary layers within the carrier (Gapes & Keller, 2009; Nogueira et al., 2015; B. Tang et al., 2017). Even if the estimate of biofilm surface area would be more precise, this does not mean that the methods are more precise. The methods based on Fick's 2nd law still amplify the input uncertainty. Fick's 2nd law can be used to describe both flat and spherical geometry, although the formulation will be slightly different. Thus, the reduced sensitivity of the diffusion coefficient applies to flat biofilms as well.

For flat biofilms, the diaphragm cell is also frequently used to measure biofilm diffusion coefficients (Horn & Morgenroth, 2006). A preliminary Monte Carlo simulation of this method showed that precise results can be achieved, with an RSD of 5% (data not shown). This implies that diffusion coefficients can be measured more precisely in flat biofilms than in spherical ones. However, biofilms have to be either grown directly on the diaphragm membrane or they have to be transferred from their natural environment onto the membrane. The biofilms have to be the exact same shape and size as the membrane to prevent leakage of solutes around the biofilm. For example, Bryers and Drummond (1998) have shown that channels in a biofilm can lead to clear overestimation of the diffusion coefficient. Therefore, although a diaphragm cell is precise, we expect that the measured diffusion coefficients are still relatively inaccurate. Obviously, experimental verification of this hypothesis is required.

Overall, we expect the findings of this paper to translate quite well to other biofilm types. We recommend researchers who want to measure diffusion coefficients in flat biofilms to perform a similar analysis to verify the precision and accuracy of their method of choice.

5.3.5 | Implications for biofilm modelling

Biofilm models are commonly used to predict performance and improve understanding of biofilm reactors. These models often rely on diffusion coefficients, which raises the question how these models are impacted by our findings. At first, it might seem likely that the descriptive and predictive power of the models is reduced with less accurate diffusion coefficients. However, we expect the impact to be limited. The principles that apply to diffusion experiments apply to biofilms models as well. Namely, biofilm models also require input parameters (biofilm thickness, surface area, etc.) that are measured with a certain precision. Furthermore, simplifications that lead to inaccuracy are often implemented in biofilm models as well (Boltz et al., 2010).

The most important reason why inaccurate diffusion coefficients have a limited impact on biofilm models is the sensitivity of the diffusion coefficient towards the predicted flux of solutes into the biofilm. We showed that the diffusion coefficient is a parameter with limited sensitivity in methods based on Fick's 2nd law. Biofilm models typically employ this same law (together with a reaction term) to determine the flux of a solute in or out of a biofilm. It is this flux combined with the biofilm area that ultimately determines the changes in bulk liquid concentration. It has been shown previously that the flux for zero-order kinetics is roughly proportional to the square root of the diffusion coefficient (Harremoës, 1978; Harris & Hansford, 1976). We briefly tested this relationship for Monod kinetics, with a numerical diffusion-reaction model, a single rate-limiting substrate, constant concentration at the granule surface, and parameters from Table 5.1 (see also Supplementary Information H). We observed that a 10% change in the diffusion coefficient led to a change in the flux between 0% and 6% (depending on the penetration depth, see Supplementary Information H for full results). Obviously, these preliminary results should be rigorously verified in future research to determine if there are certain conditions under which the reduced sensitivity does not apply.

Interestingly, the exact reasons why diffusion coefficients cannot be measured with accuracy are simultaneously the reasons why accurate values are not required. Therefore, a better, more accurate method will only marginally improve biofilm models. We suggest to treat biofilm diffusion coefficients as imprecise parameters. Practically, this means that biofilm models do not require a unique relative diffusion coefficient for each solute. It is probably sufficient to set the relative diffusion coefficient to 0.8 for all solutes. This approach is already common practice for biofilm modelling (Boltz et al., 2011; Morgenroth, 2008; Nicolella et al., 1998; Wanner et al., 2006), and our analysis shows why this approach is successful.

5.4 | CONCLUSION

In this simulation study, the theoretical precision of six different methods to measure biofilm diffusion coefficients was evaluated, as well as the theoretical accuracy for one of those methods. The precision of all methods was affected by uncertainty in experimental parameters, although the extent differed per method (RSD of 5-61%). The precision of microelectrode-based methods was higher than that of mass balance-based methods. The least precise method, *steady-state reaction*, has often been used in past research. The experimental parameters with the biggest impact were granule volume, granule radius, and biomass concentration in the granule. These parameters are difficult to identify experimentally and a direct solution for more precise measurements could not be identified. The inaccuracy of the *mass balance – uptake* method was significant, which reduces the reliability of the diffusion coefficient measurements even further. The exact impact of the systematic errors could not be quantified, but an underestimation of the true diffusion coefficient by more than 30% is likely.

Accurate methods for diffusion coefficient measurements are currently not available, but from the point of view of biofilm kinetics they are also not required. The limitations of diffusion coefficient measurements (uncertain experimental parameters, process simplifications, and reduced sensitivity to the diffusion coefficient) apply to biofilm models as well. An imprecise diffusion coefficient will most likely not have a big impact on the descriptive and predictive performance of biofilm models. It might be sufficient to use two relative diffusion coefficients in biofilm models: a high value of 0.5-0.8 for small solutes, such as oxygen, and a low value of 0.1-0.4 for medium-sized solutes, such as glucose and acetate.

SUPPLEMENTARY INFORMATION

Supplementary information A: Input parameters

The input parameters for the different methods are given below. This includes the parameters required to simulate the data and the parameter required to fit the experimental data. The parameters that are required to fit the experimental data are all uncertain, with the uncertainty listed in the main paper.

Table 5.S1. Overview of input parameters for each method for the random error analysis.

Method	Parameter		Unit	Value
1	Total volume	V	m^3	150e-6
1	Granule volume	V_G	m^3	30e-6
1	Bulk concentration	C_B	g/m^3	10
2	Total volume	V_T	m^3	150e-6
2	Granule volume	V_G	m^3	30e-6
2	Initial bulk/granule concentration	C_B	g/m^3	10
2	Experiment duration	t_{range}	min	10
2	Concentration measurements	n	-	20
3	Total volume	V_T	m^3	150e-6
3	Granule volume	V_G	m^3	30e-6
3	Initial bulk/granule concentration	C_B	g/m^3	10
3	Experiment duration	t_{range}	min	10
3	Concentration measurements	n	-	20
4	Bulk concentration	C_B	g/m^3	10
4	Microelectrode step size	rx	m	10e-6
4	Microelectrode penetration depth	d_{micro}	m	300e-6
4	Boundary layer thickness	r_{CBL}	m	100e-6
5	Total volume	V_T	m^3	150e-6
5	Granule volume	V_G	m^3	30e-6
5	Bulk concentration	C_B	g/m^3	10
5	Microelectrode step size	rx	m	10e-6
5	Microelectrode penetration depth	d_{micro}	m	300e-6
5	Boundary layer thickness	r_{CBL}	m	100e-6
6	Initial bulk concentration	C_B	g/m^3	10
6	Experiment duration	t_{range}	min	15
6	Measurement interval	t_{meas}	sec	20

Supplementary information B: Model equations for random error analysis

Steady-state reaction

The flux into the granule (J in g/m^2/s) is calculated based on the bulk volume (V_{Bulk} in m^3), the bulk concentration change over time ($(dC/dt)_{Bulk}$ in g/m^3/s), and the granule area ($A_{Granule}$ in m^2):

$$V_{Bulk}\left(\frac{dC}{dt}\right)_{Bulk} = J \cdot A_{Granule} \tag{5.S1}$$

The diffusion-reaction equation is then solved iteratively, to match the flux into the granule and the bulk concentration. The diffusion coefficient is varied to obtain the best fit. If the substrate uptake rate follows Monod kinetics, the diffusion-reaction equation is defined as follows:

$$D_{Granule}\left(\frac{\partial^2 C}{\partial r^2} + \frac{2}{r}\frac{\partial C}{\partial r}\right) = q_{max}\frac{C}{K_S + C}C_X \tag{5.S2}$$

Here, $D_{Granule}$ is the diffusion coefficient (m^2/s), r is the radial position in the granule (m), q_{max} is the maximum uptake rate (1/s), C is the solute concentration within the granule (g/m^3), K_S the half-saturation coefficient (g/m^3), and C_X the biomass concentration (g/m^3).

Transient uptake of a non-reactive solute

The equation that relates the concentration profile to the diffusion coefficient was derived by Crank (1975, pp. 93-96):

$$\frac{C_{Bulk}(t)}{C_{Bulk}(0)} = \frac{1}{1+\alpha}\left(\alpha + \sum_{n=1}^{\infty}\frac{6\alpha(1+\alpha)\exp -\frac{D_{Granule}q_n^2 t}{r_{Granule}^2}}{9 + 9\alpha + q_n^2\alpha^2}\right) \tag{5.S3}$$

Here, $C_{Bulk}(t)$ is the bulk liquid solute concentration at time t (g/m^3), α is the ratio of bulk volume over granule volume, $r_{Granule}$ is the granule radius (m), and the q_n values are the non-zero positive roots of the following non-linear equation:

$$\tan q_i = \frac{3q_i}{3 + \alpha q_i^2} \tag{5.S4}$$

Transient release of a non-reactive solute

The method can also be applied to monitor the release of a solute from the granule into the bulk liquid (Crank, 1975, pp. 93-96).

$$\frac{C_{Bulk}(t)}{C_{Granule}(0)} = \frac{1}{1+\alpha}\left(1 - \sum_{n=1}^{\infty} \frac{6\alpha(1+\alpha)\exp - \frac{D_{Granule} q_n^2 t}{r_{Granule}^2}}{9 + 9\alpha + q_n^2\alpha^2}\right) \quad (5.S5)$$

Here, α and q_n are defined as in the previous method, while $C_{Granule}(0)$ is the initial concentration inside the granules.

Steady-state concentration profiles inside and outside a granule

The diffusion coefficient in the granule can be calculated from the diffusion coefficient in water (D_{aq} in m^2/s), the concentration gradient in the boundary layer ($(dC/dr)_{BoundaryLayer}$ in g/m^4), and the concentration gradient in the granule ($(dC/dr)_{Granule}$ in g/m^4) (Cronenberg & Van Den Heuvel, 1991; Lewandowski et al., 1991):

$$D_{Granule} = D_{aq} \frac{\left(\frac{dc}{dr}\right)_{Boundary\ Layer}}{\left(\frac{dc}{dr}\right)_{Granule}} \quad (5.S6)$$

Steady-state reaction with concentration profile inside a granule

The diffusion coefficient can be calculated from the flux into the granule and the concentration gradient in the granule. The flux into the granule is determined from the bulk volume, the biofilm area and the bulk concentration change (Horn & Morgenroth, 2006):

$$D_{Granule} = \frac{J}{\left(\frac{dc}{dr}\right)_{Granule}} = \left(\frac{dc}{dt}\right)_{Bulk} \cdot \frac{V_{Bulk}}{A_{Granule}} \cdot \frac{1}{\left(\frac{dc}{dr}\right)_{Granule}} \quad (5.S7)$$

Transient penetration of a solute to the centre of a granule

The profile can be calculated with the following equation (Crank, 1975, pp. 90-91):

$$\frac{C_{Granule}(t)}{C_{Bulk}} = 1 + 2\sum_{n=1}^{\infty}(-1)^n \cdot \exp - \frac{D_{Granule} n^2 \pi^2 t}{r_{Granule}^2} \quad (5.S8)$$

Supplementary information C: Simulated datasets for random error analysis

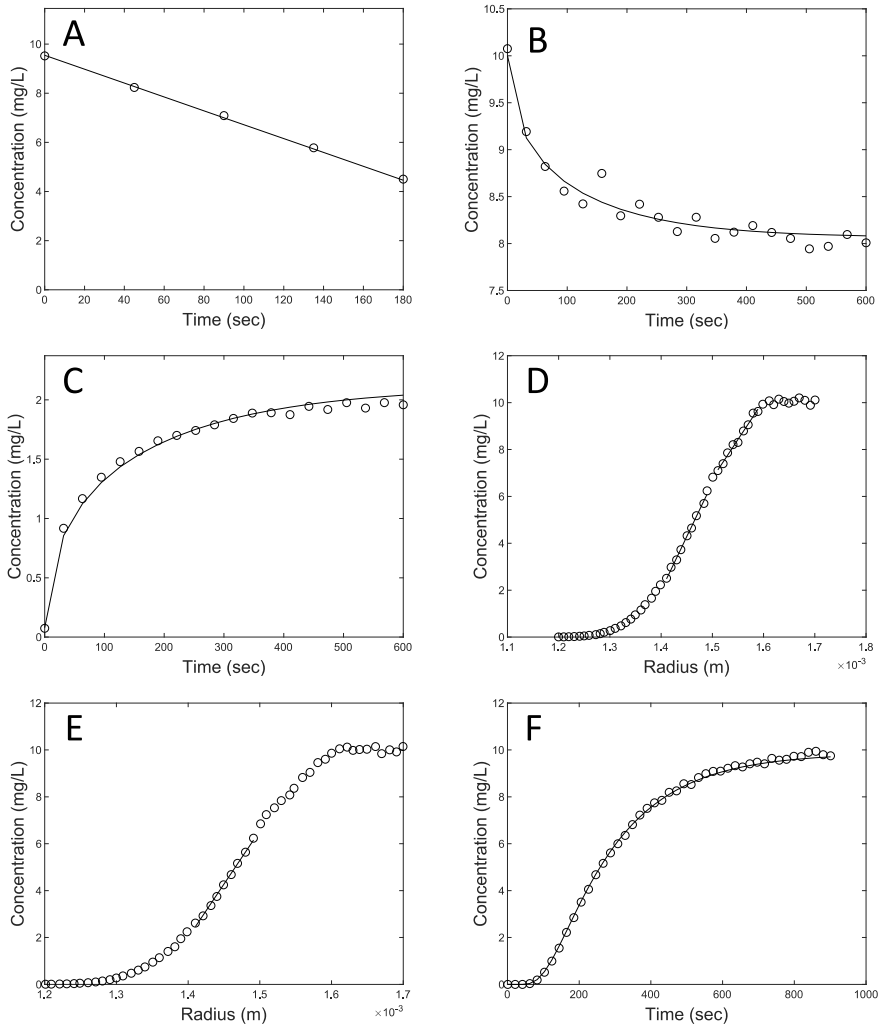

Figure 5.S1. Typical simulated datasets for the six methods included in the random error analysis. The circles represent the experimental data, while the line represent the model fit to the data. The simulated datasets are comparable to a dataset that an experimentalist might obtain with the given method. (A) Steady-state reaction, (B) Transient uptake of a non-reactive solute, (C) Transient release of a non-reactive solute, (D) Steady-state concentration profiles inside and outside a granule, (E) Steady-state reaction with concentration profile inside a granule, (F) Transient penetration of a solute to the centre of a granule.

Supplementary information D: Calculation methods for systematic error analysis

Solute sorption

In transient measurements, a solute can bind to the granule and introduce an error. We considered a solute that sorbs reversibly to the biofilm according to a linear isotherm:

$$S = k \cdot C \tag{5.S9}$$

Here, S is the adsorbed concentration (mass per non-water volume of the biofilm), k is the partition coefficient between the aqueous and biofilm phases, and C is the aqueous concentration. A mass balance over a granule section that considers both the dissolved and adsorbed component, in which only the dissolved solute diffuses, gives rise to the following equation (Stewart, 1996):

$$[\epsilon_W + (1-\epsilon_W)k]\frac{\partial C}{\partial t} = D_{Granule}\left(\frac{\partial^2 C}{\partial r^2} + \frac{2}{r}\frac{\partial C}{\partial r}\right) \tag{5.S10}$$

Here, ε_W is the volume fraction occupied by water. The mass balance in the case of no adsorption is as follows:

$$\epsilon_W \frac{\partial C}{\partial t} = D_{Granule}\left(\frac{\partial^2 C}{\partial r^2} + \frac{2}{r}\frac{\partial C}{\partial r}\right) \tag{5.S11}$$

If adsorption is not considered in the analysis of experimental data, the systematic error will thus be given by:

$$\frac{D_{Obs}}{D_{True}} = \frac{\epsilon_W}{\epsilon_W + (1-\epsilon_W)k} \tag{5.S12}$$

Table 5.S2 lists the adsorption isotherms for different solutes and biofilms that were used in the calculation, based on experiments of Bassin et al. (2011), Kennedy et al. (1992), L. Wang et al. (2019), and Beuling et al. (2000). Adsorption data is generally reported per gVSS, thus a conversion was made where necessary, with a cell density of 350 gVSS/L (Stewart, 1998) and a water fraction of 0.8.

Table 5.S2. Linear adsorption isotherms for different solutes and biomass types in L/gVSS. The units follow from the linear relation between equilibrium concentration (mg/L) and the amount of solute adsorbed (mg/gVSS).

Solute	Biomass type	Isotherm	Reference
Ammonium	Activated Sludge	0.0063	Bassin et al. (2011)
	Activated Sludge	0.0039	Bassin et al. (2011)
	Aerobic Granular Sludge	0.0375	Bassin et al. (2011)
	Aerobic Granular Sludge	0.0200	Bassin et al. (2011)
	Anammox Granular Sludge	0.0046	Bassin et al. (2011)
2-chlorophenol	Anaerobic granular sludge	0.0004	Kennedy et al. (1992)
3-chlorophenol	Anaerobic granular sludge	0.0321	Kennedy et al. (1992)
4-chlorophenol	Anaerobic granular sludge	0.0258	Kennedy et al. (1992)
2,3-dichlorophenol	Anaerobic granular sludge	0.0229	Kennedy et al. (1992)
2,4-dichlorophenol	Anaerobic granular sludge	0.0818	Kennedy et al. (1992)
2,5-dichlorophenol	Anaerobic granular sludge	0.0345	Kennedy et al. (1992)
2,6-dichlorophenol	Anaerobic granular sludge	0.0170	Kennedy et al. (1992)
3,4-dichlorophenol	Anaerobic granular sludge	0.0429	Kennedy et al. (1992)
3,5-dichlorophenol	Anaerobic granular sludge	0.0084	Kennedy et al. (1992)
2-nitrophenol	Anaerobic granular sludge	0.0191	Karim and Gupta (2002)
4-nitrophenol	Anaerobic granular sludge	0.0233	Karim and Gupta (2002)
2,4-nitrophenol	Anaerobic granular sludge	0.0265	Karim and Gupta (2002)
Dimethyl phthalate	River biofilm	0.0060	L. Wang et al. (2019)
	River biofilm	0.0058	L. Wang et al. (2019)
	River biofilm	0.0072	L. Wang et al. (2019)
	River biofilm	0.0035	L. Wang et al. (2019)
Dibutyl phthalate	River biofilm	0.0065	L. Wang et al. (2019)
	River biofilm	0.0071	L. Wang et al. (2019)
	River biofilm	0.0079	L. Wang et al. (2019)
	River biofilm	0.0043	L. Wang et al. (2019)
Di(2-ethylexyl)phtalate	River biofilm	0.0083	L. Wang et al. (2019)
	River biofilm	0.0204	L. Wang et al. (2019)
	River biofilm	0.0200	L. Wang et al. (2019)
	River biofilm	0.0089	L. Wang et al. (2019)
Oxygen	Artificial biofilm	0.0160	Beuling et al. (2000)

Deactivation procedures

For most of the methods, deactivation of the biofilm is required if a reactive solute is used. To evaluate the impact that the deactivation procedure can have on the diffusion coefficient, we used the model of Westrin and Axelsson (1991). This model allows the calculation of the overall diffusion coefficient of a granule based on the granule structure (pore volume, EPS volume, cell volume) and diffusivity inside the microbial cells. The model is formulated as follows:

$$\frac{D_{eff}}{\mathfrak{D}_{aq}} = \left(\frac{D_{eff}}{D_{eo}}\right)\left(\frac{D_{eo}}{\mathfrak{D}_{aq}}\right) \tag{5.S13}$$

Here, D_{eff} is the effective diffusive permeability of the biofilm, $\mathfrak{D}_{aq}$ is the diffusion coefficient in water, and D_{eo} is the effective diffusive permeability of the extracellular matrix. The first term describes the effect of the bacterial cells, and the second term describes the effect of the EPS. The first term is predicted with Maxwell's equation for a suspension of permeable spheres (Chresand et al., 1988):

$$\frac{D_{eff}}{D_{eo}} = \frac{2\frac{\mathfrak{D}_{aq}}{D_C} + \frac{\mathfrak{D}_{aq}}{D_{eo}} - 2\epsilon_C\left(\frac{\mathfrak{D}_{aq}}{D_C} - \frac{\mathfrak{D}_{aq}}{D_{eo}}\right)}{2\frac{\mathfrak{D}_{aq}}{D_C} + \frac{\mathfrak{D}_{aq}}{D_{eo}} + \epsilon_C\left(\frac{\mathfrak{D}_{aq}}{D_C} - \frac{\mathfrak{D}_{aq}}{D_{eo}}\right)} \tag{5.S14}$$

Here, D_c is the effective diffusive permeability in the bacterial cells, and ε_C is the volume fraction occupied by the cells. The second term of equation S13 is predicted based on the EPS and cell content of the biofilm (Westrin & Axelsson, 1991):

$$\frac{D_{eo}}{\mathfrak{D}_{aq}} = \frac{\left(1 - \frac{\epsilon_P}{1-\epsilon_C}\right)^3}{\left(1 + \frac{\epsilon_P}{1-\epsilon_C}\right)^2} \tag{5.S15}$$

Here, ε_P is the volume fraction occupied by EPS. The degree to which the deactivation procedure breaks open the cell membranes and permeabilizes the cells was simulated by varying the effective permeability in the bacterial cells (D_c). This permeability ranged from 0 (the cells are intact and a solute cannot diffuse through) to the permeability of the extracellular matrix (D_{eo}). A typical granule composition was set with a porosity of 0.8, a cell volume fraction (ε_C) of 0.17, and an EPS volume fraction (ε_P) of 0.03.

Supplementary information E: Diffusion coefficient distribution from random error analysis

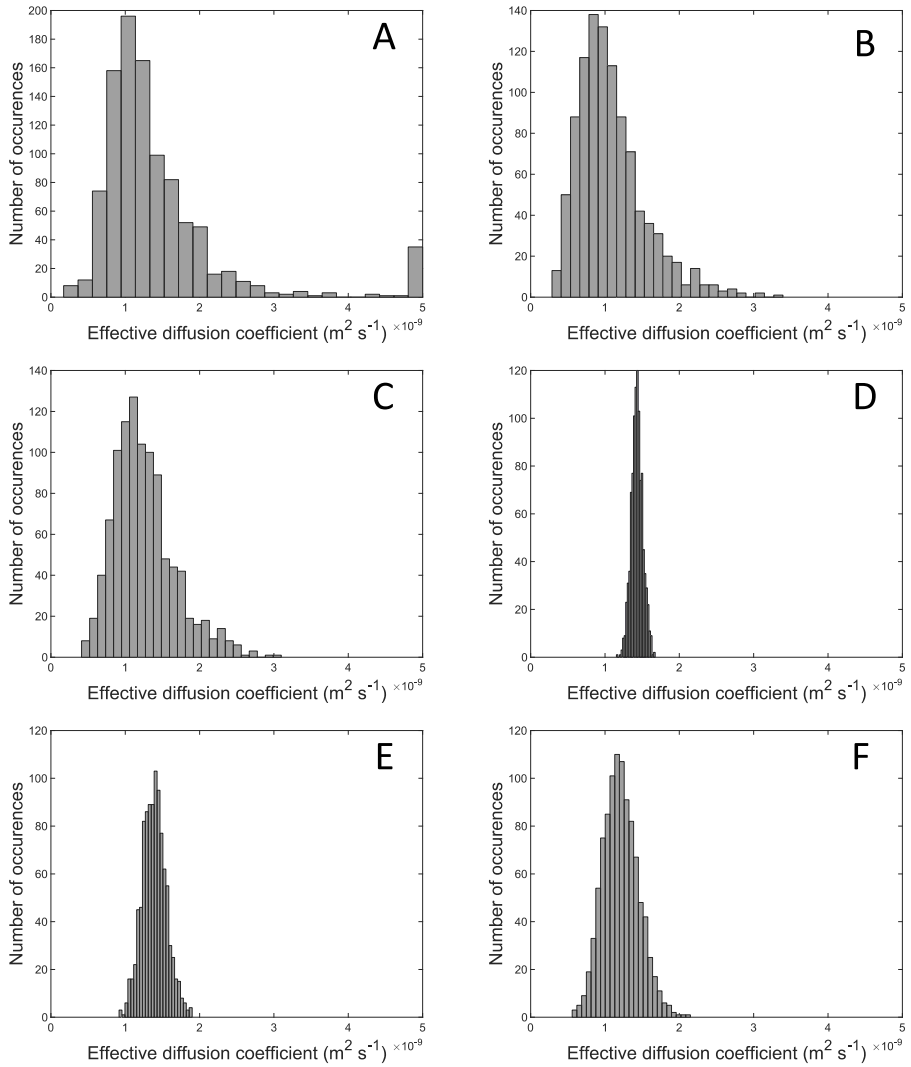

Figure 5.S2. Uncertainty analysis results: Diffusion coefficients obtained from Monte-Carlo simulations plotted as histograms. A total number of 1000 Monte-Carlo simulations were used. (A) Steady-state reaction, (B) Transient uptake of a non-reactive solute, (C) Transient release of a non-reactive solute, (D) Steady-state concentration profiles inside and outside a granule, (E) Steady-state reaction with concentration profile inside a granule, (F) Transient penetration of a solute to the centre of a granule.

Supplementary information F: Standardized regression coefficients from random error analysis

Table 5.S3. Squared standardized regression coefficients (β_i^2) of linear models of the diffusion coefficient. For a linear model, the sum of β_i^2 should be equal to 1. Typically, the sum of β_i^2 is equal to or less then the R^2. (A) Steady-state reaction, (B) Transient uptake of a non-reactive solute, (C) Transient release of a non-reactive solute, (D) Steady-state concentration profiles inside and outside a granule, (E) Steady-state reaction with concentration profile inside a granule, (F) Transient penetration of a solute to the centre of a granule.

		(A)	(B)	(C)	(D)	(E)	(F)
	R^2	0.60	0.92	0.95	0.81	0.98	1.00
1	V_g	0.0411	0.3120	0.5663	-	0.1902	-
2	V	0.0008	0.0101	0.0202	-	0.0063	-
3	C_B	0.0001	0.3324	0.0027	-	0.0001	0.0051
4	r_{micro}	-	-	-	0.2254	0.0270	-
5	r_g	0.0649	0.2300	0.3689	-	0.7358	1.0020
6	C_X	0.4883	-	-	-	-	-
7	K	0.0134	-	-	-	-	-
8	q_{max}	0.0120	-	-	-	-	-
9	C_{micro}	-	-	-	0.5653	0.0107	0.0003
Sum of β_i^2		0.62	0.88	0.96	0.79	0.97	1.01

Supplementary information G: Systematic errors: sensitivity results

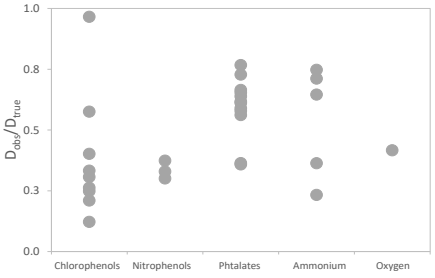

Figure 5.S3. Systematic error due to solute sorption for various types of biofilms, estimated based on reported linear isotherms or Freundlich isotherms that were approximated as linear isotherms.

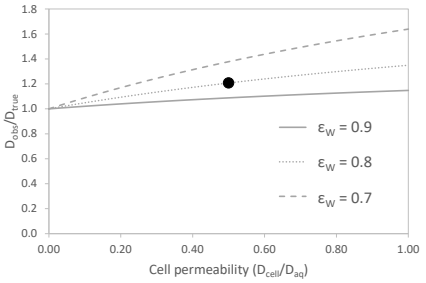

Figure 5.S4. Systematic error as a result of cell permeabilization, for different granule water volume fractions (ε_W). The red dot denotes the typical value.

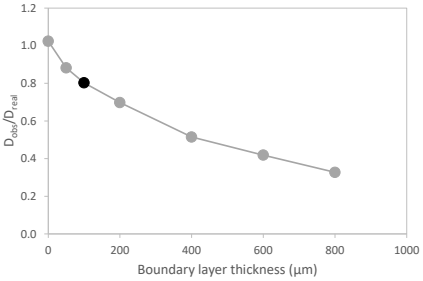

Figure 5.S5. Systematic error due to the boundary layer. The red dot denotes the typical value.

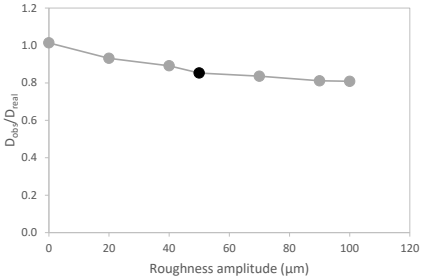

Figure 5.S6. Systematic error from the surface roughness. An amplitude of 0 represents a smooth granule. The red dot denotes the typical value.

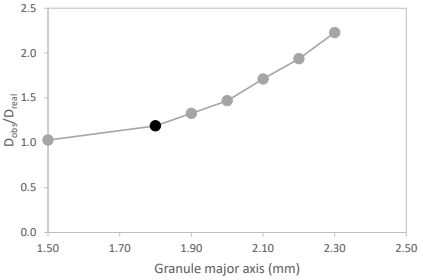

Figure 5.S7. Systematic error as a result of granule sphericity, as function of major ellipse axis for an oblate spheroid. An increase in major axis length indicates a more ellipsoidal granule. The red dot denotes the typical value for a granule major axis of 1.80 mm, and a minor axis of 1.04 mm.

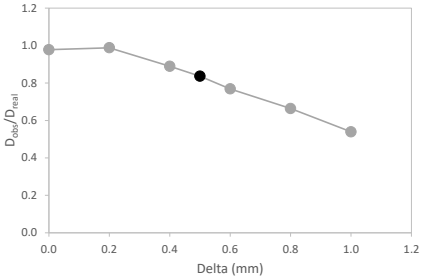

Figure 5.S8. Systematic error through polydispersity. This error was calculated with four granule sizes, two of which had the mean size (1.5 mm diameter), one was smaller by delta, and one was bigger by delta. The red dot denotes the typical value with resulting granule diameters of 1.0 mm, 1.5 mm, 1.5 mm, and 2.0 mm.

Supplementary information H: Diffusion sensitivity model

The preliminary analysis of the sensitivity of the diffusion coefficient in biofilms models was based on a one-dimensional diffusion-reaction equation in spherical coordinates:

$$D_{Granule}\left(\frac{\partial^2 C}{\partial r^2}+\frac{2}{r}\frac{\partial C}{\partial r}\right)-q_{max}\frac{C}{K_S+C}C_X=0, \qquad (5.S16)$$

where $D_{Granule}$ is the diffusion coefficient (m^2/s), r is the radial position in the granule (m), q_{max} is the maximum uptake rate (1/s), C is the solute concentration within the granule (g/m^3), K_S the half-saturation coefficient (g/m^3), and C_X the biomass concentration (g/m^3).

The equation applied to the granule as well as a mass transfer boundary layer (MTBL). The following boundary conditions were used: (1) zero flux at the granule core, (2) flux equality at the granule-MTBL interface, and (3) bulk liquid concentration at the MTBL-bulk liquid interface. The equation and boundary conditions were solved numerically in Matlab with lsqnonlin, a function for non-linear least squares fitting with constraints. A discretization scheme with central difference was applied, with a spatial stepsize of 10 µm. Input parameters were as follows: r_G 1.5 mm, $D_{Granule}$ $1.2 \cdot 10^{-9}$ m^2/s, D_{aq} $2.0 \cdot 10^{-9}$ m^2/s, C_X 10,000 gCOD/m^3, q_{max} 3.54 gO_2/gCOD/d, K_S 0.2 g/m^3, and d_{MTBL} 100 µm. The bulk liquid concentration was varied between 0.001 and 100 gO_2/m^3. This artificial range was chosen to simulate the transition from a barely penetrated granule (with concentrations below K_S) to a fully penetrated one, while only changing a single parameter. A Monte Carlo approach was used with 1000 simulations for each bulk liquid concentration. For each Monte Carlo step, a diffusion coefficient was taken randomly from a normal distribution with $D_{Granule}$ as its mean and a $0.12 \cdot 10^{-9}$ m^2/s standard deviation. The flux was calculated for each Monte Carlo step, which resulted in 1000 flux values per simulation. The sensitivity of the diffusion coefficient was evaluated by $\delta = \frac{\sigma_{Flux}}{\sigma_{DiffusionCoefficient}}$. A δ greater than 1 indicates a high sensitivity, while a δ smaller than 1 indicates a low sensitivity. The results can be seen in Figure 5.S9.

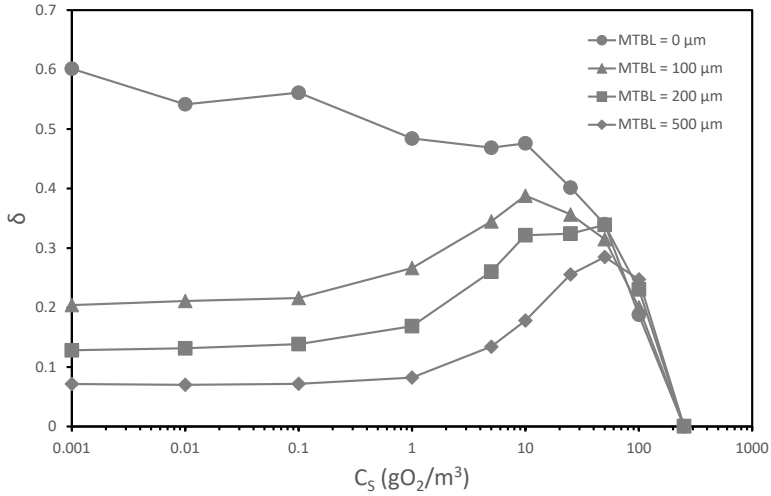

Figure 5.S9. Sensitivity of the diffusion coefficient (δ) as function of the bulk liquid substrate concentration for different mass transfer boundary layer thicknesses (0, 100, 200, and 500 µm thick). A lower δ indicates a lower sensitivity. For low bulk liquid concentrations (C_s < 1 g/m^3) the sensitivity is reduced when a boundary is included. These low concentrations lead to surface reactions. For high bulk liquid concentrations (C_s > 100 g/m^3) the sensitivity approach zero, as the granule becomes fully penetrated.

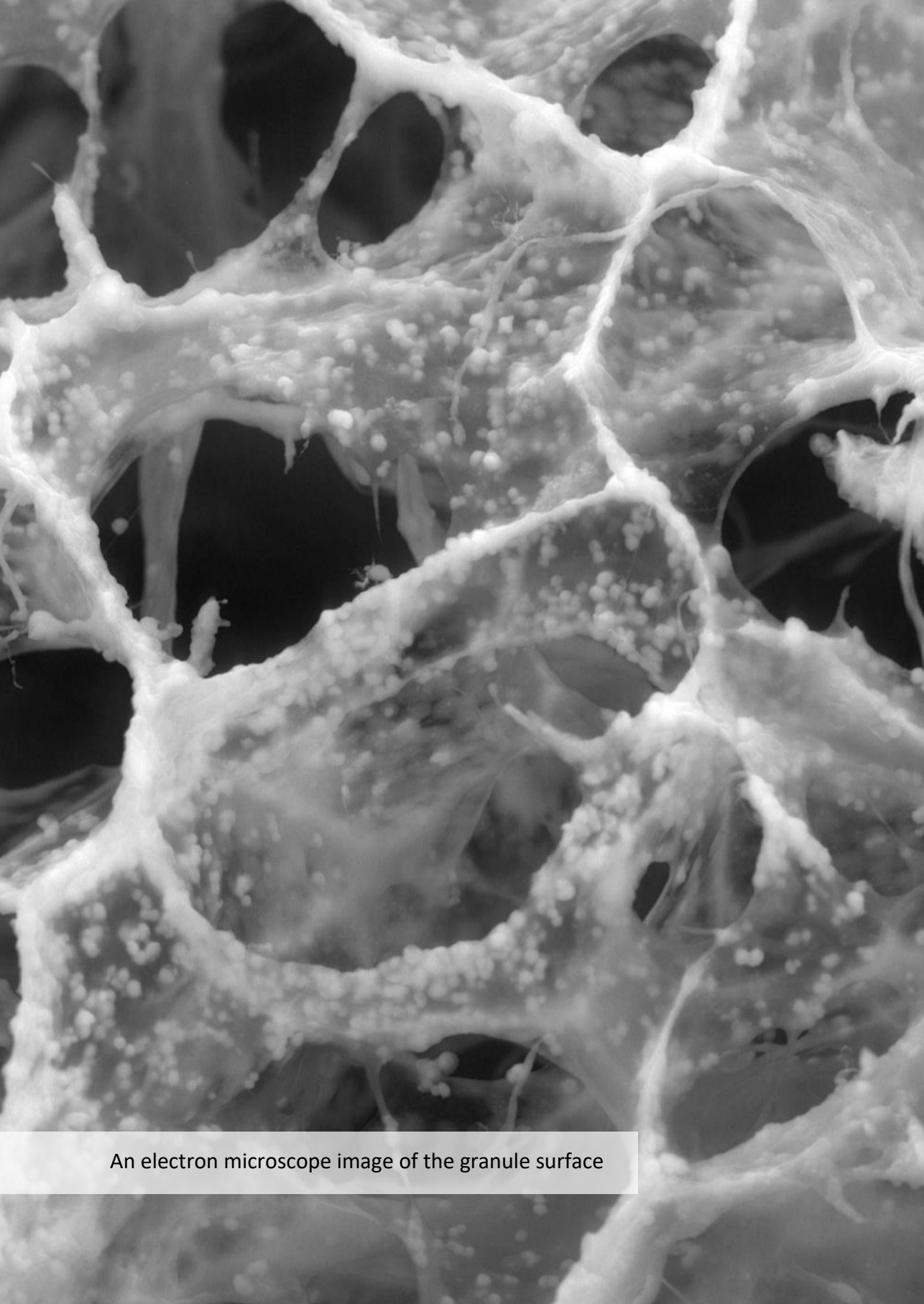

An electron microscope image of the granule surface

6

Diffusion of soluble organic substrates in aerobic granular sludge: Effect of molecular weight

Submitted for publication as: Van den Berg, L., Toja Ortega, S., van Loosdrecht, M. C. M., & de Kreuk, M. K. (2021). Diffusion of Soluble Organic Substrates in Aerobic Granular Sludge: Effect of Molecular Weight.

ABSTRACT

Background

Aerobic granular sludge (AGS) is an advanced biofilm-based technology for wastewater treatment. Diffusion of substrates into the granules is a key aspect of this technology. Domestic wastewater contains soluble organic substrates of different sizes that could potentially diffuse into the granules.

Methods

In this study, the relation between the molecular weight of a substrate and its diffusion coefficient within the granule was studied with model substrates (polyethylene glycols (PEGs) with a molecular weight between 62 and 10 000 Da). The diffusion coefficients of the model substrates within granules from a full-scale installation were measured with the 'transient uptake of a non-reactive solute' method. Furthermore, the granule structure was characterized with Environmental Scanning Electron Microscopy (ESEM). Lastly, the apparent molecular weight distribution of domestic wastewater soluble COD was determined with ultrafiltration membranes of 100, 10, and 1 kDa molecular weight cut-off.

Results

The diffusion coefficients in the granules were not significantly different from the diffusion coefficients in water, at least up to 4000 Da molecular weight. This indicates that these PEGs were not obstructed by the granule matrix. The 10 kDa PEG behaved differently from the smaller PEGs, as it could not penetrate the entire granule. The granules displayed an open structure with large macropores and semi-solid regions, which contained microbial cells. The diffusion results suggest that most diffusing molecules were unobstructed in the macropores and barely obstructed in the semi-solid regions. Only the diffusion of the 10 kDa PEG seemed to be hindered by the semi-solid regions, but not by the macropores. The influent fractionation revealed that a large part (61-69%) of the influent soluble COD was smaller than 1 kDa.

Conclusions

As molecules smaller than 1 kDa diffuse easily, the majority of the influent soluble COD can be considered as diffusible COD. These findings provide new insight into the availability of influent COD for granular sludge.

6.1 | INTRODUCTION

Aerobic granular sludge (AGS) is a recent innovation for the treatment of wastewater (Pronk et al., 2015b). The technology consists of microorganisms that produce extracellular polymeric substances (EPS) to form granular biofilms or granules. Due to the limited penetration of oxygen into the granule, different redox conditions can exist throughout the granule. Therefore, nutrient removal processes such as nitrification, denitrification, and phosphorus uptake, can occur simultaneously in a single reactor (Kishida et al., 2009; D. Wei et al., 2014). Sedimentation tanks are no longer needed due to the high settling velocity of the aerobic granules (Bengtsson et al., 2018). As a result, aerobic granular sludge technology requires less energy and land area compared to conventional activated sludge installations (de Bruin et al., 2004; Pronk et al., 2015b).

Most AGS research has been carried out with lab-scale systems that were fed with small and soluble substrates, like volatile fatty acids (VFAs) or glucose (Adav et al., 2008; de Kreuk et al., 2005; de Sousa Rollemberg et al., 2018). These substrates can diffuse readily into the granules, even into deeper zones (Pronk et al., 2015a). The diffusivity of the substrates has a major impact on the overall performance of granular sludge reactors (Layer et al., 2019). A deep penetration of substrates will contribute to the formation of stable granules and to a high denitrification activity (Layer et al., 2020; Zheng et al., 2006). At the same time, often only a small fraction of real wastewater consists of small and soluble substrates. The concentration of VFAs in domestic wastewater is generally less than 10% of the influent chemical oxygen demand (COD) (Henze et al., 1995). The other soluble substrates in the wastewater can account for 10-20% of the influent COD (Henze et al., 1995). The exact nature and size of this non-VFA soluble COD fraction is poorly understood. Soluble COD can be as small as acetate, but also as large as a colloid (up to 0.45µm). As a result, the diffusion behaviour of the soluble COD in the granules is poorly understood as well.

Diffusion in different biofilms has been researched extensively in the 1980s and the 1990s (Stewart, 1998). However, there are several limitations that hamper our knowledge on diffusion in biofilms and granules. Firstly, most studies focused on small substrates, like oxygen, ammonium, acetate, and glucose (Chiu et al., 2006; S.-Y. Liu et al., 2009; Stewart, 1998). Only a handful of studies have measured diffusion coefficients of molecules that are larger than 300 Da (Bryers & Drummond, 1998; Peulen & Wilkinson, 2011; Takenaka et al., 2009; Thurnheer et al., 2003). It is therefore not clear how the size of a solute affects its diffusion behaviour. Secondly, different studies often yield diffusion coefficients that vary greatly (Stewart, 1998). For example, the mean relative effective diffusion coefficient ($D_{biofilm}/D_{aq}$) for solutes with a molecular weight

between 44 and 342 Da was reported as 0.29 ± 0.24 (Stewart, 1998). This large variability is partially the result of differences in biofilm density between studies (Horn & Morgenroth, 2006), but it is not clear if other factors play a role as well. Lastly, our knowledge on diffusion in biofilms is limited due to the inherent inaccuracy of the methods that are commonly used to measure diffusion coefficients (van den Berg et al., 2021b). Overall, the understanding of diffusion in biofilms and granules is very limited, especially regarding larger molecules (> 300 Da).

The objectives of this study were (1) to determine the effect of the molecular weight of a molecule on its diffusion coefficient in aerobic granules and (2) to determine the distribution of soluble COD in different wastewaters. The diffusion coefficients of different polyethylene glycols (PEGs), uncharged model substrates with a molecular weight between 62 and 10 000 Da, were measured with the 'transient uptake of a non-reactive solute' method. The diffusion behaviour was related to the granule structure observed by ESEM. The distribution of soluble COD in domestic wastewater samples was determined through ultrafiltration with a 100, 10, and 1 kDa molecular weight cut-off. Implications for the design and operation of AGS reactors are discussed.

6.2 | MATERIALS & METHODS

6.2.1 | Granule source

Aerobic granules were harvested from the full-scale Nereda® plant in Utrecht, The Netherlands. The plant treats domestic wastewater with a COD of 649 ± 173 mg/L, a BOD_5 of 300 ± 95 mg/L, and a TSS of 297 ± 95 mg/L (all average values with standard deviation during the 3-month sampling period). The average sludge loading rate was 0.05 kg COD/kg DS/d. The solids retention time was 20-50 days. The reactor was operated with biological phosphate removal. The sampled granules were sieved to retain only granules with size of 2.0-2.5mm and afterward washed repeatedly to remove any non-granular material. Washing of the granules was done in three steps: First, the granules were suspended in tap water. Second, the granules were allowed to settle for a short time. Third, the liquid on top of the granules was decanted. These three steps were repeated around 5-10 times. This way, all material that did not settle well was removed from the granule sample. The granules were stored in tap water at 4 °C for a maximum of 2 weeks.

6.2.2 | Diffusion experiments

Experiments to determine solute diffusion coefficients in aerobic granules were carried out with the 'transient uptake of a non-reactive solute' method (Westrin & Zacchi, 1991). The experiments were conducted with a working volume of 300 mL in a 500 mL jacketed glass vessel. Adequate mixing was provided by an orbital shaker (Heathrow Scientific Digital Orbital Shaker, 19.2 mm orbit diameter, 170 rpm). The orbital shaker was chosen to limit granule breakage from excessive shear (de Graaff et al., 2018). The temperature was controlled at 4.0 ± 0.1 °C to limit biological activity.

Two solutions were prepared for the experiment: one with the granules and one with a specific molecule. For the granule solution, a certain amount of granules was added to a volumetric flask of 200 mL volume. The amount of the granules was chosen to obtain an α-value (the ratio of water volume, V_W, over granule volume, V_G) of roughly 4. The flask was then filled to 200 mL with tap water. For the specific molecule solution, a known mass of a specific solute was added to 100 mL of tap water. The solutions were pre-chilled and added to the jacketed glass vessel quickly to start the experiment.

Samples were taken at irregular intervals to best capture the non-linear concentration profile. For each experiment, 25 samples of 0.5 mL were taken through modified pipette tips. Regular plastic 1 mL pipette tips were covered in a stainless-steel woven mesh with a mesh size of 100 µm to prevent the granules from clogging the pipette tip. The volume lost through sampling was immediately replaced by an equal amount of a solution with a concentration of the expected final solute value, as described in Nguyen and Luong (1986). At the end of each experiment, the temperature was increased to 20 °C and the granule volume was determined with the modified Dextran Blue method (van den Berg et al., 2021a). Finally, total suspended solids and volatile suspended solids of the granules were determined according to Standard Methods (APHA, 2005).

Polyethyleneglycols (PEGs) of different molecular weight were used as solute in the diffusion experiment. Reagent-grade PEGs with average molecular weights of 62, 106, 200, 300, 400, 600, 1000, 1500, 2000, 4000, and 10 000 Da were obtained from Merck. The PEGs with molecular weight of 62 and 106 Da were monodisperse, while the other PEGs had a reported polydispersity index between 1.12 and 1.30. The initial PEG concentration in each experiment was approximately 1 mg/mL, with the exact value determined for each experiment separately. The diffusion coefficients of the different PEGs were taken from Waggoner et al. (1995).

6.2.3 | Data analysis

The diffusion coefficients (D_e) of the molecules in the granules were derived from the concentration change in the bulk liquid. If granules are initially free of substrate, the decrease in bulk liquid concentration can be described by the following equation (Crank, 1975):

$$\frac{C_B(t)}{C_B(t_0)} = \frac{1}{1+\alpha}\left(\alpha + \sum_{n=1}^{\infty} \frac{6\alpha(1+\alpha)\exp -\frac{D_e q_n^2 t}{R^2}}{9+9\alpha+q_n^2\alpha^2}\right) \quad (6.1)$$

Here, $C_B(t)$ is the bulk liquid concentration at time t, R is the granule radius, α is the ratio of liquid volume over granule volume, and the q_n's are the non-zero positive roots of

$$\tan q_n = \frac{3q_n}{3+\alpha q_n^2} \quad (6.2)$$

The granule volume, water volume (= total experimental volume – granule volume), and granule radius were determined experimentally. The initial solute concentration could not always be measured accurately in the experimental setup, since diffusion of the solute into the granule started before the liquid volume concentration was completely homogeneous. Instead, the initial concentration was calculated from the weight of solute added and the water volume in the experiment.

Non-linear least squares fitting was used to find the best approximation for the diffusion coefficient. In order to ensure that the global optimum was found, rather than a local optimum, random initial values were used repeatedly. For each experiment, 500 random initial values were used that varied between $1 \cdot 10^{-13}$ and $2 \cdot 10^{-9}$ m^2 s^{-1}. The precision of the diffusion coefficient was estimated according to the procedure of Alper and Gelb (1990). With this procedure, the uncertainty in the granule radius, granule volume, and PEG concentrations was propagated to the diffusion coefficient. One thousand Monte Carlo simulations were used to approximate the standard deviation of the fitted diffusion coefficient. The obtained diffusion coefficients at 4 °C were all converted to corresponding values at 25 °C based on Einstein (1905):

$$D_{25} = D_4 \cdot \frac{T_{25}}{T_4} \cdot \frac{\mu_4}{\mu_{25}} \quad (6.3)$$

Here, D is the diffusion coefficient (m^2/s), T is the absolute temperature (K), and μ is the dynamic viscosity of water.

6.2.4 | Environmental scanning electron microscope analysis

Several granules were examined by environmental scanning electron microscopy (ESEM) to relate diffusion with the granule pore structure. ESEM does not require desiccation or coating of the granules. Therefore, the granules can be imaged without any pre-processing and in a fully hydrated state. A Quanta FEG 650 (FEI Company, USA) was used with a gaseous secondary electron detector and a Peltier cooling stage set at 0.5 °C. The granules were imaged at pressures between 3 and 7 mbar, which corresponds to a relative humidity of 50-100%. Several granules were sliced into two halves with a scalpel to examine the inner structure of the granules with ESEM as well. As reference sample, alginate beads were included in the analysis. The beads were prepared by dissolving sodium alginate (sigma) in demineralised water to a 2% w/v solution and dripping this solution into a 2.5% w/v $CaCl_2$ solution. The alginate beads were allowed to harden for 30 min and subsequently stored in tap water.

6.2.5 | Influent characterization

Influent samples from three wastewater treatment plants (WWTP) were analysed to determine the molecular weight distribution of the soluble organic fraction. The influent samples originated from three WWTPs in The Netherlands, all treating domestic wastewater: from Utrecht WWTP in Utrecht (480 000 million population equivalents (p.e.)), from Harnaschpolder WWTP in Den Hoorn (1.3 million p.e.), and from Bath WWTP in Rilland-Bath (485 000 p.e.). These three WWTPs were selected because of the different sewer systems: Utrecht WWTP is fed from a relatively short gravity sewer system, Harnaschpolder WWTP is fed from both short and longer pressure mains, and Bath WWTP is fed from a long pressure main. Flow-proportional composite samples from a 24h period were collected after the influent screening (6 mm). The samples were collected in the months October, November, and January, during dry weather flow conditions. Immediately after collection, the samples were stored at 4 °C, for a maximum of 3 hours prior to analysis. After a brief settling period, the samples were filtered in an Amicon ultrafiltration cell (Merck Millipore). The filtration was carried out serially with a 0.45µm filter (Durapore PVDF, Merck Millipore) and ultrafiltration membranes of 100, 10, and 1 kDa nominal molecular weight cut-off (Ultracell regenerated cellulose, Merck Millipore). The membranes were treated according to the manufacturer's instructions. The filtration was performed at 20 °C and with a pressure of 2 bar from nitrogen gas.

6.2.6 | Analytical methods

Chemical oxygen demand (COD), phosphate (PO_4-P), and ammonium (NH_4–N) in the wastewater samples were measured in triplicate with Hach Lange test kits. Total suspended solids and volatile suspended solids in the wastewater samples were determined in triplicate according to Standard Methods (APHA, 2005). VFA in the wastewater were analysed with high performance liquid chromatography (HPLC; Prominence, Shimadzu, Japan), equipped with an ion exchange column (Aminex HPX-87H, Bio-rad) and a UV index detector (SPD-20A, Shimadzu, Japan). Sulphuric acid in ultrapure water (5 mM) was used as eluent. The individual VFA concentrations of acetate, propionate, and butyrate were converted to COD and lumped together to yield the total VFA concentration in mg COD/L. The concentration of PEG samples was measured with the same HPLC system, equipped with two size exclusion chromatography columns in series (SUPREMA 5µm 30Å, PSS GmbH, Germany) and a refractive index detector (RID-20A, Shimadzu, Japan). Ultrapure water was used as eluent at a flow rate of 0.8 mL/min. The size distribution of the granule samples was determined with a digital microscope (Keyence VHX-700F). The microscope images were processed with ImageJ software to obtain a granule size distribution and an average aspect ratio (Schneider et al., 2012).

6.3 | RESULTS

6.3.1 | Diffusion coefficients in AGS

The diffusion coefficients of different PEG molecules within aerobic granules were determined with the 'transient uptake of a non-reactive solute' method. Each experiment yielded a concentration profile, an average granule radius, a granule volume, and the liquid volume. Examples of the concentration profiles from the transient uptake experiments are given in Figure 6.1. Most concentration profiles followed a non-linear decrease from the initial concentration to the equilibrium concentration. There was no significant consumption of the solute during the experiments since consumption of the solute would result in a final concentration lower than the expected equilibrium concentration. A detailed overview of the individual diffusion experiments is given in Supplementary Information A and B.

For the PEG molecules between 62 and 4000 Da, the relative diffusion coefficient (D_e/D_{aq}) in the granules was between 0.73 and 1.22. The diffusion coefficients of the PEGs in the granule displayed large variability, with standard deviations ranging from 28-34%. These large standard deviations are probably the cause of the relative diffusion

coefficient larger than 1 (for PEG200, 400, 1000, 1500, and 4000). The diffusivity of PEGs in the granule decreased logarithmically with the molecular weight of the PEGs, similar to the diffusivity of PEGs in water (see Figure 6.2). The relation between diffusivity and molecular weight is given by:

$$\log D = a \cdot \log MW + b \qquad (6.4)$$

Here *D* is the diffusion coefficient, *MW* is the molecular weight, coefficient *a* is the slope, and coefficient *b* is the intercept. For PEG diffusion in water, the slope is -0.597 ± 0.020 and the intercept is -7.951 ± 0.077 (Waggoner et al., 1995). For PEG diffusion in the granules, the slope and intercept found in this study are -0.564 ± 0.044 and -8.070 ± 0.126, respectively. A t-test revealed that the slope of granules and water were not significantly different from each other, t(18) = 0.68, p = .51. The same applied for the intercept, t(18) = 0.81, p = .43. Thus, the granule matrix had no significant effect on the diffusion of PEG of all the tested molecular weights, from 62 to 4000 Da.

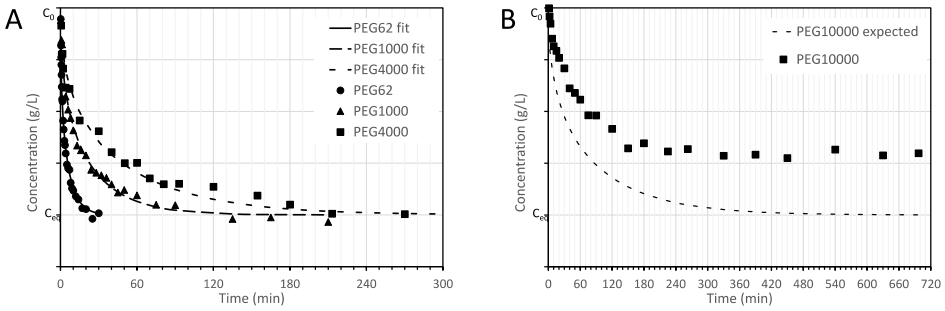

Figure 6.1. (A) Concentration profile of the diffusion experiments with PEG molecules of molecular weight 62, 1000, and 4000 Da, including a line for a fitted diffusion model. The concentration profiles all start at the initial concentration (C_0) and decrease gradually to the equilibrium concentration (C_{eq}). (B) Concentration profile of the diffusion experiment with the 10 kDa PEG, including the expected concentration profile. The expected profile is based on the assumption that the diffusion coefficient in the granule is equal to the diffusion coefficient in water.

For almost all diffusion experiments, the equilibrium concentration was equal to the expected equilibrium concentration. This indicates that the concentration in the bulk liquid was equal to the final concentration in the whole granule. There was one exception, namely the 10 kDa PEG molecule (see Figure 6.1B). The concentration in this experiment stabilized at a higher level than expected. As a result, no diffusion coefficient could be extracted from this experiment. The diffusion model that is used to determine

the diffusion coefficient (Equation 6.1) requires that the expected equilibrium is reached. The high equilibrium concentration in this experiment indicates that not all granule volume is accessible for this 10 kDa molecule. A mass balance of PEG at the final equilibrium showed that only 65% of the granule volume was accessible for this molecule size.

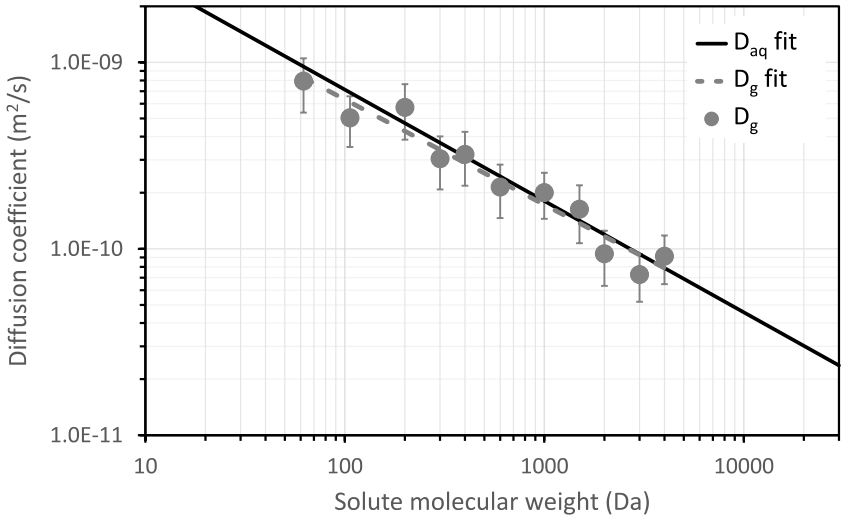

Figure 6.2. Diffusion coefficients of PEGs in aerobic granules as function of PEG molecular weight, at 25 °C. The grey dashed line indicates the fitted values for the diffusion coefficients in the granules. The black solid line indicates the fitted values for the diffusion coefficients of PEGs in water (Waggoner et al., 1995).

6.3.2 | Characterization of the granules

The hydrated structure of the granules was visualized with ESEM, to gain insight into the medium through which the PEG molecules diffused. An overview of the collected ESEM images is given in Figure 6.3. The images reveal a complex granule architecture. The majority of the granule surface was heterogeneous and many large voids with a diameter of 10-20 µm were visible (Figure 6.3A-C). It is unclear exactly how far these voids penetrate into the granules. Still, the lack of signal from these voids (the black colour in the ESEM images) suggests that they are not shallow. The granule surface also showed thick strands that form a connected network. These fibril-like strands were of similar diameter as the microbial cells which are visible as well: around 0.5-1 µm (Figure 3A-C). The length of the polymer strands was in the range of 10-30 µm. Some parts of

the granule surface were much less heterogeneous and displayed dense clusters of cells underneath a smooth surface (Figure 6.3D). However, only a minority of the granule surface had this more homogeneous nature.

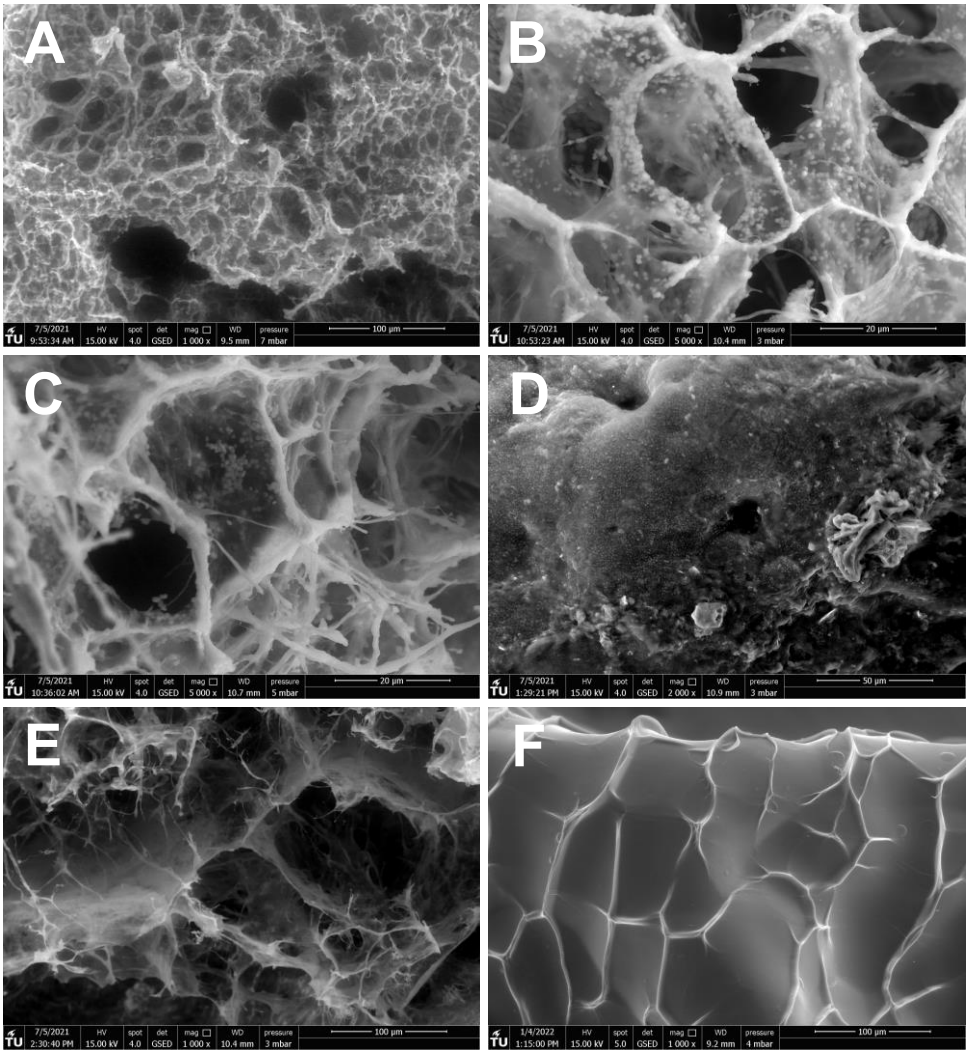

Figure 6.3. ESEM images of the surface and inner sections of aerobic granules from a full-scale WWTP. (A to C) Images that show the heterogeneous and uneven surface of the granules. The surface is characterised by several 'holes' and dense polymer strands. Individual cells are distinguishable as well, as white blobs. (D) A homogeneous section of the granule surface. In this image, the cells are clustered close together. (E) The core of a sliced granule. Large voids and a very open structure are visible. (F) The surface of an alginate bead, showing a dense surface without distinguishable pores. Note that the scales differ between images.

The inside of the granules was even more open than the granule surface. Figure 6.3E shows in the centre of the sliced granule, the structure was almost completely open and large voids were visible. The structure of the surface of alginate beads, which were included as reference material, was very different from that of the aerobic granules (Figure 6.3F). The surface of the beads showed vein-like structures, which could be the result of shrinking during the preparation of the beads. However, aside from these structures, the surface was completely smooth, and no pores could be identified.

6.3.3 | Influent characterization

Influent wastewater was collected from three WWTPs. The sewer systems feeding the WWTPs differed in terms of hydraulic retention time and sewer type. The wastewaters were all fractionated to reveal the apparent molecular weight distribution of soluble COD. As can be seen in Table 6.1, the three wastewaters showed similar characteristics. The majority of the COD was present in the particulate form (62-77%). Around 15-26% of the total COD was present in the smallest size fraction, which was below 1 kDa in size. Only a minor fraction (11-12%) of the influent COD was present in the fractions from 1 kDa to 0.45µm. This means that the majority (61-69%) of the soluble COD in all three wastewaters was smaller than 1 kDa. The VFAs were only a minor fraction of the soluble COD (17-21%).

Table 6.1. COD fractionation and other characteristics of three influent wastewater samples. All values are reported in mg/L, including standard deviation. The VFA concentration is given in mgCOD/L.

	Utrecht	Harnaschpolder	Bath
COD fractionation			
Total	605 ± 9	456 ± 20	649 ± 44
Soluble (< 0.45 µm)	175 ± 1	105 ± 1	248 ± 1
100 kDa-0.45 µm	11 ± 2	21.6 ± 0.2	23 ± 4
10-100 kDa	42 ± 2	9.5 ± 0.8	10 ± 4
1-10 kDa	17 ± 2	19.8 ± 1.1	45 ± 2
< 1 kDa	106 ± 1	67.2 ± 0.8	170 ± 1
Additional parameters			
TSS	260 ± 1	221 ± 8	268 ± 12
TN	61.7 ± 1.4	49.0 ± 0.6	59.0 ± 1.7
NH_4-N	45.9 ± 0.2	33.8 ± 0.5	42.2 ± 0.6
TP	8.0 ± 0.2	6.22 ± 0.03	10.97 ± 0.06
PO4-P	4.6 ± 0.1	3.39 ± 0.03	7.47 ± 0.15
VFA	30.8 ± 0.7	17.7 ± 0.4	36.3 ± 0.2

6.4 | DISCUSSION

6.4.1 | Diffusion coefficients of PEG molecules

In the past, many researchers have studied diffusion in biofilms. There appeared to be a relation between the molecular weight of a solute and its relative diffusivity. In biofilms, the reported relative diffusivity of small solutes (< 44 Da) was 0.46, while that of large solutes (44-342 Da) was 0.39 (Stewart, 1998). The relative diffusivities found in this study were much higher, between 0.73 and 1.22. Furthermore, there was no discernible effect of the solute molecular weight on the relative diffusivity for molecules between 62 and 4000 Da. This is surprising, as the molecular weight range used in this study is much greater than the molecular weight range included in the review of Stewart (1998).

One possible explanation for the discrepancy relates to the method used in this study. The 'transient uptake of a non-reactive solute' method has been used previously to measure diffusion coefficients in hydrogel beads and biofilms (Chresand et al., 1988; Fan et al., 1990; Pu & Yang, 1988). The limitations of this method have been described previously, highlighting the low precision as major issue (van den Berg et al., 2021b; Westrin & Zacchi, 1991). This low precision was observed here as well, but it cannot explain the large difference between our results and the results described in literature. Alternatively, the diffusion coefficients in this study could be overestimated due to systematic errors or biases. However, the effect of most systematic errors for this method is that the diffusion coefficient is underestimated (van den Berg et al., 2021b). There are only two systematic errors that lead to an overestimation: deactivation of the biomass and a non-spherical granule shape. We do not expect any bias from deactivation, as we did not use deactivating chemicals. The granule shape could have an influence, as ellipsoidal granules have a higher surface-to-volume ratio than perfectly spherical granules. As a result, the concentration in the liquid decreases faster and the diffusion coefficient is overestimated if granules are assumed to be spherical. However, the average aspect ratio of the granules was only 1.44. Our previous research has shown that this corresponds to an overestimation of the diffusion of only 10% (van den Berg et al., 2021b). Thus, it is not likely that our findings significantly overestimate the diffusion coefficient. In fact, the diffusion coefficient could even be slightly underestimated due to the rough surface of the granule, the granule size distribution, or the mass transfer boundary layer (van den Berg et al., 2021b).

Another explanation for the difference between our study and previous studies relates to the methods and types of biofilms used in the previous studies. A thorough analysis of the studies included in the review of Stewart (1998) revealed several issues (see

Supplementary Information C for full details). In total, there were 21 studies on diffusion of larger molecules (44-342 Da). From these 21 studies, 12 used the 'steady-state reaction' method, which is very imprecise and inaccurate (van den Berg et al., 2021b). Furthermore, 5 out of the remaining 9 studies were performed on biofilms with a density greater than 150 g/L. It is not surprising that the diffusion coefficient in such a high-density biofilm is much lower than in aerobic granules with a density of 90 g/L (Horn & Morgenroth, 2006). The remaining 4 studies were performed with sludge flocs (3) or without considering biomass activity (1). As a result, all studies on larger molecules that are included in Stewart (1998) have clear limitations and a direct comparison with our findings is futile.

There are several studies not included in the review of Stewart (1998) that focused on molecules in the kDa range. These studies are commonly carried out with fluorescent dextran molecules and fluorescence correlation spectroscopy or fluorescence recovery after photobleaching. These techniques measure diffusion coefficients in specific locations in a biofilm instead of the average diffusion coefficients measured in this study. Several studies of kDa-sized molecules report high relative diffusivities for molecules between 3 and 10 kDa in biofilms (Takenaka et al., 2009; Z. Zhang et al., 2011) and alginate beads (Favre et al., 2001; Puguan et al., 2015). For example, Peulen and Wilkinson (2011) found a relative diffusivity of 60-80% for a 3 kDa and a 10 kDa dextran in a *Pseudomonas fluorescens* biofilm. Others reported relative lower diffusivities, ranging from 0.01 to 0.23 for molecules with a molecular weight between 3 and 10 kDa (Bryers & Drummond, 1998; Lawrence et al., 1994; Marcotte et al., 2004; Thurnheer et al., 2003). The reason behind this wide range in reported values is unclear, but it could be due to differences in biofilm density or structure.

Overall, we believe our results are representative for diffusion in aerobic granules, despite the large standard deviations. The main result of the experiments are not the exact diffusion coefficients, but rather the relation between the molecular weight and diffusion coefficient. These results have been collected with the same method and the same type of biofilm. Thus, even if the absolute diffusion coefficients would not be reliable, the overall trend would remain the same. As it turns out, the granule matrix has no significant effect on PEG molecules of 62-4000 Da. This conclusion is in contrast with existing literature and provides a new perspective on diffusion, specifically in aerobic granules.

6.4.2 | Granule structure

The limited effect of the solute molecular weight on diffusion raised the question why the granule matrix did not provide more obstruction to the larger molecules. To address this question, we investigated the structure and porosity of the granule matrix with ESEM imaging. In contrast to conventional electron microscopy, ESEM does not require dehydration or fixation the granule. Therefore, ESEM is an appropriate technique to visualize the EPS matrix in its natural, hydrated state (Priester et al., 2007).

The ESEM images of the granules (see Figure 6.3) revealed that the granules were very heterogeneous with arguably two distinct phases: a liquid phase and a semi-solid phase. The liquid phase is present in large macropores that are visible on the granule surface and in the granule interior. The semi-solid phase in the granule was present in between the macropores, and many microorganisms were embedded within this semi-solid phase. The presence of macropores or channels and cell clusters is an established observation in biofilm literature (Bryers & Drummond, 1998; Marcotte et al., 2004; Peulen & Wilkinson, 2011; Picioreanu et al., 2016; Sankaran et al., 2019; Takenaka et al., 2009).

Generally, porosity is used as a parameter to compare the volume of the macropores with the volume of the cell clusters. However, porosity in biofilms is an ill-defined concept, since both the liquid phase in the macropores, as well as the semi-solid phase mostly consists of water (Lewandowski, 2000). Diffusion occurs both in the macropores and in the semi-solid phase. The size of micropores in the semi-solid phase could not be determined with ESEM imaging. However, alginate hydrogels have a typical pore size of 5-20 nm (Boontheekul et al., 2005; Leal-Egaña et al., 2011; Simpliciano et al., 2013; Smidsrød & Skja, 1990). The size of the micropores in the granules could be of a similar order of magnitude, since alginate gels are similar to the EPS from AGS (Felz et al., 2020a; Lin et al., 2010; Schambeck et al., 2020).

The hydrodynamic radius of the PEGs used in this study ranged from 0.15 to 2.79 nm (Devanand & Selser, 1991). Thus, the PEGs were three orders of magnitude smaller than the granule macropores. It is therefore highly likely that the PEGs diffused completely unobstructed within the macropores. At the same time, the PEGs were only slightly smaller than the hypothesized pore size of the granule micropores. Still, the diffusion experiments indicated that the PEGs with molecular weight up to 4000 Da (1.65 nm hydrodynamic radius) penetrated throughout the entire granule, as the expected equilibrium concentration was reached. Given that the expected equilibrium was not reached with 10 kDa PEG, it is possible that this molecule was excluded from the micropores. The hydrodynamic radius of the 10 kDa PEG is 2.79 nm (Devanand & Selser,

1991), which means that the diameter of the micropores might be around 5 nm. Still, the micropores are apparently large enough to allow diffusion of PEGs up to a molecular weight of 4000 Da or a hydrodynamic radius up to 1.65 nm. The notion that macropores or channels significantly enhance diffusion into the granules is therefore incorrect for molecules smaller than 4000 Da. For these molecular weights, diffusion in the macropores is only marginally faster than diffusion in the micropores. In contrast, molecules that are excluded from the micropores, can only diffuse in the macropores. The heterogeneity of the granules is therefore mainly of relevance for larger molecules (≥ 4 kDa).

This discussion highlights that diffusion behaviour in the granules is closely linked to the structure of the EPS matrix. Our results are therefore not universally applicable to all biofilm types. The aerobic granules used in this study have a distinct heterogeneous structure with macropores (10-20 µm in diameter) and fibrils. Biofilms with alginate as major component might have a structure more similar to alginate beads (see Figure 6.3F) and the diffusive behaviour in these biofilms can be very different. It is therefore of utmost importance that studies of diffusion in biofilms describe both the diffusion behaviour and the structure of the EPS matrix.

6.4.3 | Implications for practice

An important question in the design and operation of AGS systems is which fraction of influent COD can rapidly diffuse into the granules during the anaerobic phase of the sequencing batch cycle (Pronk et al., 2015a). This diffusible fraction is important for granule formation and for nutrient removal (Layer et al., 2019). The lack of a significant effect of the granule matrix on the relative diffusivity D_e/D_{aq} suggests that even larger molecules (up to 4000 Da) are likely to be available for conversion within the granules. Because of their size, larger molecules already diffuse slower in water than small molecules, but the granule matrix does not limit their diffusion further. We can evaluate the transient penetration of a molecule into a granule with the following equation (Crank, 1975):

$$\frac{C}{C_b} = 1 + 2\sum_{n=1}^{\infty}(-1)^n \exp\left(-\frac{D_e n^2 \pi^2 t}{R^2}\right) \qquad (6.5)$$

Here, C is the concentration in the granule core, C_b is the concentration in the bulk liquid, R is the granule radius, D_e is the diffusion coefficient, and t is the time. This equation can be used to estimate the concentration in the granule core after a certain time period.

We can estimate the diffusive penetration after 60 minutes, which is the length of the anaerobic feeding period for most AGS reactors (de Kreuk & Van Loosdrecht, 2004; Pronk et al., 2015b). The diffusive penetration is expressed by the relative concentration in the granule core, C/C_b. With the diffusion coefficients that were found in this study (for 62-4000 Da PEGs), granules with a 1 mm radius, and a temperature of 10 °C, the relative concentration in the granule core (C/C_b) ranges from 54-100% after 60 min; all molecules of 1 kDa and smaller reach a relative concentration in the granule core of at least 93% of the concentration in the bulk. The molecules between 1 kDa and 4 kDa penetrate less and reach a C/C_b between 47 and 93%. Of course, the *in-situ* penetration depth depends on both the diffusive properties as well as the consumption rate. Still, this analysis shows that for many molecules with different size, diffusion does not limit penetration depth.

The above analysis has even stronger implications if the distribution of soluble COD is considered. Of the soluble COD in the three analysed wastewater samples, 61-69% was smaller than 1 kDa and 70-87% was smaller than 10 kDa. This means that at least 61-69% of the soluble COD can diffuse easily into the granules. It is therefore likely that the majority of the soluble COD is converted within the granules, where it can contribute to nutrient removal (Layer et al., 2019; Layer et al., 2020). Nevertheless, the composition of wastewater can vary significantly between different locations (Henze & Harremoës, 1992). We found a similar COD distribution for three wastewaters which originated from different sewer systems in the Netherlands. Nevertheless, similar soluble COD distributions were found by other authors, for domestic and industrial wastewaters (Doğruel, 2012; Dulekgurgen et al., 2006; Hu et al., 2002; Karahan et al., 2008; Ravndal et al., 2018). It is however not clear if the abundance of < 1 kDa COD is an innate property of wastewater or if it is the result of conversion processes within the sewer. More research is required to determine how universally applicable our findings are.

There are two practical lessons that can be learned from this study. The first lesson relates to the characterization of wastewater for AGS. The majority of the soluble COD, measured by filtration over a 0.45µm filter, is small enough to diffuse into AGS. This means that a simple characterization approach suffices to know which fraction of influent COD can be converted within the granules. Even though not all soluble COD is truly diffusible, it is a reasonable approximation. The benefit of a full ultrafiltration characterization is small, especially considering the pitfalls of this method (Logan & Jiang, 1990). The second lesson relates to AGS models. The majority of AGS models are based on simple substrates, like VFAs (Baeten et al., 2019; Ni & Yu, 2010). The diffusivity of these substrates is generally assumed to be 80% of their diffusivity in water (Nicolella

et al., 1998; Wanner et al., 2006). Our findings show that the use of a single reduction factor for diffusion in granules is valid for molecules with a molecular weight up to 4000 Da. Thus, AGS models do not require a unique reduction factor for each individual molecule.

6.5 | CONCLUSION

In this study, the effect of the molecular weight of a solute on its diffusion coefficient in aerobic granules was evaluated, next to the granule structure and the distribution of soluble COD in influent wastewater. There was no statistically significant difference for the diffusion coefficients in water or granules for PEGs with a molecular weight between 62 and 4000 Da. This indicates that within this molecular weight range, diffusing molecules were only marginally obstructed by the granule matrix. A 10 kDa PEG molecule was partially excluded from the granules and only accessed 65% of the granule volume. The granule structure was heterogeneous, with large macropores (~10 µm diameter) and semi-solid regions that contained microbial cells. The partial exclusion of the 10 kDa PEG suggests that the semi-solid regions contain micropores with a diameter around 5 nm. Thus, the diffusion results provide practical information, but they also contribute to a characterization of the granule matrix.

Interestingly, a relatively large fraction (61-69%) of the soluble COD in influent wastewater is smaller than 1 kDa and thus can diffuse rapidly into the granules. These findings can be used to simplify AGS models and influent characterization approaches. AGS models do not need to consider the effect of molecular weight on the diffusion coefficients, as for most molecules the diffusion coefficient in the granule is not significantly different from its diffusion coefficient in water. The characterization of influent COD for AGS reactors can suffice with a simple filtration with a 0.45 µm pore size filter, as the majority of soluble COD in domestic wastewater is also diffusible inside aerobic granular sludge.

SUPPLEMENTARY INFORMATION

Supplementary information A: Diffusion experiment data

Table 6.S1. Diffusion experiment data, including granule properties that have been measured as part of the diffusion experiment. Here, D_{aq} is the diffusion coefficient of a molecule in water and D_e is the diffusion coefficient of a molecule within the granule. The D_e at 4 °C is the outcome of the fitting procedure, and the D_e at 25 °C is recalculated based on Einstein's equation. All values are given as mean, with or without standard deviation.

PEG	Volume	Radius	Aspect ratio	Buoyant density	Biomass density	Ash	D_{aq}	D_e (4 °C)	D_e (25 °C)	D_e/D_{aq}
	mL	mm	-	kg/m³	gVSS/L	%	x 10^{-10} m²/s	x 10^{-10} m²/s	x 10^{-10} m²/s	-
62	60.3 ± 0.5	1.43 ± 0.24	1.47 ± 0.58	1019.4	57.5	21.8	9.51	4.25 ± 1.38	7.95 ± 2.58	0.84 ± 0.27
106	52.7 ± 0.8	1.44 ± 0.20	1.44 ± 0.47	1011.7	54.8	21.0	6.91	2.70 ± 0.82	5.05 ± 1.53	0.73 ± 0.22
200	56.2 ± 1.2	1.50 ± 0.23	1.42 ± 0.44	1017.6	62.6	19.4	4.73	3.08 ± 1.01	5.75 ± 1.89	1.22 ± 0.40
300	60.0 ± 0.6	1.50 ± 0.23	1.42 ± 0.44	1020.0	58.9	21.3	3.71	1.63 ± 0.51	3.05 ± 0.96	0.82 ± 0.26
400	64.6 ± 0.9	1.50 ± 0.23	1.42 ± 0.44	1018.8	59.5	20.9	3.12	1.72 ± 0.55	3.21 ± 1.03	1.03 ± 0.33
600	58.1 ± 0.6	1.50 ± 0.23	1.42 ± 0.44	1024.2	58.0	21.0	2.45	1.15 ± 0.37	2.15 ± 0.68	0.88 ± 0.28
1000	59.9 ± 0.6	1.44 ± 0.20	1.44 ± 0.47	1017.9	53.8	20.9	1.81	1.07 ± 0.30	2.00 ± 0.56	1.11 ± 0.31
1500	64.0 ± 0.8	1.43 ± 0.24	1.47 ± 0.58	1021.2	57.8	21.7	1.42	0.87 ± 0.30	1.63 ± 0.56	1.15 ± 0.40
2000	55.4 ± 0.7	1.43 ± 0.24	1.47 ± 0.58	1017.5	56.1	21.4	1.19	0.50 ± 0.17	0.94 ± 0.31	0.79 ± 0.26
3000	65.8 ± 0.6	1.44 ± 0.20	1.44 ± 0.47	1023.4	60.7	19.5	0.94	0.39 ± 0.11	0.73 ± 0.21	0.78 ± 0.22
4000	66.7 ± 0.3	1.44 ± 0.20	1.44 ± 0.47	1019.7	58.4	20.2	0.79	0.49 ± 0.14	0.91 ± 0.27	1.16 ± 0.34
10000	65.3 ± 0.8	1.35 ± 0.24	1.43 ± 0.43	1019.8	63.3	19.8	0.46	-	-	-

Supplementary information B: Concentration profile plots

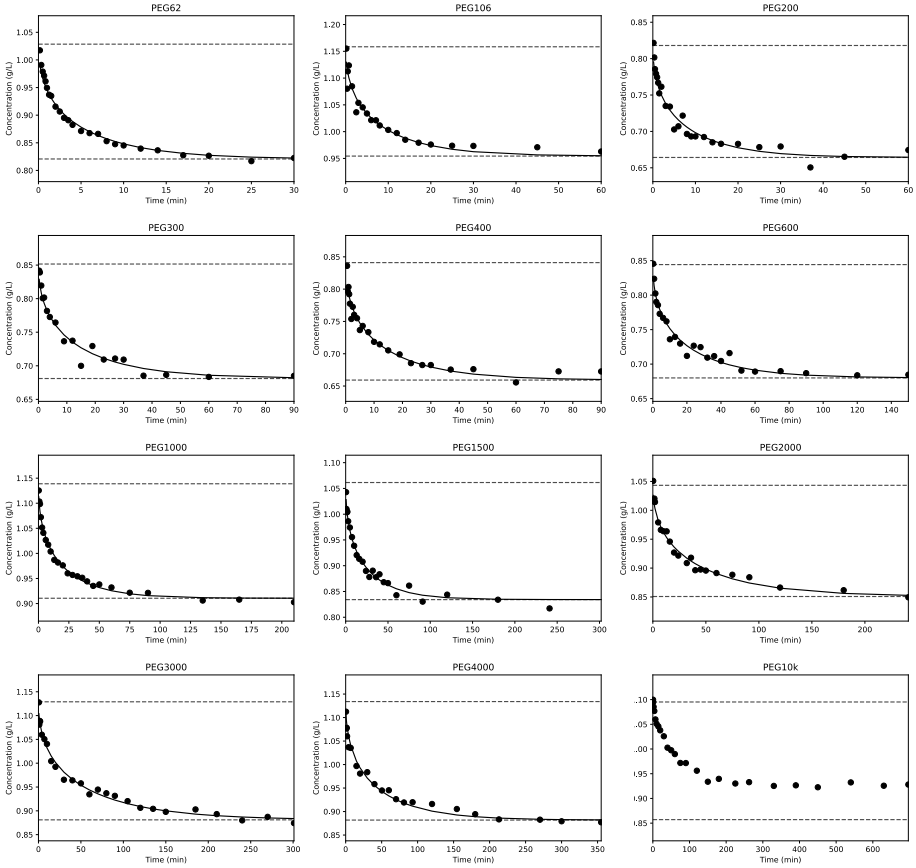

Figure 6.S1. Concentration profiles during the diffusion experiment and fitted diffusion coefficient.

Supplementary information C: Overview of previous studies

Table 6.S2. Overview of the studies included in the review of Stewart (1998) and their major limitations.

	Reference	Steady-state reaction	High biofilm density	Diffusion in compressed flocs	Reaction not considered
1	Fan et al. (1990)		X		
2	Onuma and Omura (1982)			X	
3	Pipes et al. (1974) as cited in Fan et al. (1990)			X	
4	Matson and Characklis (1976)			X	
5	Dibdin (1981)		X		
6	la Cour Jansen and Harremoes (1985)	X			
7	Dibdin (1993)		X		
8	McNee et al. (1982)		X		
9	Beyenal and Tanyolac (1994)	X			
10	Andrews and Tien (1981)	X			
11	Baillod and Boyle (1970)		X	X	
12	Fujie et al. (1979) as cited in Fan et al. (1990)	X			
13	LaMotta (1976b)	X			
14	LaMotta (1976a)	X			
15	Livingston and Chase (1989)	X		X	
16	Ozturk et al. (1989)	X		X	
17	W.T. Tang and Fan (1987)	X			
18	Tatevossian (1979)				X
19	S.C.P. Wang and Tien (1984)	X			
20	Yu and Pinder (1993)	X			
21	Yu and Pinder (1994)	X			

Granules settling inside a tube

7

Outlook

7.1 | FOREWORD

The goal of this thesis was to gain mechanistic understanding of solute diffusion in aerobic granular sludge. The research was split into six parts, as described in **Chapter 1**. The findings of the different parts are described in **Chapter 2** till **Chapter 7**. In this chapter, the separate conclusions are integrated to provide a comprehensive perspective on diffusion in AGS. Furthermore, an outlook is provided regarding diffusion and the matrix through which diffusion takes place.

7.2 | DIFFUSION IN BIOFILM MODELS

The most apparent conclusion from this thesis relates to the use of diffusion coefficients in granular sludge and biofilm models. Mathematical models of granular sludge and biofilm reactors often describe the diffusion process in the granule or biofilm as a basic process (Baeten et al., 2019; Boltz et al., 2011; Boltz et al., 2010). Generally, all heterogeneity is ignored and the diffusion coefficients in the biofilm are set to 80% of the relevant diffusion coefficients in water (Nicolella et al., 1998). This approach limits the complexity of the biofilm models, and thus provides faster computation times and less complicated results. However, the question has always remained what uncertainty is introduced with this simple approach. Perhaps, the biofilm models have been made too simple by leaving out essential diffusion processes. After all, biofilm modellers should follow the (paraphrased) principle of Albert Einstein: "*Everything should be made as simple as possible, but no simpler.*" (Robinson, 2018).

In the different chapters of this thesis, it was demonstrated that several aspects of the diffusion process could be described with a simple approach:

- In **Chapter 2**, it was shown that the granule density is very stable in different environmental conditions (i.e., salinity). As the granule density has a great influence on diffusion, it is likely that diffusion is also (mostly) independent of environmental conditions.
- In **Chapter 3**, it was demonstrated that the granules do not contain large channels that could allow flow of liquid into and out of the granules. Convective diffusion is therefore not of relevance for aerobic granular sludge.
- In **Chapter 4**, it was found that diffusive transport in granules from different full-scale treatment plants was comparable and that heterogeneous diffusion only has a limited impact on the flux of a solute into the granule.

- In **Chapter 5**, it was shown that diffusion coefficients cannot be determined with high accuracy. However, it was also shown that precise diffusion coefficients are not needed as well since the diffusion coefficient is an insensitive parameter with limited impact on the flux.
- In **Chapter 6**, it was proven that the soluble COD fraction of municipal wastewater is approximately equivalent to the diffusible COD fraction. Most soluble COD is smaller than 1 kDa and molecules up to that size can diffuse relatively easy into the granules.

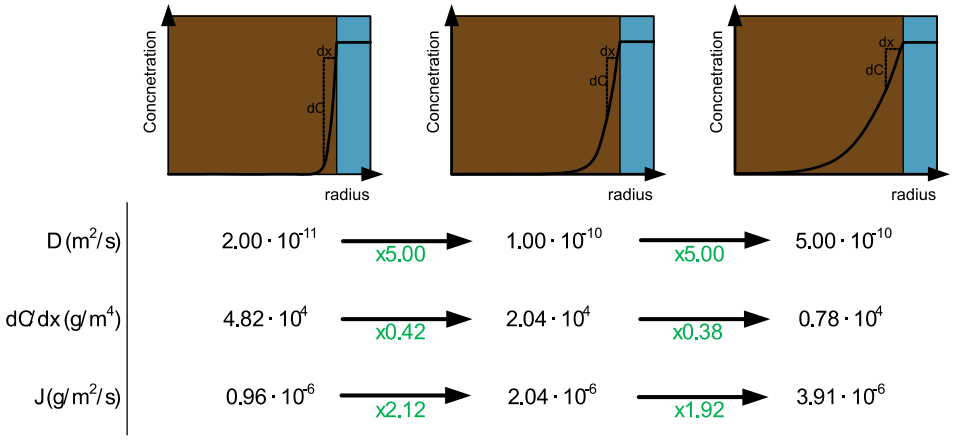

Figure 7.1. Three scenarios that illustrate the low sensitivity of the diffusion coefficient towards the flux. A 5-fold change in the diffusion coefficient only results in an approximately 2-fold change in the flux. Here, D is the diffusion coefficient, dC/dx is the concentration gradient in the biofilm, and J is the flux into the granule. Note that the concentration profiles are not drawn to scale, to emphasize the change in concentration gradients.

The conclusions of the individual chapters all point in one direction: a basic description of the diffusion process suffices for most biofilm models. The mechanisms underlying diffusion of solutes in AGS are very complex and little understood, mainly due to our lack of understanding of the granule matrix. However, there is no need to include this complexity in biofilm models. In fact, there is one key reason why the simple description is enough: the diffusion coefficient is an insensitive parameter and only has a limited impact on the flux. This reason follows from **Chapter 5** and is illustrated in Figure 7.1. The figure shows three scenarios of a granule with a certain diffusion coefficient. The concentration profile and resulting concentration gradient can be calculated for each scenario, assuming homogeneous radial diffusion and a certain homogeneous

consumption rate. From these scenarios it becomes clear that if the diffusion coefficient increases or decreases, the concentration gradient changes in the opposite direction. The flux into the granule is calculated based on the diffusion coefficient and the concentration gradient. As a result, a 5-fold change in the diffusion coefficient only leads to an approximately 2-fold change in the flux. The flux is the most important parameter in most biofilm models, and it is only partially influenced by the diffusion coefficient. Thus, the research in this thesis finally provides a thorough validation of the often-used simplifications of diffusion in biofilm models.

7.3 | DENSE SURFACE LAYER WITHIN THE GRANULES

In **Chapter 2**, different structural features of aerobic granules were visualized with MRI. One of the most surprising observations was the dense surface layer that was visible in full-scale aerobic granules (see Figure 7.2). Despite attempts to characterize this layer with different techniques (i.e., MRI, TEM, SEM-EDX), its nature remains unclear. The MRI signal is based on the local environment of water molecules, so there are many potential explanations for the presence of the surface layer. One such explanation is the high EPS density (or high charge density) in the surface layer. A high EPS density could affect the MRI measurement through exchange of protons between water and EPS functional groups (e.g., -OH, -NH_2, -SH groups). The exact impact of the EPS on the MRI measurement is a function of the concentration of exchangeable protons, the chemical shift of these protons, and their exchange rate (Hills, 1992). The chemical shift of the protons depends on the field-strength of the MRI instrument. It is therefore not surprising that the surface layer shows up more clearly in the MRI experiments with a high-field strength of 22.3T than in the experiments with a lower field strength of 5.9T.

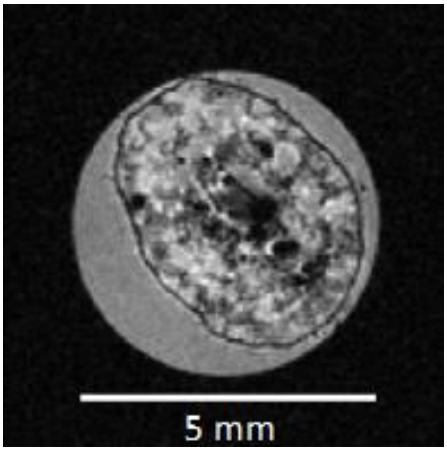

Figure 7.2. MRI of a granule from the PNU wastewater treatment plant. The image shows a dark apparent surface layer.

The MRI results show that the layer is characterized by a low signal intensity (approximately 60% of the signal intensity of water around the granule) and a reduced effective T_2 (6 ms). This effective T_2 is very close to the echo time used in the MRI

experiment (5.6 ms). This means that the effective T_2 is estimated with only a few data points. If the surface layer contained protons with an effective T_2 lower than the echo time (e.g., 2 ms), these protons would not be detected. The signal of these protons would have decayed almost completely at the first data point. It is therefore possible that the low signal intensity in the surface layer is caused by the low effective T_2 of some protons. A further characterization of this layer should involve localized NMR measurements of the T_1 and T_2 distributions in the surface layer. Our understanding of this layer can be improved as well with the help of other methods, such as ESEM, FTIR spectroscopy, or Raman spectroscopy. Several ESEM images that were collected as part of this thesis have already shown a dense outer layer that could be similar to the layer observed with the MRI (see Figure 7.3). A better characterization of this layer can help us understand what this layer is made of, why it is present, and to what extent it affects mass transfer into the granules.

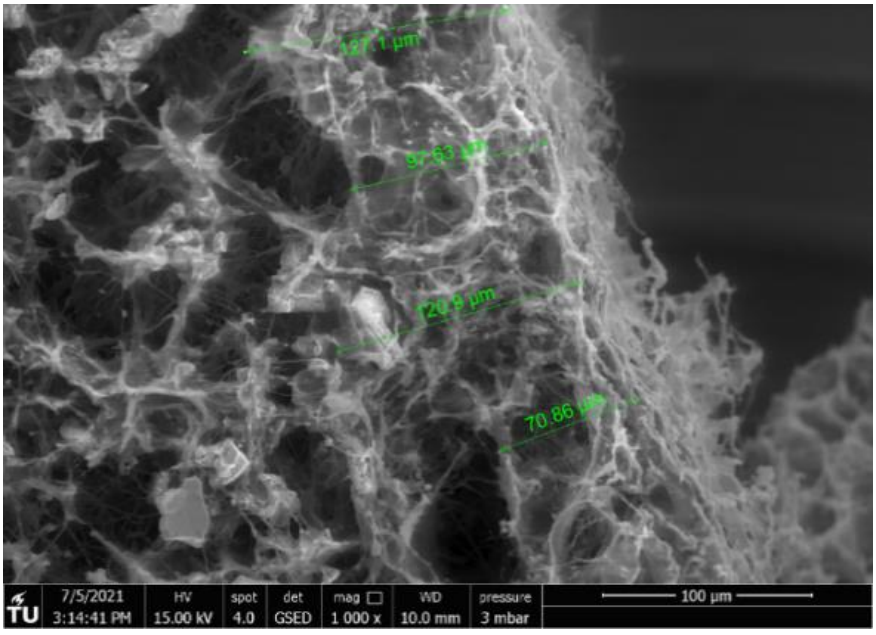

Figure 7.3. ESEM image of a sliced granule from the Utrecht wastewater treatment plant. The image shows the edge of a granule and the dense outer layer on the granule surface.

7.4 | DIFFUSION OF CHARGED MOLECULES

In **Chapter 6**, the effect of the molecular weight of a solute on its diffusion in the granules was investigated. It was found that there was no effect of the molecular weight in the

range of 60 to 4000 Da. However, all the molecules used had neutral charge. The effect of solute charge on diffusion in the granules was not investigated. The charge of a molecule could significantly impact its diffusion, as the granule contains EPS with a large number of negatively charged functional groups (Felz et al., 2020b). These functional groups will repel negatively charged diffusing molecules and will give rise to a Donnan potential (Golmohamadi & Wilkinson, 2013; Pfaff et al., 2021). Such a Donnan potential will impede diffusion of negatively charged ions and accelerate diffusion of positively charged ions. The effect of the Donnan potential will depend on the concentration of charged functional groups in the EPS and on the ionic strength of the wastewater (Siegrist & Gujer, 1985). Experiments to measure diffusion of charged molecules can provide insights into the effect of solute charge on diffusion. These experiments can be supplemented with experiments to quantify the Donnan potential through voltammetry (Golmohamadi & Wilkinson, 2013) and measurement of the ion distribution in the granule and the liquid (Pfaff et al., 2021). If the negatively charged functional groups indeed retard the diffusion of negatively charged molecules, the question follows what the evolutionary advantage is of the negatively charged polymers. After all, important molecules like acetate, propionate, and phosphate are all negatively charged. Perhaps the negatively charged polymers help accumulating the more rarely available micronutrients, like copper, iron, manganese, and cobalt.

7.5 | FIBRIL STRUCTURES

7.5.1 | Initial observations

In **Chapter 6**, the granule was studied with environmental scanning electron microscopy (ESEM). This technique does not require any sample processing and allows imaging of the granule in its natural, hydrated state (Stokes, 2001). Intriguing heterogeneous structures were visible on the granule surface and within the granule. The granules consisted of macropores of 10 µm in diameter and a semi-solid phase, through which microorganisms were dispersed. Furthermore, there were clear fibrilar structures visible on the granule surface. Such fibrilar mesh structures have already been observed in biofilms and activated sludge several decades ago, although with conventional SEM (Richards & Turner, 1984). Some authors suggested that the fibrils were a structural polymer (Tago & Aida, 1977). Others considered the fibrils as imaging artefacts that arose from fixation and dehydration of the EPS (Dohnalkova et al., 2011; Richards & Turner, 1984). It is interesting to note that we observed fibril structures with ESEM, a technique that does not involve fixation or dehydration (Stokes, 2001). The granule EPS

was fully hydrated during the collection of the ESEM images. Thus, the presence of fibrils is not purely an imaging artefact. It is very well possible that the non-fibrilar EPS collapses during drying (Dohnalkova et al., 2011; El Abed et al., 2012), which would leave the fibrils as the only structure visible with high-vacuum electron microscopy.

Besides the ESEM images, there are several other direct or indirect observations of fibrils in the biofilms or granules (Felz et al., 2020a; Larsen et al., 2007; Lin et al., 2015; Lotti et al., 2019; Pfaff et al., 2021; Romero et al., 2010). The presence of fibrils was also suggested in **Chapter 2**, where it was observed that the granule volume was hardly affected by high salinities (up to 36 g/L). This stability is different from what is commonly observed with ionic EPS (Golmohamadi & Wilkinson, 2013; N. Liu et al., 2020), indicating the presence of a non-ionic structural component, like fibrils. This suggests that the fibrils can play a major role in the rigid structure of aerobic granules. The fibrils could be the skeleton of the granule, the backbone that maintains the structural integrity of the granule. After all, similar functions have been described for fibrils in human tissues (Shoulders & Raines, 2009; Wess, 2005).

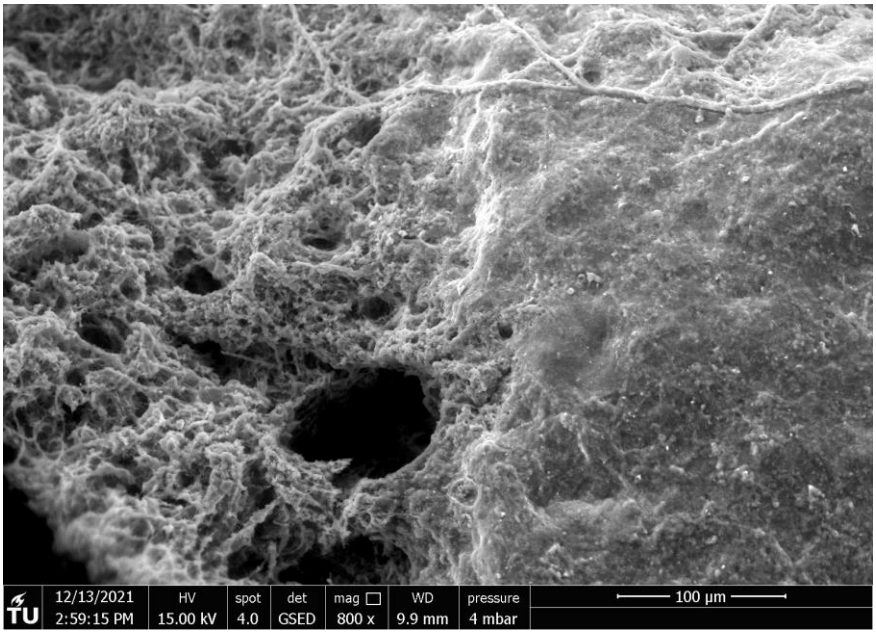

Figure 7.4. ESEM image of the surface of a granule from the Utrecht wastewater treatment plant.

However, the fibril network was not visible in all imaged granules. The granule images that were included in **Chapter 6** were from the 2-2.5 mm size fraction and all displayed the fibril structures. Other images of granules from the 1-2 mm size fraction revealed

different structures. For these granules, only part of the surface was heterogeneous, while other parts were more dense and homogeneous (see Figure 7.4). The difference between the smaller and larger granules might be related to the age of the granules. Large granules have a much higher solids retention time, so on average they are older (Ali et al., 2019). The older granules have a different microbial community, which could be reflected in the EPS composition. Alternatively, older granules might contain a higher fraction of EPS that is less biodegradable. These differences in EPS can potentially explain the observed structures.

7.5.2 | Characterization approaches

The fibril network can have a large impact on diffusion of different (macro)molecules into the granules. If the granules would consist of a homogeneous network of polymers like alginate, there would be many small pores. These pores can significantly obstruct molecules, especially larger molecules. However, the granules are not homogeneous, but they (partly) consist of a heterogeneous multi-phase network (**Chapter 6**). The microbial cells are still embedded in a homogeneous semi-solid hydrogel phase, but the granule also contains large macropores. These large pores could facilitate fast diffusion into the granules, especially for larger molecules. Even colloidal particles might be able to penetrate into the granules through the macropores, similar to the hypothesis described by Tijhuis et al. (1994a).

The physical properties of the fibril structures and the porous network can be characterized further with a combination of four techniques. Firstly, ESEM imaging has proven to be a useful method to visualize hydrated EPS. This technique can be used to image granules from different treatment plants, as well as granules after different treatments. For example, the granules could be imaged with and without dehydration to see if the ionic EPS indeed collapses onto the fibrils. Secondly, the structural properties of the granules can be evaluated through rheology. The behaviour of granules under stress can be compared with fibrilar and non-fibrilar model hydrogels. Third, the pores of the granule can be characterized with a partitioning experiment. In such an experiment, molecules (e.g., polyethylene glycols) with different sizes are allowed to diffuse into the granules. A molecule with a certain size can only enter pores that are larger than itself. With a proper mass balance, the accessible pore volume can be determined for each molecule size. Finally, the network structure within the granules can be assessed with nanoparticle diffusometry. The diffusion behaviour of different molecules is influenced by the microstructure. By measuring this diffusion behaviour, the microstructure can be characterized. Diffusometry has previously been carried out

with PFG-NMR (Brenner & Matsukawa, 2016; de Kort et al., 2018). PFG-NMR provides accurate measurements of self-diffusion coefficients over different temporal and spatial scales. In fact, PFG-NMR has already been used successfully in **Chapter 3** to study the self-diffusion of water molecules within the granules. The self-diffusion coefficients of water contained information on the granule matrix, but there is even more information that can be extracted. Hindered self-diffusion of nanoparticles can be used to quantify the mesh size or polymer strand thickness of the granule matrix (de Kort et al., 2015). Thus, diffusometry can provide exciting and fundamental insights in the architecture of the granules.

7.6 | FINAL REMARK

Overall, this work showed that the study of diffusion in granular sludge is not directly needed for improving the understanding of the conversion processes, but it holds great value for further understanding the complex matrix that constitutes the granular sludge.

The full-scale aerobic granular sludge installation in Utrecht

References

Adav, S. S., Lee, D.-J., Show, K.-Y., & Tay, J.-H. (2008). Aerobic granular sludge: recent advances. *Biotechnology Advances, 26*(5), 411-423.

Afridi, Z. U. R., Wu, J., Cao, Z. P., Zhang, Z. L., Li, Z. H., Poncin, S., & Li, H. Z. (2017). Insight into mass transfer by convective diffusion in anaerobic granules to enhance biogas production. *Biochemical Engineering Journal, 127*, 154-160.

Ali, M., Wang, Z., Salam, K. W., Hari, A. R., Pronk, M., van Loosdrecht, M. C., & Saikaly, P. E. (2019). Importance of species sorting and immigration on the bacterial assembly of different-sized aggregates in a full-scale aerobic granular sludge plant. *Environmental Science & Technology, 53*(14), 8291-8301.

Alper, J. S., & Gelb, R. I. (1990). Standard errors and confidence intervals in nonlinear regression: comparison of Monte Carlo and parametric statistics. *Journal of Physical Chemistry, 94*(11), 4747-4751.

Alphenaar, P. A., Pérez, M. C., & Lettinga, G. (1993). The influence of substrate transport limitation on porosity and methanogenic activity of anaerobic sludge granules. *Applied Microbiology and Biotechnology, 39*(2), 276-280.

Ames, J. R., Ryan, M. D., & Kovacic, P. (1986). Mechanism of antibacterial action: electron transfer and oxy radicals. *Journal of free radicals in biology medicine, 2*(5-6), 377-391.

Andrews, G. F., & Tien, C. (1981). Bacterial Film Growth in Adsorbent Surfaces. *AlChE Journal, 27*, 396-403.

APHA. (2005). *Standard methods for the examination of water and wastewater*. Washington DC, USA: American Public Health Association (APHA).

Arrojo, B., Mosquera-Corral, A., Campos, J., & Méndez, R. (2006). Effects of mechanical stress on Anammox granules in a sequencing batch reactor (SBR). *Journal of Biotechnology, 123*(4), 453-463.

Arvin, E., & Kristensen, G. H. (1982). Effect of denitrification on the pH in biofilms. *Water Science & Technology, 14*(8), 833-848.

Atkinson, M., & Bingman, C. (1997). Elemental composition of commercial seasalts. *Journal of Aquariculture and Aquatic Sciences, 8*(2), 39-43.

Axelsson, A., & Persson, B. (1988). Determination of effective diffusion coefficients in calcium alginate gel plates with varying yeast cell content. *Applied Biochemistry and Biotechnology, 18*, 231-250.

Azeredo, J., Henriques, M., Sillankorva, S., & Oliveira, R. (2003). Extraction of exopolymers from biofilms: the protective effect of glutaraldehyde. *Water Science & Technology, 47*(5), 175-179.

Baeten, J. E., Batstone, D. J., Schraa, O. J., van Loosdrecht, M. C. M., & Volcke, E. I. P. (2019). Modelling anaerobic, aerobic and partial nitritation-anammox granular sludge reactors - A review. *Water Research, 149*, 322-341.

Baeten, J. E., van Loosdrecht, M. C. M., & Volcke, E. I. P. (2018). Modelling aerobic granular sludge reactors through apparent half-saturation coefficients. *Water Research, 146*, 134-145.

Baillod, C. R., & Boyle, W. C. (1970). Mass transfer limitations in substrate removal. *Journal of the Sanitary Engineering Division, 96*(2), 525-545.

Banci, L., Bertini, I., Luchinat, C., & Mori, M. (2010). NMR in structural proteomics and beyond. *Progress in Nuclear Magnetic Resonance Spectroscopy, 56*(3), 247-266.

Bassin, J., Pronk, M., Kraan, R., Kleerebezem, R., & Van Loosdrecht, M. (2011). Ammonium adsorption in aerobic granular sludge, activated sludge and anammox granules. *Water Research, 45*(16), 5257-5265.

Bengtsson, S., de Blois, M., Wilén, B.-M., & Gustavsson, D. (2018). Treatment of municipal wastewater with aerobic granular sludge. *Critical Reviews in Environmental Science and Technology, 48*(2), 119-166.

Bengtsson, S., de Blois, M., Wilén, B.-M., & Gustavsson, D. (2019). A comparison of aerobic granular sludge with conventional and compact biological treatment technologies. *Environmental Technology, 40*(21), 2769-2778.

Beuling, E. E. (1998). *Mass transfer properties of biofilms.* (Doctoral dissertation), Universiteit van Amsterdam,

Beuling, E. E., D, v. D., Lens, P. N. L., van den Heuvel, J. C., Van As, H., & Ottengraf, S. P. P. (1998). Characterization of the diffusive properties of biofilms using pulsed field gradient-nuclear magnetic resonance. *Biotechnology and Bioengineering, 60*, 283-291.

Beuling, E. E., van den Heuvel, J. C., & Ottengraf, S. P. P. (2000). Diffusion coefficients of metabolites in active biofilms. *Biotechnology and Bioengineering, 67*, 53-60.

Beun, J., Van Loosdrecht, M., & Heijnen, J. (2002). Aerobic granulation in a sequencing batch airlift reactor. *Water Research, 36*(3), 702-712.

Beyenal, H., & Lewandowski, Z. (2002). Internal and external mass transfer in biofilms grown at various flow velocities. *Biotechnology progress, 18*(1), 55-61.

Beyenal, H., & Lewandowski, Z. (2005). Modeling mass transport and microbial activity in stratified biofilms. *Chemical Engineering Science, 60*(15), 4337-4348.

Beyenal, H., & Tanyolac, A. (1994). The calculation of simultaneous effective diffusion coefficients of the substrates in a fluidized bed biofilm reactor. *Water Science and Technology, 29*(10-11), 463.

Birmingham, J., Hughes, N., & Treloar, R. (1995). Diffusion and binding measurements within oral biofilms using fluorescence photobleaching recovery methods. *Philosophical Transactions of the Royal Society of London. Series B: Biological Sciences, 350*(1334), 325-343.

Boltz, J., Morgenroth, E., Brockmann, D., Bott, C., Gellner, W., & Vanrolleghem, P. (2011). Systematic evaluation of biofilm models for engineering practice: components and critical assumptions. *Water Science and Technology, 64*(4), 930-944.

Boltz, J., Morgenroth, E., & Sen, D. (2010). Mathematical modelling of biofilms and biofilm reactors for engineering design. *Water Science and Technology, 62*(8), 1821-1836.

Boontheekul, T., Kong, H. J., & Mooney, D. J. (2005). Controlling alginate gel degradation utilizing partial oxidation and bimodal molecular weight distribution. *Biomaterials, 26*(15), 2455-2465.

Brenner, T., & Matsukawa, S. (2016). Anomalous diffusion of poly (ethylene oxide) in agarose gels. *International Journal of Biological Macromolecules, 92*, 1151-1154.

Brownstein, K. R., & Tarr, C. E. (1979). Importance of classical diffusion in NMR studies of water in biological cells. *Physical Review A, 19*, 2446-2453.

Brumfield, S. K., Ortmann, A. C., Ruigrok, V., Suci, P., Douglas, T., & Young, M. J. (2009). Particle assembly and ultrastructural features associated with replication of the lytic archaeal virus Sulfolobus turreted icosahedral virus. *Journal of Virology, 83*(12), 5964-5970.

Bryant, L. D., McGinnis, D. F., Lorrai, C., Brand, A., Little, J. C., & Wüest, A. (2010). Evaluating oxygen fluxes using microprofiles from both sides of the sediment–water interface. *Limnol. Oceanogr.: Methods, 8*, 610-627.

Bryers, J. D., & Drummond, F. (1998). Local macromolecule diffusion coefficients in structurally non-uniform bacterial biofilms using fluorescence recovery after photobleaching (FRAP). *Biotechnology and Bioengineering, 60*(4), 462-473.

Bueno, R. d. F., Faria, J. K., Uliana, D. P., & Liduino, V. S. (2020). Simultaneous removal of organic matter and nitrogen compounds from landfill leachate by aerobic granular sludge. *Environmental Technology*, 1-15.

Callaghan, P. T. (1993). *Principles of nuclear magnetic resonance microscopy*. Oxford, UK: Oxford University Press.

Callaghan, P. T. (2011). *Translational dynamics and magnetic resonance: principles of pulsed gradient spin echo NMR*: Oxford University Press.

Callaghan, P. T., Godefroy, S., & Ryland, B. N. (2003). Diffusion–relaxation correlation in simple pore structures. *Journal of Magnetic Resonance, 162*, 320-327.

Cassidy, D., & Belia, E. (2005). Nitrogen and phosphorus removal from an abattoir wastewater in a SBR with aerobic granular sludge. *Water Research, 39*(19), 4817-4823.

Chen, M.-Y., Lee, D.-J., Tay, J.-H., & Show, K.-Y. (2007). Staining of extracellular polymeric substances and cells in bioaggregates. *Applied Microbiology and Biotechnology, 75*(2), 467-474.

Chiu, Z. C., Chen, M. Y., Lee, D. J., Tay, -. L., Tay, J. H., & Show, K. Y. (2006). Diffusivity of Oxygen in Aerobic Granules. *Biotechnology and Bioengineering, 94*(3).

Chiu, Z. C., Chen, M. Y., Lee, D. J., Wang, C. H., & Lai, J. Y. (2007a). Oxygen diffusion and consumption in active aerobic granules of heterogeneous structure. *Applied Microbiology and Biotechnology, 75*, 685-691.

Chiu, Z. C., Chen, M. Y., Lee, D. J., Wang, C. H., & Lai, J. Y. (2007b). Oxygen diffusion in active layer of aerobic granule with step change in surrounding oxygen levels. *Water Research, 41*, 884-892.

Chresand, T. J., Dale, B. E., Hanson, S. L., & Gillies, R. J. (1988). A Stirred Bath Technique for Diffusivity Measurements in Cell Matrices. *Biotechnology and Bioengineering, 32*(8).

Codd, S. L., Seymour, J. D., Gjersing, E. L., Gage, J. P., & Brown, J. R. (2006). Magnetic resonance microscopy of biofilm and bioreactor transport. In S. Stapf & S.-I. Han (Eds.), *NMR Imaging in Chemical Engineering*. Weinheim, Germany: Wiley.

Corsino, S., Campo, R., Di Bella, G., Torregrossa, M., & Viviani, G. (2016). Study of aerobic granular sludge stability in a continuous-flow membrane bioreactor. *Bioresource Technology, 200*, 1055-1059.

Crank, J. (1975). *The mathematics of difiusion* (2nd ed.). Oxford: Oxford University Press.

Cronenberg, C. C. H., & Van Den Heuvel, J. C. (1991). Determination of glucose diffusion coefficients in biofilms with micro-electrodes. *Biosensors & Bioelectronics, 6*(3), 255-262.

Csikor, Z., Mihaltz, P., Czako, L., & Hollo, J. (1994). New interpretation of expansion in biofilm-coated particle fluidization. *Applied Microbiology and Biotechnology, 41*(5), 608-614.

Daigger, G. T., & Boltz, J. P. (2011). Trickling filter and trickling filter-suspended growth process design and operation: a state-of-the-art review. *Water Environment Research, 83*(5), 388-404.

Daigger, G. T., & Littleton, H. X. (2014). Simultaneous Biological Nutrient Removal: A State-of-the-Art Review. *Water Environment Research, 86*(3), 245-257.

de Beer, D., & Stoodley, P. (1995). Relation between the structure of an aerobic biofilm and transport phenomena. *Water Science & Technology, 32*(8), 11-18.

de Beer, D., Stoodley, P., Roe, F., & Lewandowski, Z. (1994). Effects of biofilm structures on oxygen distribution and mass transport. *Biotechnology and Bioengineering, 43*, 1131-1138.

de Bruin, L. M. M., de Kreuk, M. K., van der Roest, H. F. R., Uijterlinde, C., & van Loosdrecht, M. C. M. (2004). Aerobic granular sludge technology: an alternative to activated sludge? *Water Science and Technology, 49*, 1-7.

de Graaff, D. R., van Dijk, E. J. H., van Loosdrecht, M. C. M., & Pronk, M. (2018). Strength characterization of full-scale aerobic granular sludge. *Environmental Technology*, 1-11.

de Kort, D. W., Schuster, E., Hoeben, F. J., Barnes, R., Emondts, M., Janssen, H. M., . . . van Duynhoven, J. P. (2018). Heterogeneity of network structures and water dynamics in κ-carrageenan gels probed by nanoparticle diffusometry. *Langmuir, 34*(37), 11110-11120.

de Kort, D. W., van Duynhoven, J. P., Van As, H., & Mariette, F. (2015). Nanoparticle diffusometry for quantitative assessment of submicron structure in food biopolymer networks. *Trends in Food Science & Technology, 42*(1), 13-26.

de Kreuk, M. K., Heijnen, J. J., & van Loosdrecht, M. C. M. (2005). Simultaneous COD, nitrogen, and phosphate removal by aerobic granular sludge. *Biotechnology and Bioengineering, 90*, 761-769.

de Kreuk, M. K., Kishida, N., Tsuneda, S., & van Loosdrecht, M. C. M. (2010). Behavior of polymeric substrates in an aerobic granular sludge system. *Water Research, 44*, 5929-5938.

de Kreuk, M. K., Picioreanu, C., Hosseini, M., Xavier, J. B., & van Loosdrecht, M. C. M. (2007). Kinetic model of a granular sludge SBR: Influences on nutrient removal. *Biotechnology and Bioengineering, 97*, 801-815.

de Kreuk, M. K., & Van Loosdrecht, M. C. M. (2004). Selection of slow growing organisms as a means for improving aerobic granular sludge stability. *Water Science & Technology, 49*(11-12), 9-17.

de Kreuk, M. K., & van Loosdrecht, M. C. M. (2006). Formation of aerobic granules with domestic sewage. *Journal of Environmental Engineering, 132*(6), 694-697.

de Sousa Rollemberg, S. L., Mendes Barros, A. R., Milen Firmino, P. I., & Bezerra Dos Santos, A. (2018). Aerobic granular sludge: Cultivation parameters and removal mechanisms. *Bioresource Technology, 270*, 678-688.

Devanand, K., & Selser, J. (1991). Asymptotic behavior and long-range interactions in aqueous solutions of poly (ethylene oxide). *Macromolecules, 24*(22), 5943-5947.

Di Bella, G., & Torregrossa, M. (2013). Simultaneous nitrogen and organic carbon removal in aerobic granular sludge reactors operated with high dissolved oxygen concentration. *Bioresource Technology, 142*, 706-713.

Di Iaconi, C., Ramadori, R., Lopez, A., & Passino, R. (2004). Preliminary biomass characterization in a sequencing batch biofilm reactor. *Annali di Chimica: Journal of Analytical, Environmental and Cultural Heritage Chemistry, 94*(12), 889-898.

Dibdin, G. (1981). Diffusion of sugars and carboxylic acids through human dental plaque in vitro. *Archives of oral biology, 26*(6), 515-523.

Dibdin, G. (1993). Effect of the bathing fluid on measurements of diffusion in dental plaque. *Archives of oral biology, 38*(3), 251-254.

Doğruel, S. (2012). Biodegradation characteristics of high strength municipal wastewater supported by particle size distribution. *Desalination and Water Treatment, 45*(1-3), 11-20.

Dohnalkova, A. C., Marshall, M. J., Arey, B. W., Williams, K. H., Buck, E. C., & Fredrickson, J. K. (2011). Imaging hydrated microbial extracellular polymers: comparative analysis by electron microscopy. *Applied and Environmental Microbiology, 77*(4), 1254-1262.

Dulekgurgen, E., Doğruel, S., Karahan, Ö., & Orhon, D. (2006). Size distribution of wastewater COD fractions as an index for biodegradability. *Water Research, 40*, 273-282.

Eberl, H. J., Picioreanu, C., Heijnen, J. J., & van Loosdrecht, M. C. M. (2000). A three-dimensional numerical study on the correlation of spatial structure, hydrodynamic conditions, and mass transfer and conversion in biofilms. *Chemical Engineering Science, 55*, 6209-6222.

Edzes, H. T., van Dusschoten, D., & Van As, H. (1998). Quantitative T2 Imaging of Plant Tissues By Means Of Multi-Echo MRI Microscopy. *Magnetic Resonance Imaging, 16*, 185-196.

Einstein, A. (1905). Über die von der molekularkinetischen Theorie der Wärme geforderte Bewegung von in ruhenden Flüssigkeiten suspendierten Teilchen. *Annalen der Physik, 4*.

El Abed, S., Ibnsouda, S. K., Latrache, H., & Hamadi, F. (2012). *Scanning electron microscopy (SEM) and environmental SEM: suitable tools for study of adhesion stage and biofilm formation*: Intechopen.

Engineering Toolbox. (2008). Gases solved in water - diffusion coefficients. Retrieved from https://www.engineeringtoolbox.com/diffusion-coefficients-d_1404.html

Engineering Toolbox. (2018). Air - Diffusion Coefficients of Gases in Excess of Air. Retrieved from https://www.engineeringtoolbox.com/air-diffusion-coefficient-gas-mixture-temperature-d_2010.html

Epstein, N. (1989). On tortuosity and the tortuosity factor in flow and diffusion through porous media. *Chemical Engineering Science, 44*, 777-779.

Erskine, E., MacPhee, C. E., & Stanley-Wall, N. R. (2018). Functional amyloid and other protein fibers in the biofilm matrix. *Journal of Molecular Biology, 430*(20), 3642-3656.

Etterer, T. J. (2006). *Formation, structure and function of aerobic granular sludge.* (PhD), Technische Universität München,

Etterer, T. J., & Wilderer, P. A. (2001). Generation and properties of aerobic granular sludge. *Water Science and Technology, 43*, 19-26.

Fan, L. S., Leyva-Ramos, R., Wisecarver, K., & Zehner, B. (1990). Diffusion of phenol through a biofilm grown on activated carbon particles in a draft-tube three-phase fluidized-bed bioreactor. *Biotechnology and Bioengineering, 35*(3), 279-286.

Favre, E., Leonard, M., Laurent, A., & Dellacherie, E. (2001). Diffusion of polyethyleneglycols in calcium alginate hydrogels. *Colloids and Surfaces A: Physicochemical and Engineering Aspects, 194*(1-3), 197-206.

Felz, S., Al-Zuhairy, S., Aarstad, O. A., van Loosdrecht, M. C., & Lin, Y. M. (2016). Extraction of structural extracellular polymeric substances from aerobic granular sludge. *JoVE (Journal of Visualized Experiments)*(115), e54534.

Felz, S., Kleikamp, H., Zlopasa, J., van Loosdrecht, M. C., & Lin, Y. (2020a). Impact of metal ions on structural EPS hydrogels from aerobic granular sludge. *Biofilm, 2*, 100011.

Felz, S., Neu, T. R., van Loosdrecht, M. C., & Lin, Y. (2020b). Aerobic granular sludge contains Hyaluronic acid-like and sulfated glycosaminoglycans-like polymers. *Water Research, 169*, 115291.

Fick, A. (1855). Ueber diffusion. *Annalen der Physik, 170*(1), 59-86.

Flory, P. J. (1953). *Principles of polymer chemistry*. Ithaca, New York: Cornell University Press.

Fu, Y., Zhang, T. C., & Bishop, P. (1994). Determination of effective oxygen diffusivity in biofilms grown in a completely mixed biodrum reactor. *Water Science & Technology, 29*(10-11), 455.

Fujie, K., Tsukamoto, T., & Kubota, H. (1979). Reaction kinetics of wastewater treatment with a microbial film. *J. Ferment. Technol., 57*, 539-545.

Gapes, D., & Keller, J. (2009). Impact of oxygen mass transfer on nitrification reactions in suspended carrier reactor biofilms. *Process Biochemistry, 44*(1), 43-53.

Gjaltema, A., Tijhuis, L., Van Loosdrecht, M., & Heijnen, J. (1995). Detachment of biomass from suspended nongrowing spherical biofilms in airlift reactors. *Biotechnology and Bioengineering, 46*(3), 258-269.

Gjersing, E. L., Codd, S. L., Seymour, J. D., & Stewart, P. S. (2005). Magnetic resonance microscopy analysis of advective transport in a biofilm reactor. *Biotechnology and Bioengineering, 89*(7), 822-834.

Godefroy, S., Korb, J.-P., Fleury, M., & Bryant, R. G. (2001). Surface nuclear magnetic relaxation and dynamics of water and oil in macroporous media. *Physical Review E, 64*, 021605.

Golmohamadi, M., & Wilkinson, K. J. (2013). Diffusion of ions in a calcium alginate hydrogel-structure is the primary factor controlling diffusion. *Carbohydrate Polymers, 94*, 82-87.

Gonzalez-Gil, G., & Holliger, C. (2014). Aerobic granules: microbial landscape and architecture, stages, and practical implications. *Applied and Environmental Microbiology, 80*, 3433-3441.

Gonzalez-Gil, G., Lens, P. N. L., van Aelst, A. C., Van As, H., Versprille, A. I., & Lettinga, G. (2001). Cluster structure of anaerobic aggregates of an expanded granular sludge bed reactor. *Applied and Environmental Microbiology, 67*, 3683-3692.

Guimerà, X., Dorado, A. D., Bonsfills, A., Gabriel, G., Gabriel, D., & Gamisans, X. (2016). Dynamic characterization of external and internal mass transport in heterotrophic biofilms from microsensors measurements. *Water Research, 102*, 551-560.

Hao, X., Heijnen, J. J., & van Loosdrecht, M. C. (2002). Sensitivity analysis of a biofilm model describing a one-stage completely autotrophic nitrogen removal (CANON) process. *Biotechnology and Bioengineering, 77*(3), 266-277.

Harremoës, P. (1978). Biofilm kinetics. In R. Mitchell (Ed.), *Water pollution microbiology* (pp. 71-109): John Wiley & Sons Ltd.

Harris, N. P., & Hansford, G. (1976). A study of substrate removal in a microbial film reactor. *Water Research, 10*(11), 935-943.

Helton, J. C., & Davis, F. J. (2003). Latin hypercube sampling and the propagation of uncertainty in analyses of complex systems. *Reliability Engineering & System Safety, 81*(1), 23-69.

Henze, M., Gujer, W., Mino, T., Matsuo, T., & Wentzel, M. (1995). Wastewater and biomass characterization for the activated sludge model no. 2: biological phosphorus removal. *Water Science & Technology, 31*(2), 13.

Henze, M., & Harremoës, P. (1983). Anaerobic treatment of wastewater in fixed film reactors–a literature review. *Water Science and Technology, 15*(8-9), 1-101.

Henze, M., & Harremoës, P. (1992). Characterization of Wastewater: The Effect of Chemical Precipitation on the Wastewater Composition and its Consequences for Biological Denitrification. In R. Klute & H. Hahn (Eds.), *Chemical Water and Wastewater Treatment II* (pp. 299-311). Berlin, Heidelberg: Springer, Berlin, Heidelberg.

Herrling, M. P., Fetsch, K. L., Delay, M., Blauert, F., Wagner, M., Franzreb, M., . . . Lackner, S. (2015). Low biosorption of PVA coated engineered magnetic nanoparticles in granular sludge assessed by magnetic susceptibility. *Science of the Total Environment, 537*, 43-50.

Herrling, M. P., Weisbrodt, J., Kirkland, C. M., Williamson, N. H., Lackner, S., Codd, S. L., . . . Horn, H. (2017). NMR investigation of water diffusion in different biofilm structures. *Biotechnology and Bioengineering*.

Hille, A., Neu, T. R., Hempel, D. C., & Horn, H. (2009). Effective diffusivities and mass fluxes in fungal biopellets. *Biotechnology and Bioengineering, 103*, 1202-1213.

Hills, B. P. (1992). The proton exchange cross-relaxation model of water relaxation in biopolymer systems. *Molecular Physics, 76*, 489-508.

Hinson, R. K., & Kocher, W. M. (1996). Model for effective diffusivities in aerobic biofilms. *Journal of Environmental Engineering, 122*(11), 1023-1030.

Horn, H., & Morgenroth, E. (2006). Transport of oxygen, sodium chloride, and sodium nitrate in biofilms. *Chemical Engineering Science, 61*, 1347-1356.

Hornemann, J. A., Lysova, A. A., Codd, S. L., Seymour, J. D., Busse, S. C., Stewart, P. S., & Brown, J. R. (2008). Biopolymer and water dynamics in microbial biofilm extracellular polymeric substance. *Biomacromolecules, 9*(9), 2322-2328.

Hoskins, B. C., Fevang, L., Majors, P. D., Sharma, M. M., & Georgiou, G. (1999). Selective imaging of biofilms in porous media by NMR relaxation. *Journal of Magnetic Resonance, 139*(1), 67-73.

Hu, Z., Chandran, K., Smets, B. F., & Grasso, D. (2002). Evaluation of a rapid physical-chemical method for the determination of extant soluble COD. *Water Research, 36*(3), 617-624.

Huisman, J. W., Van den Heuvel, J. C., & Ottengraf, S. P. P. (1990). Enhancement of external mass transfer by gaseous end products. *Biotechnology Progress, 6*, 425-429.

Hürlimann, M., Venkataramanan, L., & Flaum, C. (2002). The diffusion–spin relaxation time distribution function as an experimental probe to characterize fluid mixtures in porous media. *The journal of chemical physics, 117*(22), 10223-10232.

Isanta, E., Suárez-Ojeda, M. E., del Río, Á. V., Morales, N., Pérez, J., & Carrera, J. (2012). Long term operation of a granular sequencing batch reactor at pilot scale treating a low-strength wastewater. *Chemical Engineering Journal, 198*, 163-170.

Ivanov, V., Tay, S.-L., Liu, Q.-S., Wang, X.-H., Wang, Z.-W., & Tay, J.-H. (2005). Formation and structure of granulated microbial aggregates used in aerobic wastewater treatment. *Water Science and Technology, 52*(7), 13-19.

Jenkins, D., & Wanner, J. (2014). *Activated sludge-100 years and counting*: IWA publishing.

Jimenez, B., Noyola, A., & Capdeville, B. (1988a). Selected dyes for residence time distribution evaluation in bioreactors. *Biotechnology Techniques, 2*(2), 77-82.

Jimenez, B., Noyola, A., Capdeville, B., Roustan, M., & Faup, G. (1988b). Dextran blue colorant as a reliable tracer in submerged filters. *Water Research, 22*(10), 1253-1257.

Jones, E. R., van Vliet, M. T., Qadir, M., & Bierkens, M. F. (2021). Country-level and gridded estimates of wastewater production, collection, treatment and reuse. *Earth System Science Data, 13*(2), 237-254.

Kagawa, Y., Tahata, J., Kishida, N., Matsumoto, S., Picioreanu, C., Van Loosdrecht, M., & Tsuneda, S. (2015). Modeling the nutrient removal process in aerobic granular sludge system by coupling the reactor-and granule-scale models. *Biotechnology and Bioengineering, 112*(1), 53-64.

Karahan, Ö., Dogruel, S., Dulekgurgen, E., & Orhon, D. (2008). COD fractionation of tannery wastewaters-Particle size distribution, biodegradability and modeling. *Water Research, 42*, 1083-1092.

Karim, K., & Gupta, S. (2002). Biosorption of nitrophenols on anaerobic granular sludge. *Environmental Technology, 23*(12), 1379-1384.

Kennedy, K., Lu, J., & Mohn, W. W. (1992). Biosorption of chlorophenols to anaerobic granular sludge. *Water Research, 26*(8), 1085-1092.

Khan, A., & Richardson, J. (1987). The resistance to motion of a solid sphere in a fluid. *Chemical Engineering Communications, 62*(1-6), 135-150.

Khlebnikov, A., Samb, F., & Péringer, P. (1998). A transient mathematical model for maximum respiration activity and oxygen diffusion coefficient estimation in non-steady-state biofilms. *Journal of Chemical Technology & Biotechnology, 73*(3), 274-280.

Kirkland, C. M., Krug, J. R., Vergeldt, F. J., van den Berg, L., Velders, A. H., Seymour, J. D., . . . de Kreuk, M. K. (2020). Characterizing the structure of aerobic granular sludge using ultra-high field magnetic resonance. *Water Science and Technology*.

Kishida, N., Tsuneda, S., Kim, J., & Sudo, R. (2009). Simultaneous nitrogen and phosphorus removal from high-strength industrial wastewater using aerobic granular sludge. *Journal of Environmental Engineering, 135*(3), 153-158.

Kühl, M., & Jørgensen, B. B. (1992). Microsensor measurements of sulfate reduction and sulfide oxidation in compact microbial communities of aerobic biofilms. *Appl. Environ. Microbiol., 58*(4), 1164-1174.

la Cour Jansen, J., & Harremoes, P. (1985). Removal of soluble substrates in fixed films. *Water Science & Technology, 17*(2-3), 1-14.

Lai, V. K., Nedrelow, D. S., Lake, S. P., Kim, B., Weiss, E. M., Tranquillo, R. T., & Barocas, V. H. (2016). Swelling of collagen-hyaluronic acid co-gels: an in vitro residual stress model. *Annals of Biomedical Engineering, 44*(10), 2984-2993.

LaMotta, E. J. (1976a). External mass transfer in a biological film reactor. *Biotechnology and Bioengineering, 18*(10), 1359-1370.

LaMotta, E. J. (1976b). Internal diffusion and reaction in biological films. *Environmental Science & Technology, 10*(8), 765-769.

Larsen, P., Nielsen, J. L., Dueholm, M. S., Wetzel, R., Otzen, D., & Nielsen, P. H. (2007). Amyloid adhesins are abundant in natural biofilms. *Environmental Microbiology, 9*(12), 3077-3090.

Lawrence, J. R., Wolfaardt, G. M., & Korber, D. R. (1994). Determination of diffusion coefficients in biofilms by confocal laser microscopy. *Appl Environ Microbiol, 60*(4), 1166-1173.

Layer, M., Adler, A., Reynaert, E., Hernandez, A., Pagni, M., Morgenroth, E., . . . Derlon, N. (2019). Organic substrate diffusibility governs microbial community composition, nutrient removal performance and kinetics of granulation of aerobic granular sludge. *Water research X, 4*, 100033.

Layer, M., Villodres, M. G., Hernandez, A., Reynaert, E., Morgenroth, E., & Derlon, N. (2020). Limited simultaneous nitrification-denitrification (SND) in aerobic granular sludge systems treating municipal wastewater: Mechanisms and practical implications. *Water research X, 7*, 100048.

Leal-Egaña, A., Braumann, U.-D., Díaz-Cuenca, A., Nowicki, M., & Bader, A. (2011). Determination of pore size distribution at the cell-hydrogel interface. *Journal of nanobiotechnology, 9*(1), 1-7.

Lefebvre, O., & Moletta, R. (2006). Treatment of organic pollution in industrial saline wastewater: a literature review. *Water Research, 40*(20), 3671-3682.

Lemaire, R., Webb, R. I., & Yuan, Z. (2008). Micro-scale observations of the structure of aerobic microbial granules used for the treatment of nutrient-rich industrial wastewater. *The ISME journal, 212*, 528-541.

Lens, P. N. L., De Beer, D., Cronenberg, C. C. H., Houwen, F. P., Ottengraf, S. P. P., & Verstraetel, W. H. (1993). Heterogeneous Distribution of Microbial Activity in Methanogenic Aggregates: pH and Glucose Microprofiles. *Applied and Environmental Microbiology, 59*(11), 3803-3815.

Lens, P. N. L., Gastesi, R., Vergeldt, F. J., van Aelst, A. C., Pisabarro, A. G., & Van As, H. (2003). Diffusional properties of methanogenic granular sludge: 1H NMR characterization. *Applied and Environmental Microbiology, 69*(11), 6644-6649.

Lens, P. N. L., Pol, L. H., Lettinga, G., & Van As, H. (1997). Use of 1H NMR to study transport processes in sulfidogenic granular sludge. *Water Science and Technology, 36*.

Lewandowski, Z. (2000). Notes on biofilm porosity. *Water Research, 34*(9), 2620-2624.

Lewandowski, Z., Stoodley, P., Altobelli, S., & Fukushima, E. (1994). Hydrodynamics and kinetics in biofilm systems-recent advances and new problems. *Water Science and Technology, 29*(10-11), 223.

Lewandowski, Z., Walser, G., & Characklis, W. G. (1991). Reaction kinetics in biofilms. *Biotechnology and Bioengineering, 38*(8), 877-882.

Li, W., Zheng, P., Wang, L., Zhang, M., Lu, H., Xing, Y., . . . Ghulam, A. (2013). Physical characteristics and formation mechanism of denitrifying granular sludge in high-load reactor. *Bioresource Technology, 142*, 683-687.

Li, X., Luo, J., Guo, G., Mackey, H. R., Hao, T., & Chen, G. (2017). Seawater-based wastewater accelerates development of aerobic granular sludge: A laboratory proof-of-concept. *Water Research, 115*, 210-219.

Li, Y., Liu, Y., Shen, L., & Chen, F. (2008). DO diffusion profile in aerobic granule and its microbiological implications. *Enzyme and Microbial Technology, 43*, 349-354.

Libicki, S. B., Salmon, P. M., & Robertson, C. R. (1988). The effective diffusive permeability of a nonreacting solute in microbial cell aggregates. *Biotechnology and Bioengineering, 32*(1), 68-85.

Lin, Y., de Kreuk, M. K., Van Loosdrecht, M. C. M., & Adin, A. (2010). Characterization of alginate-like exopolysaccharides isolated from aerobic granular sludge in pilot-plant. *Water Research, 44*(11), 3355-3364.

Lin, Y., Nierop, K., Girbal-Neuhauser, E., Adriaanse, M., & Van Loosdrecht, M. (2015). Sustainable polysaccharide-based biomaterial recovered from waste aerobic granular sludge as a surface coating material. *Sustainable Materials and Technologies, 4*, 24-29.

Lin, Y., Reino, C., Carrera, J., Pérez, J., & van Loosdrecht, M. C. M. (2018). Glycosylated amyloid-like proteins in the structural extracellular polymers of aerobic granular sludge enriched with ammonium-oxidizing bacteria. *Microbiology Open*, e00616.

Lin, Y., Zhang, H., & Adin, A. (2009). Characterization of bacterial alginate extracted from biofilm matrix. *Desalination and Water Treatment, 8*(1-3), 250-255.

Liu, L., Sheng, G.-P., Liu, Z.-F., Li, W.-W., Zeng, R. J., Lee, D.-J., . . . Yu, H.-Q. (2010). Characterization of Multiporous Structure and Oxygen Transfer Inside Aerobic Granules with the Percolation Model. *Environmental Science & Technology, 44*, 8535-8540.

Liu, N., Dopffel, N., Hovland, B., Alagic, E., Vik, B. F., & Bødtker, G. (2020). High osmotic stress initiates expansion and detachment of Thalassospira sp. biofilms in glass microchannels. *Journal of Environmental Chemical Engineering, 8*(6), 104525.

Liu, S.-Y., Chen, Y.-P., Fang, F., Xu, J., Sheng, G.-P., Yu, H.-Q., . . . Tian, Y.-C. (2009). Measurement of dissolved oxygen and its diffusivity in aerobic granules using a lithographically-fabricated microelectrode array. *Environmental Science & Technology, 43*(4), 1160-1165.

Liu, Y.-Q., Tay, J.-H., & Moy, B. Y.-P. (2006). Characteristics of aerobic granular sludge in a sequencing batch reactor with variable aeration. *Applied Microbiology and Biotechnology, 71*(5), 761-766.

Liu, Y., Wang, Z. W., Liu, Y. Q., Qin, L., & Tay, J. H. (2005). A generalized model for settling velocity of aerobic granular sludge. *Biotechnology progress, 21*(2), 621-626.

Livingston, A. G., & Chase, H. A. (1989). Modeling phenol degradation in a fluidized-bed bioreactor. *AIChE journal, 35*(12), 1980-1992.

Logan, B. E., & Jiang, Q. (1990). Molecular size distributions of dissolved organic matter. *Journal of Environmental Engineering, 116*(6), 1046-1062.

López-Palau, S., Dosta, J., Pericas, A., & Mata-Álvarez, J. (2011). Partial nitrification of sludge reject water using suspended and granular biomass. *Journal of Chemical Technology & Biotechnology, 86*(12), 1480-1487.

Lotti, T., Carretti, E., Berti, D., Martina, M. R., Lubello, C., & Malpei, F. (2019). Extraction, recovery and characterization of structural extracellular polymeric substances from anammox granular sludge. *Journal of Environmental Management, 236*, 649-656.

Marcotte, L., Therien-Aubin, H., Sandt, C., Barbeau, J., & Lafleur, M. (2004). Solute Size Effects on the Diffusion in Biofilms of Streptococcus mutans. *Biofouling, 20*, 189-201.

Matson, J. V., & Characklis, W. G. (1976). Diffusion into microbial aggregates. *Water Research, 10*, 877-885.

McDonnell, G., & Russell, A. D. (1999). Antiseptics and disinfectants: activity, action, and resistance. *Clinical Microbiology Reviews, 12*(1), 147-179.

McKay, M. D., Beckman, R. J., & Conover, W. J. (1979). Comparison of three methods for selecting values of input variables in the analysis of output from a computer code. *Technometriccs, 21*(2), 239-245.

McNee, S., Geddes, D., & Weetman, D. (1982). Diffusion of sugars and acids in human dental plaque in vitro. *Archives of oral biology, 27*(11), 975-979.

Mcswain, B. S., Irvine, R. L., Hausner, M., & Wilderer, P. A. (2005). Composition and Distribution of Extracellular Polymeric Substances in Aerobic Flocs and Granular Sludge. *Applied and Environmental Microbiology, 71*, 1051-1057.

Meyer, R. L., Saunders, A. M., Zeng, R. J., Keller, J., & Blackall, L. L. (2003). Microscale structure and function of anaerobic—aerobic granules containing glycogen accumulating organisms. *FEMS Microbiology Ecology, 45*(3), 253-261.

Möller, M., Botti, H., Batthyany, C., Rubbo, H., Radi, R., & Denicola, A. (2005). Direct measurement of nitric oxide and oxygen partitioning into liposomes and low density lipoprotein. *Journal of Biological Chemistry, 280*(10), 8850-8854.

Morgenroth, E. (2008). Modelling biofilms. In M. Henze, M. C. M. Van Loosdrecht, G. A. Ekama, & D. Brdjanovic (Eds.), *Biological Wastewater Treatment: Principles, Modelling and Design*. London, UK: IWA Publishing.

Morgenroth, E., Eberl, H. J., & van Loosdrecht, M. C. M. (2000). Evaluating 3-D and 1-D mathematical models for mass transport in heterogeneous biofilms. *Water Science and Technology, 41*.

Morgenroth, E., Eberl, H. J., Van Loosdrecht, M. C. M., Noguera, D., Pizarro, G., Picioreanu, C., . . . Wanner, O. (2004). Comparing biofilm models for a single species biofilm system. *Water Science & Technology, 49*(11-12), 145-154.

Morgenroth, E., Sherden, T., Van Loosdrecht, M., Heijnen, J., & Wilderer, P. (1997). Aerobic granular sludge in a sequencing batch reactor. *Water Research, 31*(12), 3191-3194.

Mosquera-Corral, A., de Kreuk, M. K., Heijnen, J. J., & van Loosdrecht, M. C. M. (2005). Effects of oxygen concentration on N-removal in an aerobic granular sludge reactor. *Water Research, 39*, 2676-2686.

Mu, Y., Yu, H.-Q., & Wang, G. (2006). Permeabilities of anaerobic CH4-producing granules. *Water Research, 40*(9), 1811-1815.

Mulcahy, L. T., Shieh, W. K., & LaMotta, E. J. (1981). Kinetic model of biological denitrification in a fluidized bed biofilm reactor (FBBR). In S. H. Jenkins (Ed.), *Water Pollution Research and Development* (pp. 143-157): Elsevier.

Nguyen, A. L., & Luong, J. (1986). Diffusion in κ-carrageenan gel beads. *Biotechnology and Bioengineering, 28*(8), 1261-1267.

Ni, B.-J., & Yu, H.-Q. (2010). Mathematical modeling of aerobic granular sludge: A review. *Biotechnology Advances, 28*, 895-909.

Nicolella, C., Van Loosdrecht, M., & Heijnen, J. (1998). Mass transfer and reaction in a biofilm airlift suspension reactor. *Chemical Engineering Science, 53*(15), 2743-2753.

Nicolella, C., van Loosdrecht, M. C., Di Felice, R., & Rovatti, M. (1999). Terminal settling velocity and bed-expansion characteristics of biofilm-coated particles. *Biotechnology and Bioengineering, 62*(1), 62-70.

Nicolella, C., van Loosdrecht, M. C. M., & Heijnen, J. J. (2000). Particle-based biofilm reactor technology. *Trends in Biotechnology, 18*, 312-320.

Ning, Y.-F., Chen, Y.-P., Shen, Y., Zeng, N., Liu, S.-Y., Guo, J.-S., & Fang, F. (2014). A new approach for estimating aerobic–anaerobic biofilm structure in wastewater treatment via dissolved oxygen microdistribution. *Chemical Engineering Journal, 255*, 171-177.

Nogueira, B. L., Pérez, J., van Loosdrecht, M. C., Secchi, A. R., Dezotti, M., & Biscaia Jr, E. C. (2015). Determination of the external mass transfer coefficient and influence of mixing intensity in moving bed biofilm reactors for wastewater treatment. *Water Research, 80*, 90-98.

Nor-Anuar, A., Ujang, Z., Van Loosdrecht, M., De Kreuk, M., & Olsson, G. (2012). Strength characteristics of aerobic granular sludge. *Water Science and Technology, 65*(2), 309-316.

Ødegaard, H. (2006). Innovations in wastewater treatment:–the moving bed biofilm process. *Water Science and Technology, 53*(9), 17-33.

Onuma, M., & Omura, T. (1982). Mass-transfer characteristics within microbial systems. *Water Science & Technology, 14*(6-7), 553-568.

Ozturk, S. S., Palsson, B. O., & Thiele, J. H. (1989). Control of interspecies electron transfer flow during anaerobic digestion: dynamic diffusion reaction models for hydrogen gas transfer in microbial flocs. *Biotechnology and Bioengineering, 33*(6), 745-757.

Pertoft, H., Laurent, T. C., Låås, T., & Kågedal, L. (1978). Density gradients prepared from colloidal silica particles coated by polyvinylpyrrolidone (Percoll). *Analytical Biochemistry, 88*(1), 271-282.

Peulen, T.-O., & Wilkinson, K. J. (2011). Diffusion of nanoparticles in a biofilm. *Environmental Science & Technology, 45*(8), 3367-3373.

Pfaff, N.-M., Kleijn, J. M., van Loosdrecht, M. C., & Kemperman, A. J. (2021). Formation and ripening of alginate-like exopolymer gel layers during and after membrane filtration. *Water Research, 195*, 116959.

Phoenix, V. R., & Holmes, W. M. (2008). Magnetic resonance imaging of structure, diffusivity, and copper immobilization in a phototrophic biofilm. *Applied and Environmental Microbiology, 74*, 4934-4943.

Picioreanu, C., Pérez, J., & van Loosdrecht, M. C. M. (2016). Impact of cell cluster size on apparent half-saturation coefficients for oxygen in nitrifying sludge and biofilms. *Water Research, 106*, 371-382.

Picioreanu, C., van Loosdrecht, M. C. M., & Heijnen, J. J. (2000). A theoretical study on the effect of surface roughness on mass transport and transformation in biofilms. *Biotechnology and Bioengineering, 68*, 355-369.

Pipes, D. M., Characklis, W. G., & Matson, J. V. (1974). Discussion of "Substrate Removal Mechanism of Trickling Filters". *Journal of the Environmental Engineering Division, 100*(1), 225-226.

Priester, J. H., Horst, A. M., Van De Werfhorst, L. C., Saleta, J. L., Mertes, L. A., & Holden, P. A. (2007). Enhanced visualization of microbial biofilms by staining and environmental scanning electron microscopy. *Journal of Microbiological Methods, 68*(3), 577-587.

Pronk, M., Abbas, B., Al-Zuhairy, S., Kraan, R., Kleerebezem, R., & Van Loosdrecht, M. (2015a). Effect and behaviour of different substrates in relation to the formation of aerobic granular sludge. *Applied Microbiology and Biotechnology, 99*(12), 5257-5268.

Pronk, M., de Kreuk, M. K., de Bruin, B., Kamminga, P., Kleerebezem, R., & van Loosdrecht, M. C. M. (2015b). Full scale performance of the aerobic granular sludge process for sewage treatment. *Water Research, 84*, 207-217.

Pronk, M., Giesen, A., Thomphson, A., Robertson, S., & van Loosdrecht, M. C. M. (2017). Aerobic granular biomass technology: advancements in design, applications and further developments. *Water Practice & Technology, 12*, 987-996.

Provencher, S. W. (1982). A constrained regularization method for inverting data represented by linear algebraic or integral equations. *Computer Physics Communications, 27*(3), 213-227.

Pu, H. T., & Yang, R. Y. K. (1988). Diffusion of sucrose and yohimbine in calcium alginate gel beads with or without entrapped plant cells. *Biotechnology and Bioengineering, 32*, 891-896.

Puguan, J. M. C., Yu, X., & Kim, H. (2015). Diffusion characteristics of different molecular weight solutes in Ca–alginate gel beads. *Colloids and Surfaces A: Physicochemical and Engineering Aspects, 469*, 158-165.

Quoc, B. N., Wei, S., Armenta, M., Bucher, R., Sukapanpotharam, P., Stahl, D. A., . . . Winkler, M.-K. H. (2021). Aerobic granular sludge: Impact of size distribution on nitrification capacity. *Water Research, 188*, 116445.

Rasmussen, K., & Lewandowski, Z. (1998). Microelectrode measurements of local mass transport rates in heterogeneous biofilms. *Biotechnology and Bioengineering, 59*(3), 302-309.

Ravndal, K. T., Opsahl, E., Bagi, A., & Kommedal, R. (2018). Wastewater characterisation by combining size fractionation, chemical composition and biodegradability. *Water Research*.

Renslow, R. S., Babauta, J. T., Majors, P. D., & Beyenal, H. (2013). Diffusion in biofilms respiring on electrodes. *Energy Environ. Sci., 6*, 595-607.

Renslow, R. S., Majors, P. D., McLean, J. S., Fredrickson, J. K., Ahmed, B., & Beyenal, H. (2010). In situ effective diffusion coefficient profiles in live biofilms using pulsed-field gradient nuclear magnetic resonance. *Biotechnology and Bioengineering, 106*, 928-937.

Revsbech, N. P., Madsen, B., & Jørgensen, B. (1986). Oxygen production and consumption in sediments determined at high spatial resolution by computer simulation of oxygen microelectrode data. *Limnology and Oceanography, 31*(2), 293-304.

Richards, S., & Turner, R. (1984). A comparative study of techniques for the examination of biofilms by scanning electron microscopy. *Water Research, 18*(6), 767-773.

Robinson, A. (2018). Did Einstein really say that? Retrieved from https://www.nature.com/articles/d41586-018-05004-4

Romero, D., Aguilar, C., Losick, R., & Kolter, R. (2010). Amyloid fibers provide structural integrity to Bacillus subtilis biofilms. *Proceedings of the National Academy of Sciences, 107*(5), 2230-2234.

Royal HaskoningDHV. (2021). Nereda. Retrieved from https://www.royalhaskoningdhv.com/nereda

Saitoh, S., Araki, Y., Kon, R., Katsura, H., & Taira, M. (2000). Swelling/deswelling mechanism of calcium alginate gel in aqueous solutions. *Dental materials journal, 19*(4), 396-404.

Saltelli, A., Ratto, M., Andres, T., Campolongo, F., Cariboni, J., Gatelli, D., . . . Tarantola, S. (2008). *Global sensitivity analysis: the primer*: John Wiley & Sons.

Sankaran, J., Tan, N., But, K. P., Cohen, Y., Rice, S. A., & Wohland, T. (2019). Single microcolony diffusion analysis in Pseudomonas aeruginosa biofilms. *NPJ Biofilms Microbiomes, 5*(1), 35.

Schambeck, C. M., Girbal-Neuhauser, E., Boni, L., Fischer, P., Bessiere, Y., Paul, E., . . . Derlon, N. (2020). Chemical and physical properties of alginate-like exopolymers of aerobic granules and flocs produced from different wastewaters. *Bioresource Technology, 312*, 123632.

Schmidt, J. E., & Ahring, B. K. (1996). Granular sludge formation in upflow anaerobic sludge blanket (UASB) reactors. *Biotechnology and Bioengineering, 49*(3), 229-246.

Schneider, C. A., Rasband, W. S., & Eliceiri, K. W. (2012). NIH Image to ImageJ: 25 years of image analysis. *Nature Methods, 9*(7), 671-675.

Seviour, T., Pijuan, M., Nicholson, T., Keller, J., & Yuan, Z. (2009). Understanding the properties of aerobic sludge granules as hydrogels. *Biotechnology and Bioengineering, 102*, 1483-1493.

Seviour, T., Yuan, Z., van Loosdrecht, M. C., & Lin, Y. (2012). Aerobic sludge granulation: a tale of two polysaccharides? *Water Research, 46*(15), 4803-4813.

Seymour, J. D., Codd, S. L., Gjersing, E. L., & Stewart, P. S. (2004). Magnetic resonance microscopy of biofilm structure and impact on transport in a capillary bioreactor. *Journal of Magnetic Resonance*.

Shanahan, J., Cole, A., Semmens, M., & LaPara, T. M. (2005). Acetate and ammonium diffusivity in membrane-aerated biofilms: improving model predictions using experimental results. *Water Science and Technology, 52*(7), 121-126.

Shoulders, M. D., & Raines, R. T. (2009). Collagen structure and stability. *Annual review of biochemistry, 78*, 929-958.

Siegrist, H., & Gujer, W. (1985). Mass transfer mechanisms in a heterotrophic biofilm. *Water Research, 19*(11), 1369-1378.

Simpliciano, C., Clark, L., Asi, B., Chu, N., Mercado, M., Diaz, S., . . . Mobed-Miremadi, M. (2013). Cross-linked alginate film pore size determination using atomic force microscopy and validation using diffusivity determinations. *Journal of Surface Engineered Materials and Advanced Technology, 3*(4), 1-12.

Sin, G., Gernaey, K. V., Neumann, M. B., van Loosdrecht, M. C. M., & Gujer, W. (2009). Uncertainty analysis in WWTP model applications: A critical discussion using an example from design. *Water Research, 43*, 2894-2906.

Sin, G., Gernaey, K. V., Neumann, M. B., van Loosdrecht, M. C. M., & Gujer, W. (2011). Global sensitivity analysis in wastewater treatment plant model applications: Prioritizing sources of uncertainty. *Water Research, 45*, 639-651.

Smidsrød, O., & Skja, G. (1990). Alginate as immobilization matrix for cells. *Trends in Biotechnology, 8*, 71-78.

Stejskal, E. O., & Tanner, J. E. (1965). Spin diffusion measurements: spin echoes in the presence of a time-dependent field gradient. *The journal of chemical physics, 42*(1), 288-292.

Stewart, P. S. (1996). Theoretical aspects of antibiotic diffusion into microbial biofilms. *J Antimicrobial agents chemotherapy, 40*(11), 2517-2522.

Stewart, P. S. (1998). A review of experimental measurements of effective diffusive permeabilities and effective diffusion coefficients in biofilms. *Biotechnology and Bioengineering, 59*, 261-272.

Stewart, P. S. (2003). Diffusion in biofilms. *Journal of Bacteriology, 185*, 1485-1491.

Stewart, P. S., Murga, R., Srinivasan, R., & de Beer, D. (1995). Biofilm structural heterogeneity visualized by three microscopic methods. *Water Research, 29*(8), 2006-2009.

Stokes, D. J. (2001). Characterisation of soft condensed matter and delicate materials using environmental scanning electron microscopy (ESEM). *Advanced Engineering Materials, 3*(3), 126-130.

Stoodley, P., Boyle, J. D., DeBeer, D., & Lappin-Scott, H. M. (1999). Evolving perspectives of biofilm structure. *Biofouling, 14*(1), 75-90.

Stoodley, P., De Beer, D., & Lewandowski, Z. (1994). Liquid flow in biofilm systems. *Applied and Environmental Microbiology, 60*(8), 2711-2716.

Tago, Y., & Aida, K. (1977). Exocellular mucopolysaccharide closely related to bacterial floc formation. *Applied and Environmental Microbiology, 34*(3), 308-314.

Takács, I., Bye, C., Chapman, K., Dold, P., Fairlamb, P., & Jones, R. (2007). A biofilm model for engineering design. *Water Science and Technology, 55*(8-9), 329-336.

Takenaka, S., Pitts, B., Trivedi, H. M., & Stewart, P. S. (2009). Diffusion of macromolecules in model oral biofilms. *Applied and Environmental Microbiology, 75*(6), 1750-1753.

Tang, B., Song, H., Bin, L., Huang, S., Zhang, W., Fu, F., . . . Chen, Q. (2017). Determination of the profile of DO and its mass transferring coefficient in a biofilm reactor packed with semi-suspended bio-carriers. *Bioresource Technology, 241*, 54-62.

Tang, W. T., & Fan, L. S. (1987). Steady state phenol degradation in a draft-tube, gas-liquid-solid fluidized-bed bioreactor. *AlChE Journal, 33*(2), 239-249.

Tassew, F. A., Bergland, W. H., Dinamarca, C., & Bakke, R. (2019). Settling velocity and size distribution measurement of anaerobic granular sludge using microscopic image analysis. *Journal of Microbiological Methods, 159*, 81-90.

Tatevossian, A. (1979). Diffusion of radio tracers in human dental plaque. *Carries research, 13*(3), 154-162.

Tay, J.-H., Ivanov, V., Pan, S., & Tay, S. T.-L. (2002). Specific layers in aerobically grown microbial granules. *Letters in Applied Microbiology, 34*, 254-257.

Tay, J.-H., Liu, Q. S., & Liu, Y. (2001). The role of cellular polysaccharides in the formation and stability of aerobic granules. *Letters in Applied Microbiology, 33*(3), 222-226.

Thurnheer, T., Gmür, R., Shapiro, S., & Guggenheim, B. (2003). Mass Transport of Macromolecules within an In Vitro Model of Supragingival Plaque. *Applied and Environmental Microbiology, 69*, 1702-1709.

Tijhuis, L., van Benthum, W. A. J., van Loosdrecht, M. C. M., & Heijnen, J. J. (1994a). Solids Retention Time in Spherical Biofilms in a Biofilm Airlift Suspension Reactor. *Biotechnology and Bioengineering, 44*, 867-879.

Tijhuis, L., Van Loosdrecht, M., & Heijnen, J. (1994b). Formation and growth of heterotrophic aerobic biofilms on small suspended particles in airlift reactors. *Biotechnology and Bioengineering, 44*(5), 595-608.

Torfs, E., Nopens, I., Winkler, M., Vanrolleghem, P. A., Balemans, S., & Smets, I. Y. (2016). Settling tests. In M. C. M. van Loosdrecht, P. Nielsen, C. M. Lopez-Vazquez, & D. Brdjanovic (Eds.), *Experimental Methods in Wastewater Treatment* (pp. 235-262). London: IWA Publishing.

Trego, A. C., Morabito, C., Mills, S., Connelly, S., Bourven, I., Guibaud, G., . . . Collins, G. (2018). Diversity converges during community assembly in methanogenic granules, suggesting a biofilm life-cycle. *BioRxiv*, 484642.

UN Habitat, & WHO. (2021). *Progress on wastewater treatment – Global status and acceleration needs for SDG indicator 6.3.1*. Geneva: United Nations Human Settlements Programme (UN-Habitat) and World Health Organization (WHO).

Valko, E., & DuBois, A. (1944). The antibacterial action of surface active cations. *Journal of Bacteriology, 47*(1), 15.

Van As, H., & Lens, P. N. L. (2001). Use of 1 H NMR to study transport processes in porous biosystems. *Journal of Industrial Microbiology and Biotechnology, 26*, 43-52.

Van Benthum, W., Van Den Hoogen, J., Van der Lans, R., Van Loosdrecht, M., & Heijnen, J. (1999). The biofilm airlift suspension extension reactor. Part I: Design and two-phase hydrodynamics. *Chemical Engineering Science, 54*(12), 1909-1924.

van den Berg, L., Pronk, M., van Loosdrecht, M. C., & de Kreuk, M. K. (2021a). Density Measurements of Aerobic Granular Sludge. *Environmental Technology*(just-accepted), 1-27.

van den Berg, L., van Loosdrecht, M. C. M., & de Kreuk, M. K. (2021b). How to measure diffusion coefficients in biofilms: A critical analysis. *Biotechnology and Bioengineering, 118*(3), 1273-1285.

Van den Heuvel, J. C., Portegies Zwart, I., & Vredenbregt, L. H. J. (1996). Convective acceleration of mass transfer in three-phase systems by pressure oscillations. *Chemical Engineering Science, 51*, 2391-2398.

Van den Heuvel, J. C., Verschuren, P. G., & Ottengraf, S. P. P. (1997). Acceleration of mass transfer in loop reactors. *Water Science and Technology, 36*, 311-319.

van der Roest, H. F., de Bruin, L. M. M., Gademan, G., & Coelho, F. (2011). Towards sustainable waste water treatment with Dutch Nereda® technology. *Water Practice and Technology, 6*.

van Dijk, E. J., Pronk, M., & van Loosdrecht, M. C. (2020). A settling model for full-scale aerobic granular sludge. *Water Research, 186*, 116135.

Van Loosdrecht, M. C. M., Tijhuis, L., Wijdieks, A., & Heijnen, J. (1995). Population distribution in aerobic biofilms on small suspended particles. *Water Science & Technology, 31*(1), 163-171.

Van Schadewijk, R., Van Den Berg, T. E., Gupta, K. B. S. S., Ronen, I., De Groot, H. J., & Alia, A. (2018). Non-invasive magnetic resonance imaging of oils in Botryococcus braunii green algae: Chemical shift selective and diffusion-weighted imaging. *PloS one, 13*(8).

Verawaty, M., Pijuan, M., Yuan, Z., & Bond, P. (2012). Determining the mechanisms for aerobic granulation from mixed seed of floccular and crushed granules in activated sludge wastewater treatment. *Water Research, 46*(3), 761-771.

Vlaeminck, S., De Clippeleir, H., & Verstraete, W. (2012). Microbial resource management of one-stage partial nitritation/anammox. *Microbial Biotechnology, 5*(3), 433-448.

Vogt, M., Flemming, H.-C., & Veeman, W. S. (2000). Diffusion in Pseudomonas aeruginosa biofilms: a pulsed field gradient NMR study. *Journal of Biotechnology, 77*, 137-146.

Voutouri, C., Polydorou, C., Papageorgis, P., Gkretsi, V., & Stylianopoulos, T. (2016). Hyaluronan-derived swelling of solid tumors, the contribution of collagen and cancer cells, and implications for cancer therapy. *Neoplasia, 18*(12), 732-741.

Waggoner, R. A., Blum, F. D., & Lang, J. C. (1995). Diffusion in aqueous solutions of poly (ethylene glycol) at low concentrations. *Macromolecules, 28*(8), 2658-2664.

Wagner, K., & Hempel, D. (1988). Biodegradation by immobilized bacteria in an airlift-loop reactor—influence of biofilm diffusion limitation. *Biotechnology and Bioengineering, 31*(6), 559-566.

Wang, L., Li, Y., Zhang, P., Zhang, S., Li, P., Wang, P., & Wang, C. (2019). Sorption removal of phthalate esters and bisphenols to biofilms from urban river: From macroscopic to microcosmic investigation. *Water Research, 150*, 261-270.

Wang, S. C. P., & Tien, C. (1984). Bilayer film model for the interaction between adsorption and bacterial activity in granular activated carbon columns part I: Formulation of equations and their numerical solutions. *AlChE Journal, 30*(5), 786-794.

Wang, W., Wang, W., Zhang, X., & Wang, D. (2002). Adsorption of p-chlorophenol by biofilm components. *Water Research, 36*(3), 551-560.

Wanner, O., Eberl, H. J., Morgenroth, E., Morgenroth, E., Noguera, D., Picioreanu, C., . . . Van Loosdrecht, M. M. (2006). *Mathematical Modelling of Biofilms*. In.

Wei, D., Shi, L., Yan, T., Zhang, G., Wang, Y., & Du, B. (2014). Aerobic granules formation and simultaneous nitrogen and phosphorus removal treating high strength ammonia wastewater in sequencing batch reactor. *Bioresource Technology, 171*, 211-216.

Wei, S. P., Quoc, B. N., Shapiro, M., Chang, P. H., Calhoun, J., & Winkler, M. K. (2021). Application of aerobic kenaf granules for biological nutrient removal in a full-scale continuous flow activated sludge system. *Chemosphere, 271*, 129522.

Weissbrodt, D. G., Neu, T. R., Kuhlicke, U., Rappaz, Y., & Holliger, C. (2013). Assessment of bacterial and structural dynamics in aerobic granular biofilms. *Frontiers in microbiology, 4*, 175.

Wess, T. J. (2005). Collagen fibril form and function. *Advances in Protein Chemistry, 70*, 341-374.

Westrin, B. A., & Axelsson, A. (1991). Diffusion in gels containing immobilized cells: A critical review. *Biotechnology and Bioengineering, 38*(5), 439-446.

Westrin, B. A., Axelsson, A., & Zacchi, G. (1994). Diffusion measurement in gels. *Journal of Controlled Release, 30*, 189-199.

Westrin, B. A., & Zacchi, G. (1991). Measurement of diffusion coefficients in gel beads: random and systematic errors. *Chemical Engineering Science, 46*(8), 1911-1916.

Wieland, A., de Beer, D., Damgaard, L. R., Kühl, M., van Dusschoten, D., & Van As, H. (2001). Fine-scale measurement of diffusivity in a microbial mat with nuclear magnetic resonance imaging. *Limnology and Oceanography, 46*(2), 248-259.

Wilén, B.-M., Gapes, D., & Keller, J. (2004). Determination of external and internal mass transfer limitation in nitrifying microbial aggregates. *Biotechnology and Bioengineering, 86*, 445-457.

Wilén, B.-M., Liébana, R., Persson, F., Modin, O., & Hermansson, M. (2018). The mechanisms of granulation of activated sludge in wastewater treatment, its optimization, and impact on effluent quality. *Applied Microbiology and Biotechnology, 102*(12), 5005-5020.

Wilke, C. R., & Chang, P. (1955). Correlation of diffusion coefficients in dilute solutions. *AlChE Journal, 1*, 264-270.

Wilking, J. N., Zaburdaev, V., De Volder, M., Losick, R., Brenner, M. P., & Weitz, D. A. (2013). Liquid transport facilitated by channels in Bacillus subtilis biofilms. *Proceedings of the National Academy of Sciences, 110*(3), 848-852.

Williamson, K., & McCarty, P. L. (1976). Verification studies of the biofilm model for bacterial substrate utilization. *J. Wat. Pollut. Cont. Fed*, 281-296.

Winkler, M. K. H., Bassin, J., Kleerebezem, R., Van der Lans, R., & Van Loosdrecht, M. (2012). Temperature and salt effects on settling velocity in granular sludge technology. *Water Research, 46*(16), 5445-5451.

Winkler, M. K. H., Kleerebezem, R., Strous, M., Chandran, K., & Van Loosdrecht, M. (2013). Factors influencing the density of aerobic granular sludge. *Applied Microbiology and Biotechnology, 97*(16), 7459-7468.

Witten, J., & Ribbeck, K. (2017). The particle in the spider's web: transport through biological hydrogels. *Nanoscale, 9*(24), 8080-8095.

Xavier, J. B., de Kreuk, M. K., Picioreanu, C., & van Loosdrecht, M. C. M. (2007). Multi-Scale Individual-Based Model of Microbial and Bioconversion Dynamics in Aerobic Granular Sludge. *Environmental Science & Technology, 41*, 6410-6417.

Xu, D., Fan, J., Li, W., Chen, W., Pan, C., Kang, D., . . . Zheng, P. (2021). Deciphering correlation between permeability and size of anammox granule:“pores as medium”. *Water Research, 191*, 116832.

Xu, D., Kang, D., Yu, T., Ding, A., Lin, Q., Zhang, M., . . . Zheng, P. (2019). A secret of high-rate mass transfer in anammox granular sludge: “Lung-like breathing”. *Water Research, 154*, 189-198.

Yan, J., Nadell, C. D., Stone, H. A., Wingreen, N. S., & Bassler, B. L. (2017). Extracellular-matrix-mediated osmotic pressure drives Vibrio cholerae biofilm expansion and cheater exclusion. *Nature communications, 8*(1), 1-11.

Yang, S., & Lewandowski, Z. (1995). Measurement of local mass transfer coefficient in biofilms. *Biotechnology and Bioengineering, 48*(6), 737-744.

Yano, T., Kodama, T., & Yamada, K. (1961). Fundamental Studies on the Aerobic Fermentation. *Agricultural and Biological Chemistry, 25*(7), 580-584.

Yilmaz, G., Lemaire, R., Keller, J., & Yuan, Z. (2008). Simultaneous nitrification, denitrification, and phosphorus removal from nutrient-rich industrial wastewater using granular sludge. *Biotechnology and Bioengineering, 100*(3), 529-541.

Yu, J., & Pinder, K. (1993). Diffusion of lactose in acidogenic biofilms. *Biotechnology and Bioengineering, 41*(7), 736-744.

Yu, J., & Pinder, K. L. (1994). Effective diffusivities of volatile fatty acids in methanogenic biofilms. *Bioresource Technology, 48*(2), 155-161.

Yuan, S., Gao, M., Zhu, F., Afzal, M. Z., Wang, Y.-K., Xu, H., . . . Wang, X.-H. (2017). Disintegration of aerobic granules during prolonged operation. *Environmental Science: Water Research & Technology, 3*(4), 757-766.

Zhang, T. C., & Bishop, P. L. (1994a). Density, porosity, and pore structure of biofilms. *Water Research, 28*, 2267-2277.

Zhang, T. C., & Bishop, P. L. (1994b). Evaluation of tortuosity factors and effective diffusivities in biofilms. *Water Research, 28*, 2279-2287.

Zhang, Z., Nadezhina, E., & Wilkinson, K. J. (2011). Quantifying Diffusion in a Biofilm of Streptococcus mutans. *Antimicrobial Agents and Chemotherapy, 55*, 1075-1081.

Zheng, Y.-M., & Yu, H.-Q. (2007). Determination of the pore size distribution and porosity of aerobic granules using size-exclusion chromatography. *Water Research, 41*, 39-46.

Zheng, Y.-M., Yu, H.-Q., Liu, S.-J., & Liu, X.-Z. (2006). Formation and instability of aerobic granules under high organic loading conditions. *Chemosphere, 63*, 1791-1800.

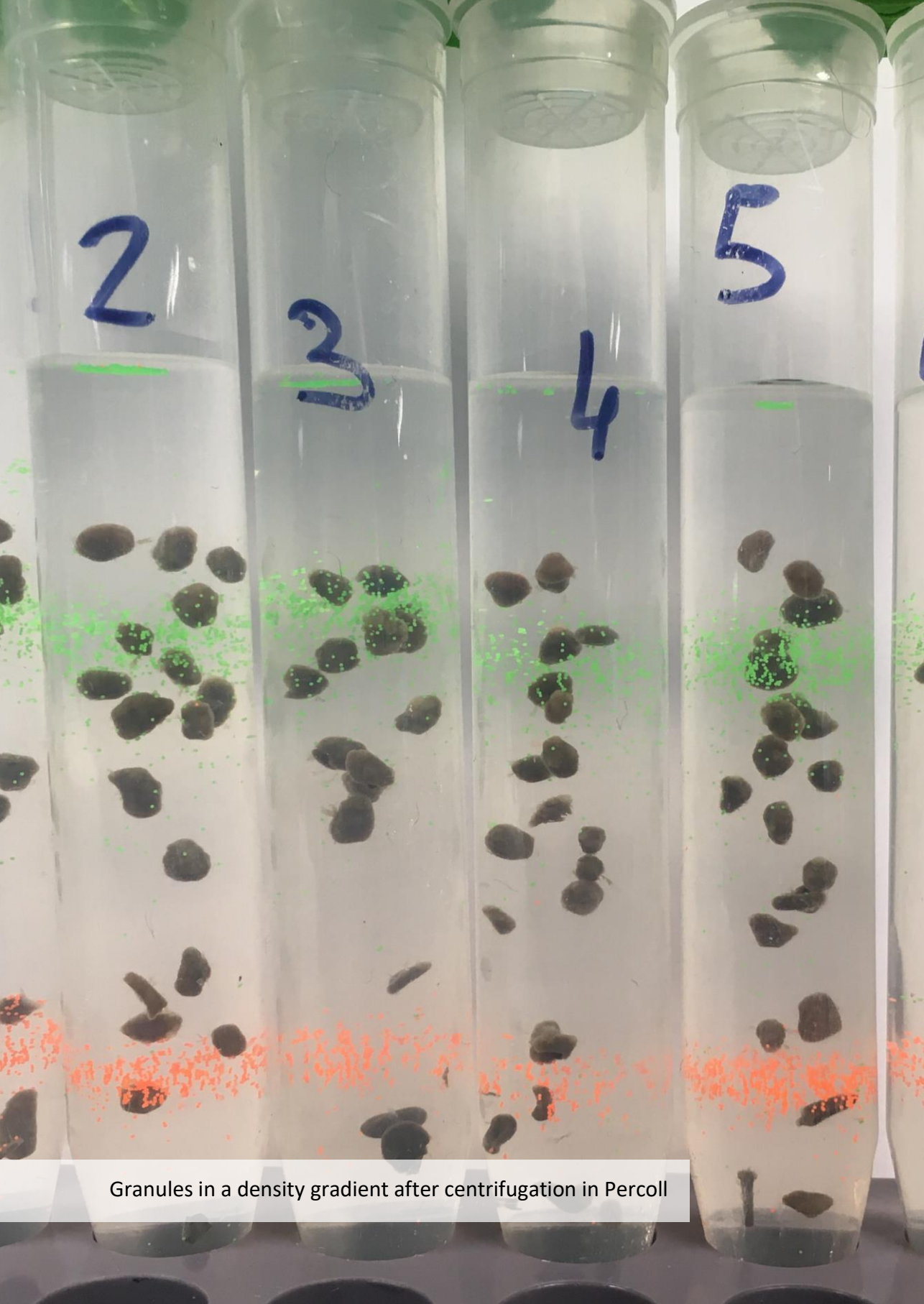

Granules in a density gradient after centrifugation in Percoll

Acknowledgements

Curriculum Vitae

List of Publications

Acknowledgements

This book is the results of four years of work. There are many people that contributed to this book and that made these four years an exciting time. I would like to dedicate the next pages to thank several of those people specifically.

First of all, **Merle**, thank you for guiding me through my studies and offering me this amazing PhD opportunity. You were always supportive, warm and friendly and you managed to create an environment of growth, with room for mistakes and trying out new things. Your support stimulated me to develop myself. Our weekly meetings were always one of the highlights of my week. **Mark**, thank you for your support and your great insights. You always pushed me to take my research to a higher level and you were my guide in the academic world. I really appreciate that you pushed me to share my research and overcome my perfectionism.

Sara, thank you for making the last years very enjoyable. You were always ready to listen to me, when I was excited about new plans and ideas. Many PhDs feel like they work alone on their little island, but we were lucky to work on the 'granular sludge' island together. Thank you for the nice moments, the laughs and the conversations.

Emiel, thank you for being my paranymph. You are a great colleague, and I enjoyed our lunches and coffee breaks. Our research topics were not very similar, but there were still interesting discussions about science and research, and the 'Dutch approach'. It was a shame that you worked so much from home the last year, because it was always nice to have you around in the lab.

During my PhD, I had the opportunity to spend three great months at Montana State University with **Catherine**, **Joe**, and **Sarah**. Thank you for hosting me and teaching me so much about NMR and MRI. It was wonderful to experience the beautiful state of Montana. I would love to come back one day. **Julia**, thank you for helping me with the MRI measurements in Utrecht.

I am grateful for all the nice and friendly colleagues at the Sanitary Engineering group. I especially want to thank all the PhDs that started around the same time as I did and with whom I shared the big call centre office: **Antonella**, **Carina**, **Bruno**, **Javier**, **Daniel**, **Max**, **Mingliang**, **Bin Lin**, and **Lihua**. Thank you for the warm welcome to the department and for all the good times we had. Of course, there are more people that I crossed paths with and deserve to be mentioned: **Adrian**, **Hongxiao, Peng, Niels, Victor, Magela, Pamela,** and **Steef**. Thank you for the positive atmosphere, the chaotic red lab meetings,

and for everything else. I wish you the all the best for the future. Thank you, **Armand**, **Patricia**, **Mohammed**, **Jane**, and **Jasper** for all your help in the lab. Thank you, **Mariska**, **Tamara**, and **Riëlle** for all your help with practical matters. I would like to thank my students who helped me with my project: **Shiyu**, **Sarah**, and **Shkenca**. I enjoyed working with you, the (mostly) online meetings, and the time in the lab.

Thank you, granular sludge colleagues outside my own department. **Mario**, you were always interested in what I was doing. We did not meet that often, but each meeting with you would reignite my enthusiasm. Thank you for that. **Viktor**, I was always amazed about your grand ideas and insights. I enjoyed our discussions about modelling, granule formation, and mass transfer. The discussions really boosted my enthusiasm and motivation. **Mark Stevens**, jouw gastvrijheid en enthousiasme kennen geen grenzen. Het was altijd een plezier om langs te komen voor korrels en voor de gezelligheid! Dankzij jouw hulp heb ik al mijn experimenten kunnen doen. Ik hoop dat ik je in de toekomst nog eens tegen kom.

I would like to thank my family, and especially my **parents**. Dank voor jullie steun tijdens mijn studie en tijdens mijn promotie. Dank voor al jullie advies en voor de aanmoediging om mezelf te ontwikkelen. Ik heb het getroffen met jullie als ouders. I also want to thank **Christi-Janne, Norah and Luuk**. Jullie zijn er altijd voor me en jullie hebben me de motivatie gegeven om mijn proefschrift te voltooien. Jullie betekenen meer voor me dan ik in woorden kan vatten. Finally, I am thankful to God, who has guided me throughout my life and has provided me with everything I needed to finalize my PhD. *For from Him and through Him and to Him are all things. To him be glory forever* (Romans 11:36).

Soli Deo Gloria

Curriculum Vitae

Lenno van den Berg was born on March 4th, 1994, in Zeist, The Netherlands. In 2011, he started with the bachelor of Civil Engineering at Delft University of Technology. During this study, he developed an interest in water treatment. He completed his bachelor in 2014 with a bachelor end project on pre-treatment technologies for sludge digestion, at Royal Haskoning DHV. From 2014 until 2017, he continued his education with an individual double degree program, also at Delft University of Technology. The double degree program combined the master Watermanagement and the master Life Science and Technology. He completed his first MSc thesis on modelling and characterization of full-scale aerobic granular sludge, at Royal HaskoningDHV. His second MSc thesis was focused on anaerobic ATP generation in *Candidatus Accumulibacter phosphatis*, an important organism in wastewater treatment.

In October 2017, he started his PhD at the Sanitary Engineering Section at the Delft University of Technology under the supervision of Merle de Kreuk and Mark van Loosdrecht. The aim of the project was to better understand the fate of complex contaminants in the aerobic granular sludge process. His research was focused on diffusion of complex contaminants within the granules. The project was carried out together with PhD candidate Sara Toja Ortega, who focused on the biological conversion of complex contaminants. During his PhD, he spent 3 months at the Center for Biofilm Engineering in Bozeman, Montana to study diffusion in aerobic granules with nuclear magnetic resonance methods.

He is currently working as consultant R&D at the advisory group waste water at Royal HaskoningDHV.

List of Publications

Publications

Kirkland, C. M. K., Krug, J. R., Vergeldt, F. J., **Van den Berg, L**., Velders, A. H., Seymour, J. D., Codd, S.L., Van As, H., & De Kreuk, M. K. (2020). Characterizing the structure of aerobic granular sludge using ultra-high field magnetic resonance. *Water Science and Technology*, 82(4), 627-639. doi:10.2166/wst.2020.341

Van den Berg, L., Kirkland, C. M. K., Seymour, J. D., Codd, S. L., Van Loosdrecht, M. C. M., & De Kreuk, M. K. (2020). Heterogeneous diffusion in aerobic granular sludge. *Biotechnology and bioengineering*, 117(12), 3809-3819. doi:10.1002/bit.27522

Van den Berg, L., Van Loosdrecht, M. C. M., & De Kreuk, M. K. (2021). How to measure diffusion coefficients in biofilms: A critical analysis. *Biotechnology and bioengineering*, 118(3), 1273-1285. doi:10.1002/bit.27650

Van den Berg, L., Pronk, M., Van Loosdrecht, M. C. M., & De Kreuk, M. K. (2021). Density Measurements of Aerobic Granular Sludge. *Environmental Technology*. doi:10.1080/09593330.2021.2017492

Van den Berg, L., Toja Ortega, S., Van Loosdrecht, M. C. M., & De Kreuk, M. K. (submitted). Diffusion of Soluble Organic Substrates in Aerobic Granular Sludge: Effect of Molecular Weight.

Conference contributions

Van den Berg, L., Kirkland, C. M. K., Van Loosdrecht, M. C. M., & De Kreuk, M. K. (2019, July 2). Heterogeneous diffusion in aerobic granules does not improve granule performance [Poster presentation]. TU Delft Bioday, Delft, The Netherlands.

Van den Berg, L., Kirkland, C. M. K., Van Loosdrecht, M. C. M., & De Kreuk, M. K. (2020, Februari 12-14). How significant is heterogeneity and variability of diffusion in aerobic granular sludge? [Oral presentation]. IWA Young Water Professionals Conference, Luxembourg, Luxembourg.

Van den Berg, L., Kirkland, C. M. K., Van Loosdrecht, M. C. M., & De Kreuk, M. K. (2020, September 1-3). The key role of diffusion in simultaneous nitrification and denitrification by aerobic granular sludge [Oral presentation]. IWA Nutrient Removal and Recovery Conference, Helsinki, Finland.

Van den Berg, L., Van Loosdrecht, M. C. M., & De Kreuk, M. K. (2020, September 29-October 1). How to measure diffusion coefficients in biofilms? [Oral presentation]. Biofilms 9 Online Conference, Karlsruhe, Germany.

Van den Berg, L., Van Loosdrecht, M. C. M., & De Kreuk, M. K. (2020, December 7-9). Modelling of heterogeneous granule structures [Workshop presentation]. IWA Biofilms Virtual Conference, Notre Dame, IN, United States.

Van den Berg, L., Van Loosdrecht, M. C. M., & De Kreuk, M. K. (2020, December 7-9). How sensitive are biofilm models to the diffusion coefficient? [Poster presentation]. IWA Biofilms Virtual Conference, Notre Dame, IN, United States.

Van den Berg, L., Van Loosdrecht, M. C. M., & De Kreuk, M. K. (2021, December 6-8). Effect of molecular weight on diffusion in aerobic granular sludge [Oral presentation]. IWA Biofilm Reactors Virtual Conference, Notre Dame, IN, United States.